Cell

Directed evolution of a family of AAV capsid variants enabling potent muscle-directed gene delivery across species

Graphical abstract

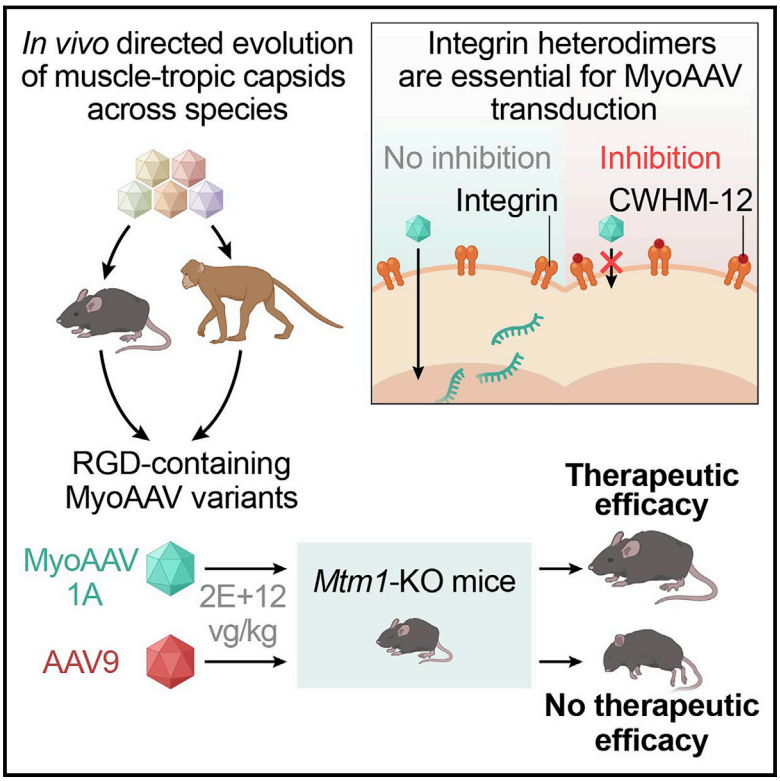

Highlights

- A family of muscle-tropic capsids identified by directed evolution in mice and primates
- MyoAAV transduction is dependent on integrin heterodimers in mouse and human cells
- MyoAAV administration at low dose results in therapeutic efficacy in disease models
- Systemically administrated MyoAAV transduces primate muscles highly efficiently

Authors

Mohammadsharif Tabebordbar, Kim A. Lagerborg, Alexandra Stanton, ..., Alan H. Beggs, Amy J. Wagers, Pardis C. Sabeti

Correspondence

tabebord@fas.harvard.edu (M.T.), amy_wagers@harvard.edu (A.J.W.), pardis@broadinstitute.org (P.C.S.)

In brief

Tabebordbar et al. evolved a family of RGD-containing AAV capsid variants in mice and primates that enable highly effective systemic gene delivery to muscles. They show these capsids are dependent on integrin heterodimers for transduction across species and enable achieving therapeutic efficacy after systemic administration at low dose.

Tabebordbar et al., 2021, Cell *184*, 4919–4938
September 16, 2021
https://doi.org/10.1016/j.cell.2021.08.028

CellPress

Cell

CellPress
OPEN ACCESS

Article

Directed evolution of a family of AAV capsid variants enabling potent muscle-directed gene delivery across species

Mohammadsharif Tabebordbar,[1,13,14,*] Kim A. Lagerborg,[1,2,13] Alexandra Stanton,[1,3] Emily M. King,[1] Simon Ye,[1,4] Liana Tellez,[1] Allison Krunnfusz,[1] Sahar Tavakoli,[5,6,7,8] Jeffrey J. Widrick,[9] Kathleen A. Messemer,[5,6,7] Emily C. Troiano,[9] Behzad Moghadaszadeh,[9] Bryan L. Peacker,[5,6,7] Krystynne A. Leacock,[5,6,7] Naftali Horwitz,[5,6,7,11] Alan H. Beggs,[1,9] Amy J. Wagers,[5,6,7,11,*] and Pardis C. Sabeti[1,10,12,*]

[1]Broad Institute of MIT and Harvard, Cambridge, MA 02142, USA
[2]Harvard Program in Biological and Biomedical Sciences, Harvard Medical School, Boston, MA 02115, USA
[3]Harvard Program in Virology, Harvard Medical School, Boston, MA 02115, USA
[4]Harvard-MIT Health Sciences and Technology, Massachusetts Institute of Technology, Cambridge, MA 02139, USA
[5]Department of Stem Cell and Regenerative Biology, Harvard University, Cambridge, MA 02138, USA
[6]Harvard Stem Cell Institute, Cambridge, MA 02138, USA
[7]Paul F. Glenn Center for the Biology of Aging, Harvard Medical School, Boston, MA 02115, USA
[8]Stem Cell Program and Division of Hematology/Oncology, Boston Children's Hospital, Boston, MA 02115, USA
[9]Division of Genetics and Genomics, The Manton Center for Orphan Disease Research, Boston Children's Hospital, Harvard Medical School, Boston, MA 02115, USA
[10]Department of Organismic and Evolutionary Biology, FAS Center for Systems Biology, Harvard University, Cambridge, MA 02138, USA
[11]Section on Islet Cell and Regenerative Biology, Joslin Diabetes Center, Boston, MA 02215, USA
[12]Howard Hughes Medical Institute, Chevy Chase, MD 20815, USA
[13]These authors contributed equally
[14]Lead contact
*Correspondence: tabebord@fas.harvard.edu (M.T.), amy_wagers@harvard.edu (A.J.W.), pardis@broadinstitute.org (P.C.S.)
https://doi.org/10.1016/j.cell.2021.08.028

SUMMARY

Replacing or editing disease-causing mutations holds great promise for treating many human diseases. Yet, delivering therapeutic genetic modifiers to specific cells *in vivo* has been challenging, particularly in large, anatomically distributed tissues such as skeletal muscle. Here, we establish an *in vivo* strategy to evolve and stringently select capsid variants of adeno-associated viruses (AAVs) that enable potent delivery to desired tissues. Using this method, we identify a class of RGD motif-containing capsids that transduces muscle with superior efficiency and selectivity after intravenous injection in mice and non-human primates. We demonstrate substantially enhanced potency and therapeutic efficacy of these engineered vectors compared to naturally occurring AAV capsids in two mouse models of genetic muscle disease. The top capsid variants from our selection approach show conserved potency for delivery across a variety of inbred mouse strains, and in cynomolgus macaques and human primary myotubes, with transduction dependent on target cell expressed integrin heterodimers.

INTRODUCTION

Recombinant adeno-associated viruses (rAAVs) are the most commonly used vehicles for *in vivo* gene replacement therapy and gene editing in preclinical and clinical studies, yet selective transduction of specific tissues after systemic delivery remains a challenge. Recombinant AAVs generated using naturally occurring capsids are predominantly sequestered in the liver after systemic injection. This sequestration limits the efficiency of transduction in other organs (Gao et al., 2006; Murrey et al., 2014; Zincarelli et al., 2008) and poses a particular challenge for gene delivery to skeletal muscle. Because muscle comprises up to 40% of total body mass, achieving therapeutic thresholds in muscle with natural capsid variants requires extremely high virus doses (~2E+14 vg/kg) (Duan, 2018), which creates a formidable hurdle for vector manufacturing and can result in therapy-limiting toxicity, as observed in some recent clinical trials (Morales et al., 2020).

AAV capsid protein engineering coupled with *in vivo* selection is a promising approach to enable potent and selective gene delivery to a variety of tissues. AAV capsid-directed evolution strategies typically involve generating diverse capsid libraries followed by selection of variants with desired tropism in cell culture and/or animal models. This approach has generated

modified vectors for augmented delivery to a number of tissues (Choudhury et al., 2016; Dalkara et al., 2013; Deverman et al., 2016; Körbelin et al., 2016; Li et al., 2016; Michelfelder et al., 2009; Nonnenmacher et al., 2020; Tse et al., 2017; Yang et al., 2009; Yang and Xiao, 2013).

To be most successful, a directed evolution approach must enable stringent selection of functional capsid variants at the mRNA level across different strains and species. AAV transduction is a multi-step process including binding to receptors on the cell surface, intracellular trafficking, endosomal escape, nuclear entry, vector genome second strand DNA synthesis, and transgene expression (Berry and Asokan, 2016; Ding et al., 2005; Figure S1A), and inefficiency in any of these steps can limit vector potency. Therefore, successful identification of potent capsids requires selecting variants that proceed effectively through all stages of transduction. However, the majority of *in vivo* capsid directed evolution strategies select successful capsid variants based on presence in the tissue of interest of the vector genome DNA, rather than the transgene mRNA (Li and Samulski, 2020). Species- and strain-specific differences in the coding sequence and expression of genes involved in AAV transduction have presented yet another challenge, as capsid variants selected in specific mouse strains may not yield potent transduction in other strains or other species (Hordeaux et al., 2018).

Here, we developed the DELIVER (directed evolution of AAV capsids leveraging *in vivo* expression of transgene RNA) strategy to combine diverse capsid library generation with stringent transcript-based *in vivo* selection and to enable directed evolution followed by identification of functional capsid variants in any tissue of interest and any animal model. We apply DELIVER to develop muscle-tropic capsids in mice and non-human primates (NHPs) and compare our results to AAV9 and AAVrh74, both of which are naturally occurring AAV capsids currently used in gene replacement trials for Duchenne muscular dystrophy (DMD) (clinicaltrials.gov identifiers: NCT03362502, NCT03368742, NCT03375164, and NCT03769116). Overall, our muscle-directed vectors demonstrate superior potency and selectivity for transduction of both skeletal muscle and cardiac tissue when compared to AAV9 and AAVrh74. These vectors further demonstrate conserved transduction potency across mice, NHPs, and human muscle cells. Cross-comparison of muscle-enriched variant capsid sequences in mice and NHPs identified a common arginine-glycine-aspartic acid (RGD) motif among the top variants, and additional analyses uncovered a strong interaction with, and dependence on, target cell expression of RGD-binding integrin heterodimers. Taken together, this work provides a class of AAV capsid variants with particular utility for therapeutics development and testing in striated muscle. It additionally presents a comprehensive experimental framework for future evolution of additional families of AAVs with alternative tissue tropism, emphasizing the crucial advantages of independent screening efforts performed in multiple species and strains based on functional variant transduction from high diversity capsid libraries and of applying mechanistic insight to guide directed evolution for vector optimization.

RESULTS

In vivo evolution of AAV9 capsid using DELIVER identifies a class of muscle-tropic variants

The AAV9-based capsid libraries we designed for this study included several key features to facilitate identification of muscle-directed vectors with high potency for *in vivo* use. First, each variant included a random 7-mer peptide inserted between amino acids 588 and 589 in the hypervariable region VIII of the AAV9 capsid, a design that ensures exposure of the variable peptide sequence on the capsid surface (Börner et al., 2020; DiMattia et al., 2012; Figure 1A). Each variant also encapsulated a transgene encoding its own capsid sequence under the control of either a ubiquitous or a cell type-specific mammalian promoter, which allowed for expression of the transgene (capsid variant) in both the HEK293 cells used for virus library production (Figure 1B) and the animal tissues transduced with the virus after *in vivo* delivery (Figures 1C and 1D).

We initially evaluated DELIVER's stringency for selecting capsid variants that functionally transduce discrete mouse tissues in C57BL/6J mice, using a virus library in which capsid variants were expressed under the ubiquitous cytomegalovirus (CMV) promoter. We identified variants that were enriched relative to the virus library at the DNA and mRNA levels in various tissues. Selection of variants based on mRNA expression yielded fewer capsids compared to selection based on the presence of vector genome DNA (Figures S1B–S1H), which could suggest that only a small fraction of capsid variants that physically enter target cells can functionally transduce these cells to express their encoded transgene. In line with this possibility, we found that while capsid variants with higher abundance in the injected virus library were more abundant in the liver of injected animals at the vector genome DNA level, there was almost no correlation between abundance of each variant in the virus library and the level of transgene mRNA from the same variant in the liver (Figures S1I and S1J). Furthermore, we assessed the abundance of each capsid variant identified in the liver (Figure S1K) and muscle (Figures S1L–S1N) at the vector genome DNA and transgene mRNA levels and found no correlation between DNA and mRNA.

We next investigated the feasibility of using muscle-specific promoters to enhance selection for potent muscle-tropic capsid variants. Skeletal and cardiac muscle contain several different cell types, but AAV capsids capable of effective transgene delivery to two cell types in particular—muscle fibers and cardiomyocytes—are most desired for therapeutic gene delivery for genetic myopathies. To enable selection of variants specifically expressed in these cell types *in vivo*, we generated AAV capsid libraries in HEK293 cells using inverted terminal repeat (ITR)-containing constructs in which expression of capsid coding sequences was controlled by the muscle-specific CK8 or MHCK7 promoters. These constructs produced similar titers of rAAV as those produced using a construct expressing the capsid under the ubiquitous CMV promoter (Figure 1B). Furthermore, within the skeletal and cardiac muscles of injected mice, virus libraries expressed under CK8 or MHCK7 promoters yielded similar or higher transgene mRNA expression compared to those expressed under CMV, greatly facilitating identification of

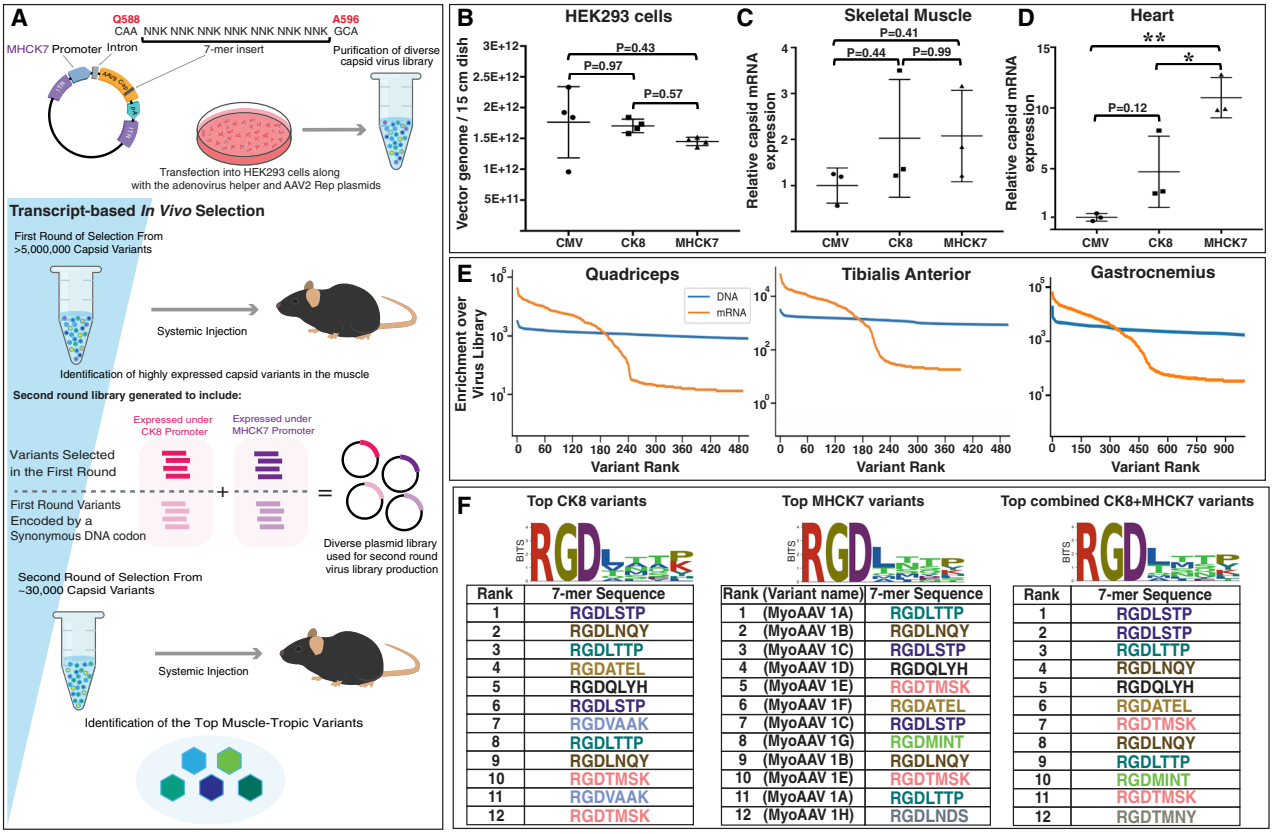

Rank	7-mer Sequence
1	RGDLSTP
2	RGDLNQY
3	RGDLTTP
4	RGDATEL
5	RGDQLYH
6	RGDLSTP
7	RGDVAAK
8	RGDLTTP
9	RGDLNQY
10	RGDTMSK
11	RGDVAAK
12	RGDTMSK

Rank (Variant name)	7-mer Sequence
1 (MyoAAV 1A)	RGDLTTP
2 (MyoAAV 1B)	RGDLNQY
3 (MyoAAV 1C)	RGDLSTP
4 (MyoAAV 1D)	RGDQLYH
5 (MyoAAV 1E)	RGDTMSK
6 (MyoAAV 1F)	RGDATEL
7 (MyoAAV 1C)	RGDLSTP
8 (MyoAAV 1G)	RGDMINT
9 (MyoAAV 1B)	RGDLNQY
10 (MyoAAV 1E)	RGDTMSK
11 (MyoAAV 1A)	RGDLTTP
12 (MyoAAV 1H)	RGDLNDS

Rank	7-mer Sequence
1	RGDLSTP
2	RGDLSTP
3	RGDLTTP
4	RGDLNQY
5	RGDQLYH
6	RGDATEL
7	RGDTMSK
8	RGDLNQY
9	RGDLTTP
10	RGDMINT
11	RGDTMSK
12	RGDTMNY

Figure 1. DELIVER identifies a class of muscle-tropic AAV capsid variants containing an RGD motif

(A) Schematic of virus library production and capsid variant selection using DELIVER.

(B) Comparison of rAAV titers produced using ITR-containing constructs that express the AAV9 capsid coding sequence under the control of CMV, CK8, or MHCK7 promoters. Data are presented as mean ± SD (n = 4). p value calculated by one-way analysis of variance (ANOVA) with Tukey-Kramer multiple comparisons test (MCT).

(C and D) *In vivo* expression of the AAV9 capsid library mRNA expressed under the control of CMV, CK8, or MHCK7 promoters in skeletal muscle (C) and heart (D) of 8-week-old C57BL/6J mice systemically injected with 1E+12 vg of the capsid library. Data are presented as mean ± SD (n = 3). p value calculated by one-way ANOVA with Tukey-Kramer MCT. *p < 0.05, **p < 0.01.

(E) Graphs showing enrichment of capsid variants expressed under MHCK7 promoter over virus library at the DNA and mRNA level in different mouse skeletal muscles.

(F) Sequence of the 7-mer insertion in the top highly expressed capsid variants in muscles of 8-week-old C57BL/6J mice injected with 1E+12 vg virus library after the second round of transcript-based selection. Variants with the same color in each group are encoded by synonymous DNA codons. Variant rank is based on the sum of mRNA expression for each variant in quadriceps, tibialis anterior, gastrocnemius, triceps, abdominal, diaphragm, and heart.

See also Figure S1.

functional variants that transduce muscle fibers and cardiomyocytes (Figures 1C and 1D).

We performed two rounds of *in vivo* selection with directed evolution, screening capsid variants expressed from the MHCK7 promoter in multiple different muscles of C57BL/6J mice. Sequencing the first-round virus library identified more than 5,000,000 unique capsid variants. After the first round of selection, we selected the top 30,000 variants that were highly expressed in seven muscles (quadriceps, tibialis anterior [TA], gastrocnemius, triceps, abdominal, diaphragm, and heart) (Figures 1A and 1E). For the second round of *in vivo* selection, we incorporated two kinds of controls. The first was a synonymous codon control in which the same 7-mer inserted peptides identified for each selected variant from the primary screen were encoded using synonymous DNA codons. The second was an expression control in which duplicate virus libraries were generated to express the two replicates of those 30,000 variants under either of two skeletal muscle specific promoters, CK8 or MHCK7 (Figure 1A).

Strikingly, in the second round of selection, all 12 of the top capsid variants highly expressed in muscles from either the CK8 or MHCK7 libraries contained the same RGD motif in the first three amino acid positions of the 7-mer insert (Figure 1F; Table S4). Further implicating the specific peptide sequences included in these capsid variants in their superior transduction of muscle, 10 of the top 12 hits in the CK8 group and 8 of the top 12 hits in the MHCK7 group were from synonymous pairs (i.e., the corresponding variant encoded by synonymous DNA codons was also within the top 12 muscle-expressed variants).

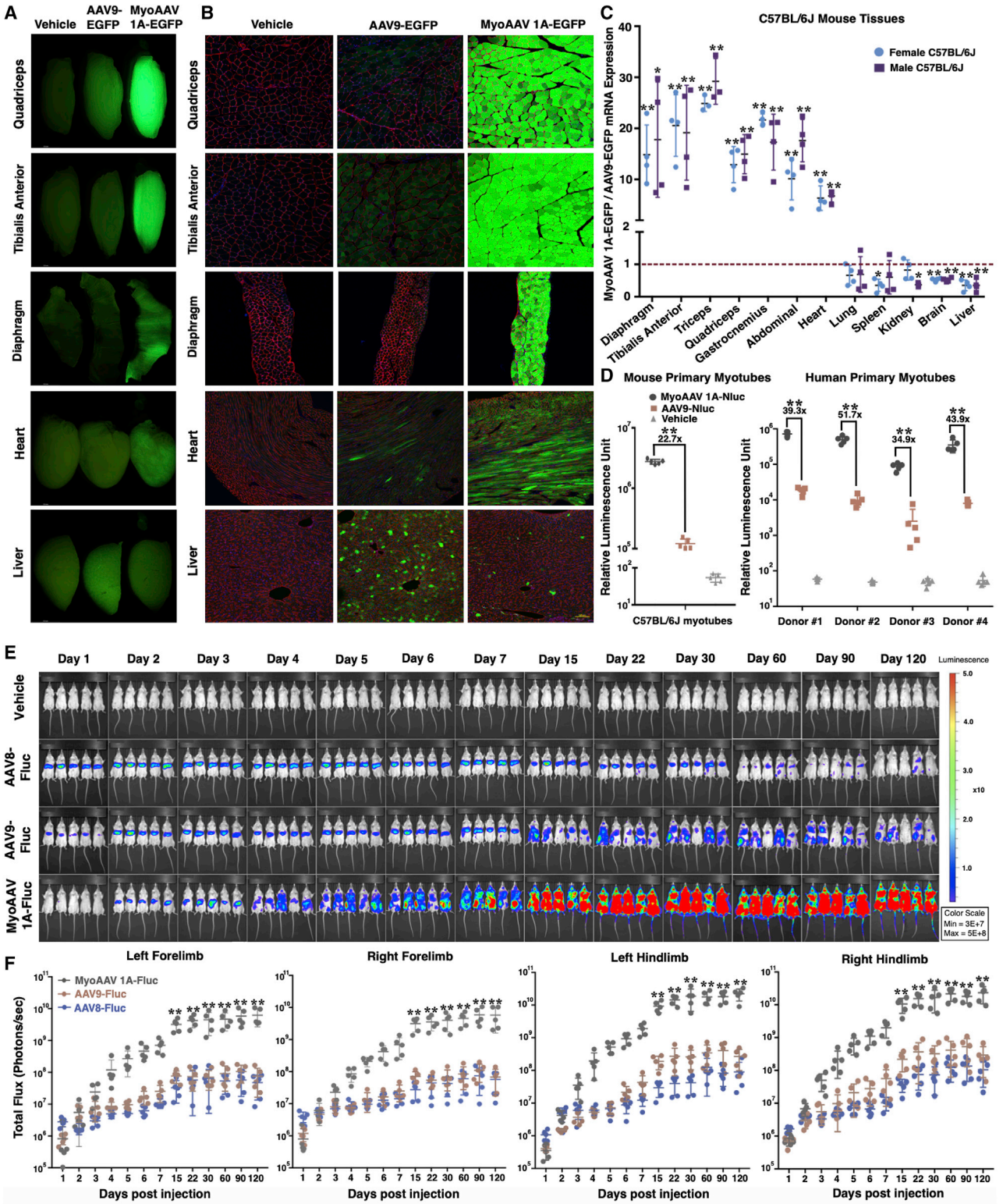

Figure 2. MyoAAV 1A transduces mouse skeletal muscles with high efficiency after systemic injection

(A and B) Whole mount fluorescent (A) and cross section (B) images of skeletal muscles, heart, and liver from 8-week-old C57BL/6J mice systemically injected with 1E+12 vg of AAV9- or MyoAAV 1A-CMV-EGFP. Green, EGFP; red: laminin for muscles, lectin for liver; blue, Hoechst. Scale bar in cross sections: 100 μm.

(legend continued on next page)

Moreover, 10 of the top 12 hits were shared between the CK8 and MHCK7 groups.

In order to select one of the variants for further characterization, we considered the variant rank and evaluated the production yield of the top five unique RGD-containing capsid variants. We quantified titers of rAAVs produced using the top five unique RGD-containing capsid variants. This comparison showed no significant difference between these and the parental AAV9 capsid (Figure S2F). With all this data together, we selected the variant containing the RGDLTTP peptide insertion for further characterization and named this variant "MyoAAV 1A." This variant was selected as it was the highest ranked capsid in the MHCK7 group, and one of the two highest overall (the other was RGDLSTP). RGDLTTP also matches the consensus amino acids at each position from the top 12 RGD-containing hits in both groups.

MyoAAV 1A transduces mouse muscles with high efficiency after systemic administration

To investigate the transduction profile and biodistribution of MyoAAV 1A after systemic delivery, we injected adult C57BL/6J mice with 1E+12 vg (~4E+13 vg/kg) AAV9- or MyoAAV 1A-CMV-EGFP and analyzed transgene expression and vector genome abundance in different tissues 2 weeks after injection. Whole mount fluorescent imaging of harvested tissues revealed far greater fluorescence intensity in muscles of mice injected with MyoAAV 1A as compared to AAV9-injected mice (Figures 2A and S2A). Importantly, MyoAAV 1A transduced the heart, a key affected organ in many genetic myopathies, more effectively than AAV9. Strong transgene expression in muscle fibers and cardiomyocytes of MyoAAV 1A injected mice was further confirmed by immunofluorescence analysis (Figures 2B and S2B). Remarkably, MyoAAV 1A showed relatively diminished transduction of liver after systemic delivery in C57BL/6J mice, suggesting a liver-detargeted transduction profile for this variant compared to AAV9 (Figures 2A–2C).

Quantification of EGFP mRNA in different skeletal muscles of male and female C57BL/6J mice revealed 10 to 29 times higher transgene expression in muscles of MyoAAV 1A-injected compared to AAV9-injected mice (Figure 2C). EGFP mRNA expression was 6.3 times higher in the heart and 2.8 times lower in the liver of MyoAAV 1A injected animals (Figure 2C). Notably, improved transduction efficiency by MyoAAV 1A was restricted to striated muscle tissues, and this engineered capsid variant transduced the lung, kidney, spleen, and brain of injected animals with similar or lower efficiency compared to AAV9 (Figures 2C and S2C). Western blot analysis confirmed dramatically higher expression of EGFP protein in the gastrocnemius and triceps muscles and lower EGFP expression in the liver of MyoAAV 1A-injected animals compared to AAV9-injected mice (Figure S2D). Biodistribution analysis demonstrated that MyoAAV 1A delivered vector genomes to muscles of C57BL/6J mice more effectively than AAV9 and resulted in a significantly lower number of vector genomes per diploid genome (vg/dg) in the liver after systemic administration (Figure S2E).

To investigate the possibility of liver damage following systemic MyoAAV 1A administration, we measured levels of alanine aminotransferase (ALT) and aspartate aminotransferase (AST) enzymes in the serum of C57BL/6J mice injected with vehicle (saline), or 1E+12 vg (~4E+13 vg/kg) of AAV9- or MyoAAV 1A-CMV-EGFP, before injection, as well as 14 and 28 days after injection. Levels of ALT and AST in the serum of AAV9- or MyoAAV 1A-injected mice were not significantly different compared to the vehicle-injected animals, suggesting lack of liver damage at the dose injected (Figures S3I and S3J).

We further tested cross reactivity of anti-AAV9 antibodies with MyoAAV 1A by analyzing inhibition of AAV9 and MyoAAV 1A transduction after addition of serum isolated from mice previously injected with AAV9- or MyoAAV 1A-EGFP. Results from this experiment demonstrated that antibodies produced against AAV9 cross react with MyoAAV 1A and vice versa (Figures S3K and S3L).

To evaluate the efficiency of muscle transduction after systemic administration of MyoAAV 1A in different mouse strains, we injected male and female mice from the BALB/cJ and DBA/2J backgrounds with 1E+12 vg (~4E+13 vg/kg) of AAV9- or MyoAAV 1A-CMV-EGFP and compared transgene expression in different tissues of the injected mice. Whole organ imaging and EGFP mRNA quantification showed that potent muscle transduction and liver detargeting characteristics of MyoAAV 1A extend to BALB/cJ and DBA/2J mice as well (Figures S3A–S3E).

We also assessed the efficiency of muscle transduction after intramuscular delivery of MyoAAV 1A compared to AAV9. Intramuscular administration of 2E+10 vg of AAV9- or MyoAAV 1A-CMV-EGFP to the TA muscle in C57BL/6J mice resulted in 14 times higher EGFP mRNA expression, as well as dramatically higher EGFP protein expression, analyzed by western blot and immunofluorescence, in the MyoAAV 1A-injected muscles relative to the muscles of AAV9-injected mice (Figures S3F–S3H).

(C) Quantification of fold difference in EGFP mRNA expression in various tissues of male and female 8-week-old C57BL/6J mice injected with 1E+12 vg of AAV9- or MyoAAV 1A-CMV-EGFP. Dashed red line indicates relative expression from AAV9-CMV-EGFP. Data are presented as mean ± SD (n = 3–4); *p < 0.05, **p < 0.01 (Student's t test between AAV9 and MyoAAV 1A-injected mice for each group).

(D) Quantification of *in vitro* transduction in mouse (left) and human (right) primary myotubes transduced with vehicle, AAV9- or MyoAAV 1A-CK8-Nluc. Data are presented as mean ± SD (n = 5); **p < 0.01 (Student's t test). Donor 1: 29-year-old male; donor 2: 19-year-old female; donor 3: 20-year-old male; donor 4: 34-year-old female.

(E) Whole-body *in vivo* bioluminescence images of 8-week-old BALB/cJ mice systemically injected with 4E+11 vg of AAV8-, AAV9-, or MyoAAV 1A-CMV-Fluc, taken over 120 days.

(F) Quantification of total luminescence from forelimbs and hindlimbs of animals injected with AAV8-, AAV9-, or MyoAAV 1A-CMV-Fluc, assessed over 120 days. p value calculated between AAV8, AAV9, and MyoAAV 1A groups by two-way ANOVA with Tukey-Kramer MCT; Data are presented as mean ± SD (n = 5). **p < 0.01 for both MyoAAV 1A versus AAV8 and MyoAAV 1A versus AAV9. Difference between AAV8 and AAV9 groups is not statistically significant at any of the time points.

See also Figures S2 and S3.

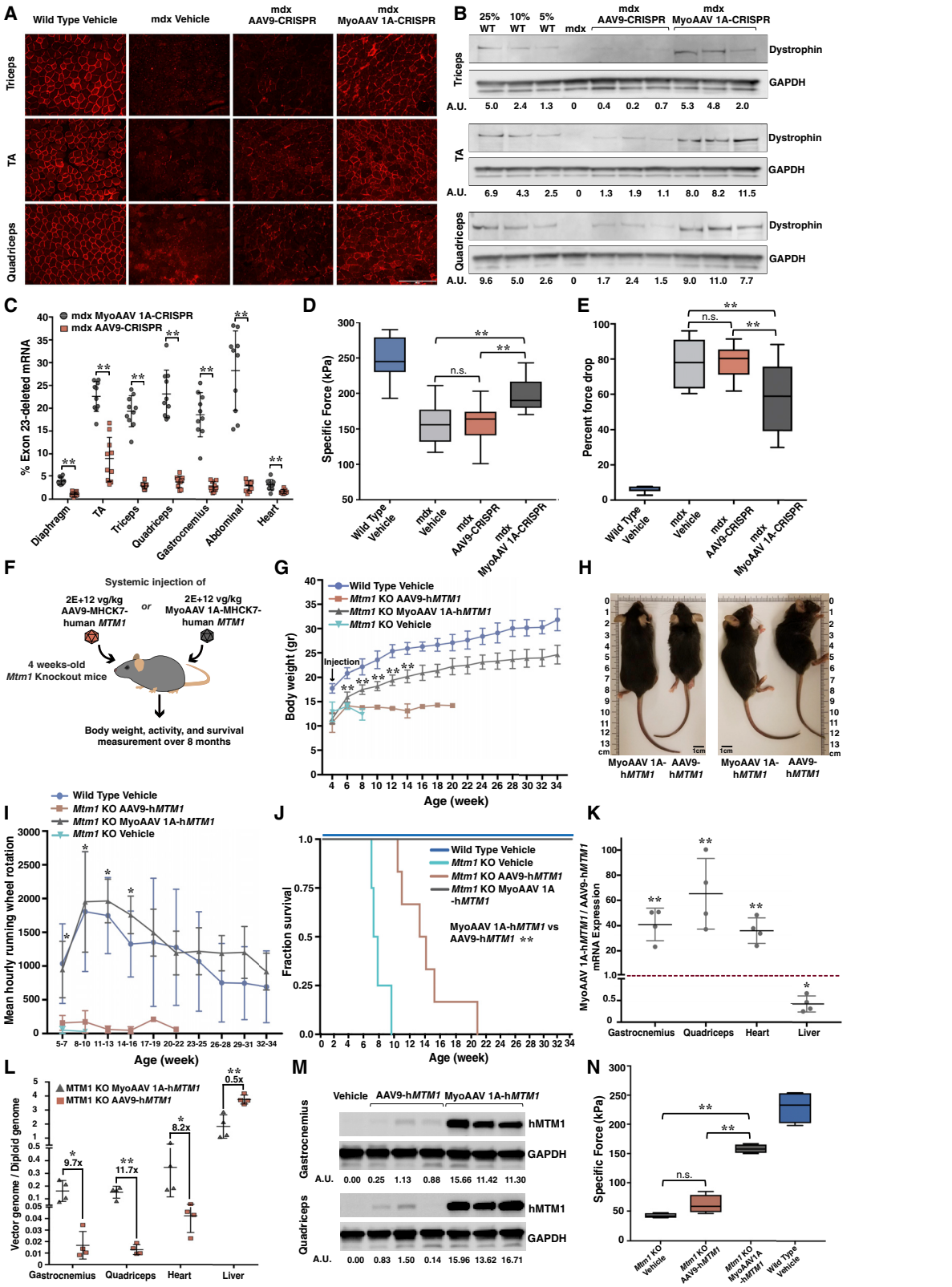

(legend on next page)

We next analyzed MyoAAV 1A's efficiency in transducing human skeletal muscle. Human primary myotubes from four different donors (two males and two females) were transduced *in vitro* with AAV9- or MyoAAV 1A-CK8-nanoluciferase (Nluc). MyoAAV 1A transduced myotubes from different donors with 35 to 52 times greater efficiency than AAV9 (Figure 2D). MyoAAV 1A also transduced mouse primary myotubes from C57BL/6J mice with 23 times higher efficiency compared to AAV9 (Figure 2D).

Additionally, we evaluated the efficiency of muscle stem cell (satellite cell) transduction by MyoAAV 1A after intravenous administration in 6-month-old mdx-Ai9 mice. Dystrophin-deficient mdx mice are a genetic model for human DMD (carrying a nonsense mutation in *Dmd* exon 23). Mdx-Ai9 mice additionally carry a Cre-activatable tdTomato transgene, which serves as a reporter for transduction by Cre-encoding AAVs. Fluorescence-activated cell sorting (FACS) of satellite cells from the muscle of mice injected with AAV8-, AAV9-, or MyoAAV 1A-CMV-Cre showed MyoAAV 1A transduces satellite cells with 2.6 and 3.2 times higher efficiency compared to AAV9 and AAV8, respectively (Figures S2G–S2K).

To investigate the kinetics of *in vivo* gene expression after systemic delivery of MyoAAV 1A, we injected adult BALB/cJ mice with 4E+11 vg (~1.6E+13 vg/kg) AAV8-, AAV9-, or MyoAAV 1A-CMV-Firefly luciferase (Fluc) and performed whole-body bioluminescence imaging at different time points over 120 days following injection. Mice receiving MyoAAV 1A showed faster kinetics and significantly higher overall levels of transgene expression in their limbs and throughout their bodies compared to mice injected with AAV8 or AAV9 (Figures 2E and 2F). Whole-organ bioluminescence imaging from muscles of mice harvested 4 months after injection confirmed dramatically higher luciferase expression in the muscles of MyoAAV 1A injected animals (Figures S3M–S3O).

Systemic administration of therapeutic transgenes using MyoAAV 1A leads to functional improvement in mouse models of DMD and X-linked myotubular myopathy

To investigate the feasibility of using MyoAAV 1A for *in vivo* delivery of therapeutic transgenes, we injected adult mdx mice with AAV9 or MyoAAV 1A carrying constructs encoding SaCas9, together with guide RNAs (gRNAs) targeting 5′ and 3′ of the mdx mutation (Figures S4A and S4B). We and others have previously shown that this CRISPR-Cas9-mediated approach results in excision of exon 23 from the genome of mdx cells and expression of a truncated but still in-frame and functional version of dystrophin protein that provides therapeutic benefit in dystrophic muscle (Nelson et al., 2016; Tabebordbar et al., 2016).

MyoAAV 1A-*Dmd* CRISPR administration produced exon 23-deleted *Dmd* mRNA with efficiencies ranging from 3.4% to 25% of total *Dmd* mRNA in different mdx muscles. In contrast, the

Figure 3. Systemic administration of MyoAAV 1A-*Dmd* CRISPR and MyoAAV 1A-human *MTM1* results in therapeutic benefit in mouse models of DMD and XLMTM, respectively

(A) Representative immunofluorescence images for dystrophin (red) in muscles from 8-week-old mdx mice injected with AAV9- or MyoAAV 1A-*Dmd* CRISPR (4.5E+12 vg of AAV-SaCas9 and 9E+12 vg of AAV-gRNA). Scale bar: 400 μm.

(B) Western blots detecting dystrophin and GAPDH in muscles of 8-week-old mdx mice injected with AAV9- or MyoAAV 1A-*Dmd* CRISPR, with relative signal intensity determined by densitometry at the bottom. A.U.: arbitrary unit, normalized to GAPDH.

(C) Taqman-based quantification of exon 23-deleted mRNA in different muscles of 8-week-old mdx mice injected with AAV9- or MyoAAV 1A- *Dmd* CRISPR. Data are presented as mean ± SD (n = 9-10); **p < 0.01 (Student's t test).

(D and E) Tibialis anterior muscle specific force (D) and decrease in isometric force after five eccentric contractions (E) for WT C57BL/6J mice injected with vehicle (n = 11) and mdx mice injected with vehicle (n = 15), AAV9-*Dmd* CRISPR (n = 15), or MyoAAV 1A-*Dmd* CRISPR (n = 17). **p < 0.01 (one-way ANOVA with Tukey-Kramer MCT).

(F) Schematic of the experiment to investigate the efficacy of 2E+12 vg/kg of AAV9- or MyoAAV 1A-MHCK7-human *MTM1* (h*MTM1*) systemically delivered to 4-week-old *Mtm1* knockout (KO) mice.

(G) Total body weight of *Mtm1* KO mice injected with vehicle or 2E+12 vg/kg of AAV9- or MyoAAV 1A-MHCK7-h*MTM1*, and WT littermate controls injected with vehicle. Data are presented as mean ± SD (n = 6 for KO AAV9, n = 6 for KO MyoAAV 1A, n = 3 for WT vehicle, n = 4 for KO vehicle). p value calculated between MyoAAV 1A and AAV9 groups; **p < 0.01 (multiple t tests with Holm-Sidak MCT).

(H) Pictures of *Mtm1* KO mice injected with 2E+12 vg/kg of either MyoAAV 1A-h*MTM1* or AAV9-h*MTM1* 16 weeks after injection of the virus.

(I) Mean hourly passive activity assessed by in-cage running wheel rotation from WT mice injected with vehicle, or *Mtm1* KO mice injected with vehicle, AAV9-h*MTM1*, or MyoAAV 1A-h*MTM1,* both at 2E+12 vg/kg. Data are presented as mean ± SD (n = 6 for KO AAV9, n = 6 for KO MyoAAV 1A, n = 3 for WT vehicle, n = 3 for KO vehicle) for weekly measurements averaged across three-week time periods. p value calculated between MyoAAV 1A and AAV9 groups; **: p < 0.01 (Multiple t tests with Holm-Sidak MCT).

J) Survival curve for *Mtm1* KO animals injected with vehicle, 2E+12 vg/kg AAV9-h*MTM1*, or MyoAAV 1A-h*MTM1*, as well as WT littermates injected with vehicle. (n = 6 for KO AAV9, n = 6 for KO MyoAAV 1A, n = 3 for WT vehicle, n = 4 for KO vehicle). Data points for the *Mtm1* KO mice injected with vehicle are from a previous experiment. p value calculated between MyoAAV 1A and AAV9 groups; **p < 0.01 (Mantel-Cox test).

(K) Quantification of fold difference in hMTM1 mRNA expression in gastrocnemius, quadriceps, heart, and liver of *Mtm1* KO mice injected with 2E+12 vg/kg AAV9- or MyoAAV 1A-h*MTM1* at 4 weeks of age and analyzed 4 weeks after injection. Dashed red line indicates relative expression from AAV9-h*MTM1*. Data are presented as mean ± SD (n = 4); *p < 0.05, **p < 0.01 (Student's t test between AAV9- and MyoAAV 1A-injected groups for each tissue).

(L) Quantification of vector genome per diploid genome in various tissues of *Mtm1* KO mice injected with 2E+12 vg/kg AAV9- or MyoAAV 1A-h*MTM1* at 4 weeks of age and analyzed 4 weeks after injection. Data are presented as mean ± SD (n = 4). *p < 0.05, **p < 0.01 (Student's t test).

(M) Western blots detecting hMTM1 and GAPDH in muscles of *Mtm1* KO mice injected with vehicle or 2E+12 vg/kg AAV9- or MyoAAV 1A-h*MTM1* at 4 weeks of age and analyzed 4 weeks after injection, with relative signal intensity determined by densitometry at the bottom. A.U.: arbitrary unit, normalized to GAPDH.

(N) Extensor digitorum longus (EDL) muscle specific force for WT C57BL/6J mice injected with vehicle (n = 4), and *Mtm1* KO mice injected with vehicle (n = 4), 2E+12 vg/kg AAV9-h*MTM1* (n = 4), or MyoAAV 1A-h*MTM1* (n = 4) at 4 weeks of age and analyzed 4 weeks after injection. **p < 0.01 (one-way ANOVA with Tukey-Kramer MCT).

See also Figure S4.

efficiency of production of exon 23-deleted mRNA in muscles of mdx mice injected with the same dose of AAV9-*Dmd* CRISPR ranged from only 1.3% to 8.7% (Figure 3C). Quantification of SaCas9 and gRNA expression indicated 6.7 to 19 times higher SaCas9 expression and 3.5 to 7.8 times higher gRNA expression in the muscles of MyoAAV 1A-injected mice compared to AAV9 injected animals (Figures S4D and S4E).

Several findings point to the superior rescue of dystrophin expression with MyoAAV 1A-*Dmd* CRISPR compared to AAV9-*Dmd* CRISPR. Immunofluorescence and western blot analysis confirmed greater and more widespread dystrophin restoration in muscles of mice injected with MyoAAV 1A-*Dmd* CRISPR as compared to AAV9-*Dmd* CRISPR (Figures 3A, 3B and S4C), with protein levels generally correlating with the level of exon 23-deleted *Dmd* mRNA detected in each muscle. Physiological assessment of the TA muscles of AAV-CRISPR-treated animals demonstrated significantly higher specific force (Figure 3D) and decreased percent force drop after eccentric contraction (Figure 3E) in MyoAAV 1A-*Dmd* CRISPR-injected mdx mice when compared to either vehicle or AAV9-*Dmd* CRISPR-injected controls. Thus, MyoAAV 1A exhibits markedly enhanced potency for delivery of therapeutic gene editing complexes to muscle compared to conventional and widely utilized AAV9.

We further assessed MyoAAV 1A's performance for gene replacement after low-dose systemic administration in a mouse model of X-linked myotubular myopathy (XLMTM). *Mtm1* knockout (KO) mice provide an excellent genetic and phenotypic model of XLMTM; they show marked muscle wasting, loss of mobility, and dramatically shortened lifespans. We injected 4-week-old *Mtm1* KO mice with 2E+12 vg/kg of AAV9 or MyoAAV 1A encoding the human *MTM1* (h*MTM1*) expressed under the control of the MHCK7 promoter (Figure S4F). We measured body weight, activity, and survival for each group over an 8-month period (Figure 3F). The dose of virus that we used in this experiment was 50–150 times lower than the dose being used in an ongoing human clinical trial for XLMTM (clinicaltrials.gov identifier: NCT03199469) and 15–250 times lower than the doses used in previously published preclinical studies for XLMTM gene therapy (Childers et al., 2014; Elverman et al., 2017; Mack et al., 2017). MyoAAV 1A-MHCK7-h*MTM1*-injected mice manifested striking improvements in muscle function and survival. All mice injected with 2E+12 vg/kg of AAV9-MHCK7-h*MTM1* were minimally active and reached the humane endpoint for euthanasia between 11–21 weeks after the injection. In contrast, all mice injected with the same dose of MyoAAV 1A-MHCK7-h*MTM1* survived with a similar trajectory to wild-type (WT) mice and also gained weight and were noticeably more active compared to the AAV9-injected mice throughout the study (Figures 3G–3J and S4G).

We quantified vector genome biodistribution, transgene mRNA and protein expression, and muscle-specific force in the tissues of *Mtm1* KO mice injected with 2E+12 vg/kg AAV9- or MyoAAV 1A-MHCK7-h*MTM1* 4 weeks after AAV administration. Quantification of h*MTM1* mRNA expression and vector genome biodistribution in the gastrocnemius, quadriceps, heart, and liver of the injected mice showed significantly higher transgene expression and vg/dg in the muscles of the MyoAAV 1A-MHCK7-h*MTM1*-injected mice compared to the AAV9-MHCK7-h*MTM1* injected animals, while the converse was observed in the liver (Figures 3K and 3L). Western blot analysis confirmed higher h*MTM1* protein expression in the gastrocnemius and quadriceps of mice injected with MyoAAV 1A-MHCK7-h*MTM1* (Figure 3M) and physiological analysis of the extensor digitorum longus (EDL) muscle demonstrated significantly higher specific force in MyoAAV 1A-MHCK7-h*MTM1* injected mice when compared to either vehicle or AAV9-MHCK7-h*MTM1* injected controls (Figure 3N).

MyoAAV 1A is dependent on integrin heterodimers for transducing mouse and human primary myotubes

Given the presence of an RGD motif in MyoAAV 1A and all of the other top variants from our selection, we assessed the role of RGD-binding integrin heterodimers in MyoAAV 1A transduction. The RGD motif was first recognized in 1984 as the minimal sequence in fibronectin that facilitates binding to its receptor, later identified as the integrin heterodimer α5β1 (Pierschbacher and Ruoslahti, 1984; Pytela et al., 1985). RGD has since been identified as a recognition motif for several different integrin heterodimers: specifically, αIIbβ3, α5β1, α8β1, αVβ1, αVβ3, αVβ5, αVβ6, and αVβ8 (Ruoslahti, 1996).

We compared transduction efficiency of MyoAAV 1A-CMV-Nluc in HEK293 cells transfected with plasmids encoding for each of these eight human RGD-binding integrin heterodimers or the pUC19 plasmid as a control. Overexpression of α8β1, αVβ1, αVβ3, αVβ6, or αVβ8 increased the transduction efficiency of MyoAAV 1A in the transfected HEK293 cells compared to pUC19-transfected controls (Figures 4A and S5A–S5K). We next analyzed the effect of different integrin heterodimers on the binding efficiency of MyoAAV 1A to the cell surface through overexpression experiments. We quantified the vector genomes bound to the surface of HEK293 cells transfected with each of the eight RGD-binding integrin heterodimers or a pUC19 control plasmid and found that αVβ6, and to a lesser extent α8β1 and αVβ1, increased binding of MyoAAV 1A to integrin-transfected cells compared to pUC19-transfected controls (Figure 4B).

We also investigated the impact of two different pan-αV integrin antagonists (CWHM-12 and GLPG-0187) on MyoAAV 1A transduction efficiency in primary cells. Both inhibitors impeded MyoAAV 1A transduction in a dose-dependent manner in both mouse (Figures S6A and S6B) and human (Figures 4C, 4D, and S6C–S6H) primary skeletal muscle myotubes, while neither inhibitor had a dose-dependent effect on AAV9 transduction efficiency. These results demonstrate that inhibiting αV-containing integrin heterodimers almost completely eliminates the ability of MyoAAV 1A to transduce both mouse and human primary myotubes.

To further elucidate the impact of individual αV-containing integrin heterodimers on MyoAAV 1A's binding affinity, we transduced human primary myotubes with MyoAAV 1A or AAV9 after pre-incubation of these viruses with αVβ1, αVβ3, αVβ6, αVβ8 recombinant soluble integrin heterodimers, or maltose-binding protein (MBP) as a control. Remarkably, pre-incubation of MyoAAV 1A with increasing concentrations of αVβ6 resulted in a dose-dependent inhibition of transduction of human primary myotubes, while none of the other recombinant proteins that we tested had a dose-dependent effect on transduction of the cells by either MyoAAV 1A or AAV9 (Figures 4E and 4F).

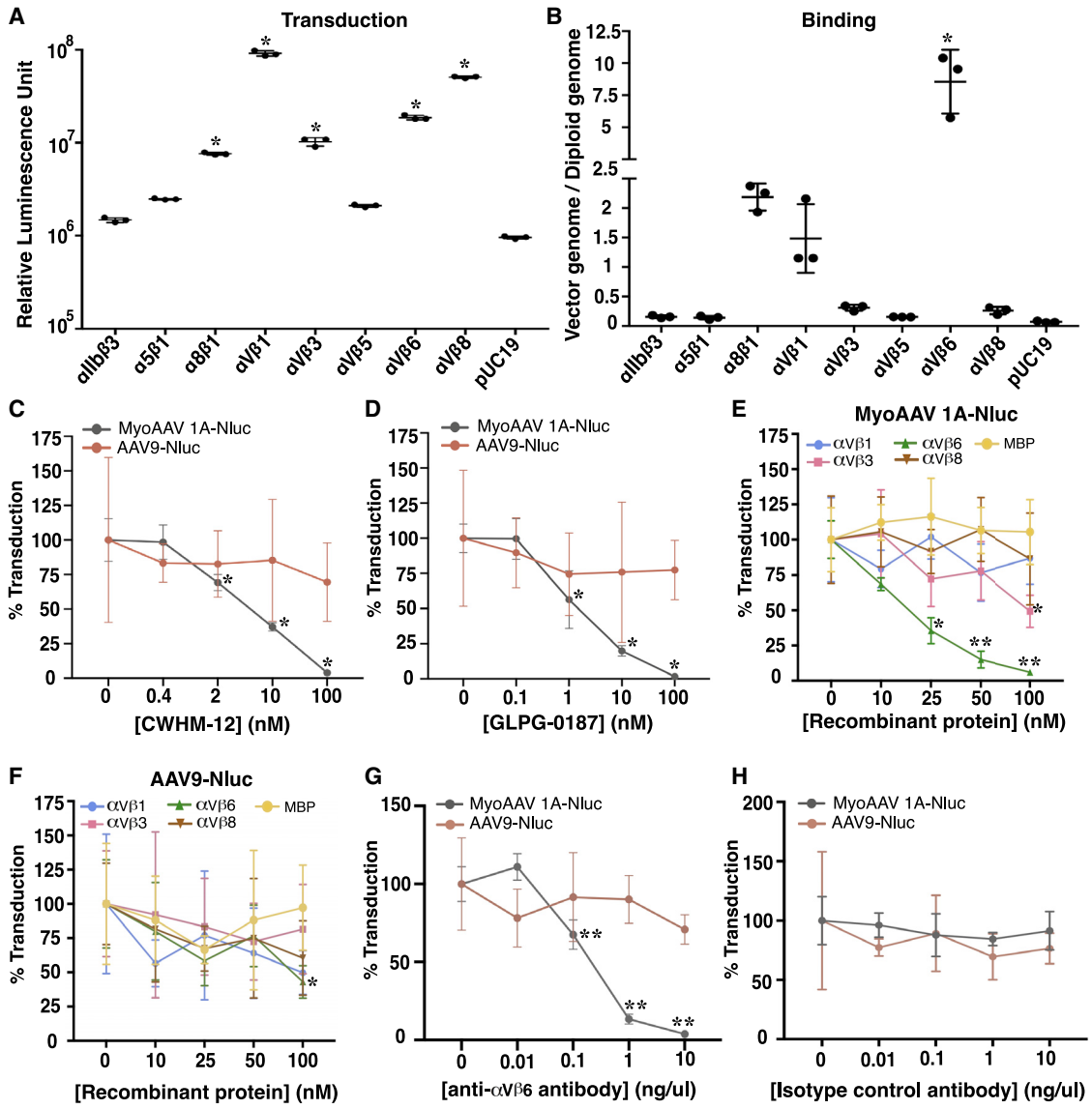

Figure 4. MyoAAV 1A transduction is dependent on integrin heterodimers

(A and B) Quantification of *in vitro* transduction (A) and viruses bound to cell surface (B) in HEK293 cells transfected with plasmids encoding for RGD-binding integrin heterodimers or with pUC19 and transduced with MyoAAV 1A-CMV-Nluc. Data are presented as mean ± SD (n = 3); *p < 0.01 (one-way ANOVA with Dunnett's MCT with the pUC19 transfected cells set as the control).

(C and D) *In vitro* transduction efficiency in human primary myotubes treated with different concentrations of CWHM-12 (C) or GLPG-0187 (D) pan-integrin αV antagonists and transduced with AAV9- or MyoAAV 1A-CK8-Nluc. Data are presented as mean ± SD (n = 5). p value calculated compared to the 0 nM small molecule condition in each group. *p < 0.01 (one-way ANOVA with Dunnett's MCT).

(E and F) *In vitro* transduction efficiency in human primary myotubes transduced with MyoAAV 1A-CK8-Nluc (E) or AAV9-CK8-Nluc (F) incubated with different concentrations of αVb1, αVb3, αVb6, αVb8, or MBP recombinant proteins. Data are presented as mean ± SD (n = 5). *p < 0.01, **p < 0.001 (one-way ANOVA with Dunnett's MCT with the 0 nM recombinant protein set as the control for each group).

(G and H) *In vitro* transduction efficiency in human primary myotubes treated with different concentrations of anti-αVb6 (G) or isotype control (H) antibody and transduced with AAV9- or MyoAAV 1A-CK8-Nluc. Data are presented as mean ± SD (n = 5). p value calculated compared to the 0 ng/ul antibody condition in each group; *p < 0.01, **p < 0.001 (one-way ANOVA with Dunnett's MCT).

See also Figures S5 and S6.

Furthermore, pre-incubation of human myotubes with increasing concentrations of anti-αVβ6 antibody decreased transduction efficiency by MyoAAV 1A in a dose-dependent manner and did not affect transduction of myotubes by AAV9 (Figures 4G and 4H). These data suggest that among the αV-containing integrin heterodimers that have the capability to facilitate MyoAAV 1A transduction, αVβ6 has the highest affinity to bind to this capsid variant. Additionally, αVβ6 must be available on the surfaces of

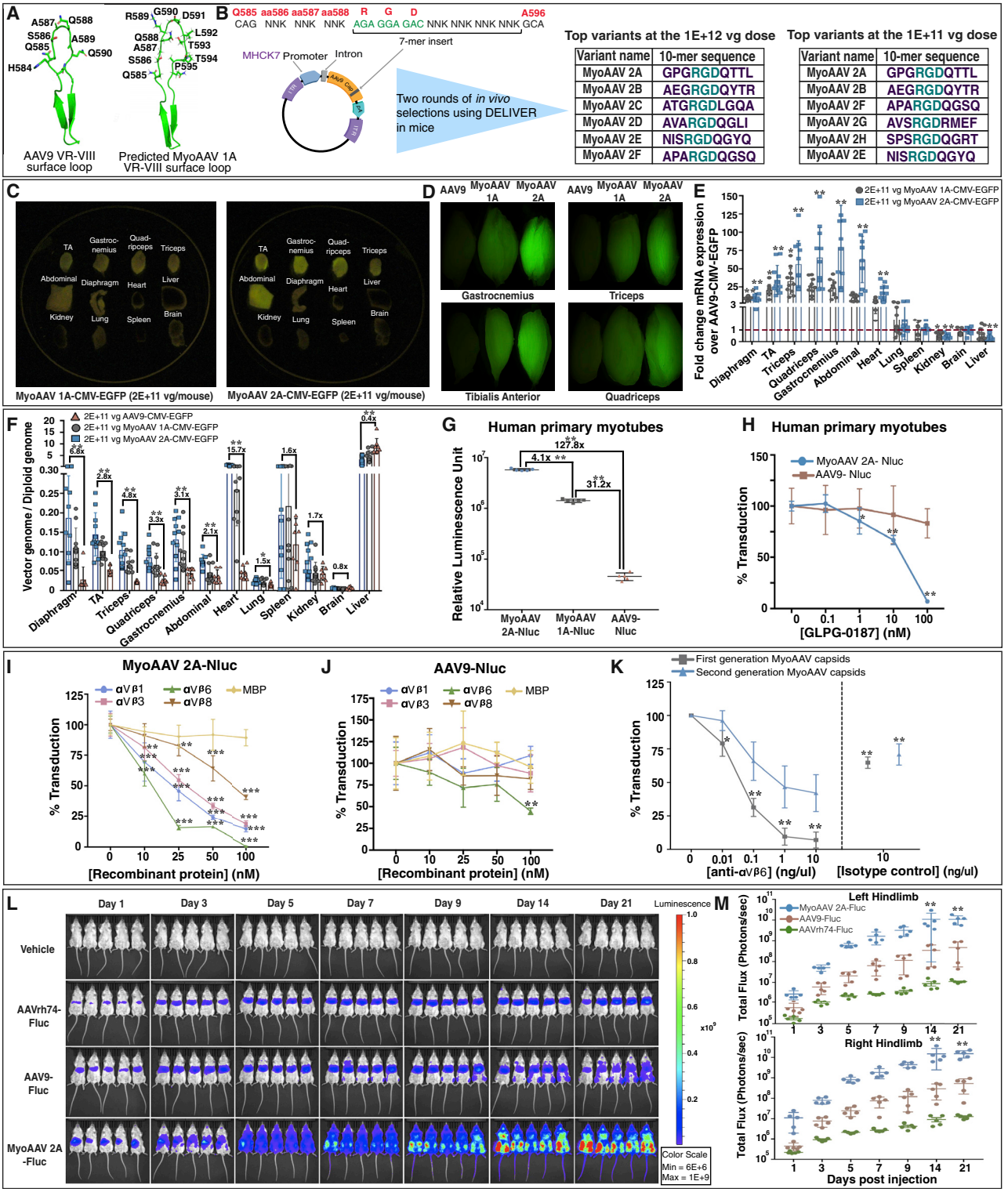

Figure 5. Further evolution of MyoAAV 1A using DELIVER generates more enhanced muscle-tropic capsid variants

(A) Structure of the AAV9 VR-VIII surface loop and the predicted structure of the MyoAAV 1A VR-VIII surface loop with the amino acids annotated.

(B) Schematic of virus library design and sequence of the top hits identified from mouse muscles after injection of the second-round virus library at two different doses.

(legend continued on next page)

human muscle cells to enable their optimal transduction by MyoAAV 1A.

Given the importance of glycans with terminal sialic acid on transduction and binding of AAV9 to cells (Bell et al., 2011), we assessed the role of glycan moieties on MyoAAV 1A transduction and binding. Treatment of HEK293 cells with neuraminidase (NA), which cleaves the sialic acid linkages to glycans on the cell surface, resulted in 172 times higher transduction and 4 times more effective binding by MyoAAV 1A to the treated cells compared to untreated controls (Figures S6I and S6J). We further tested if the terminal galactose is important in transduction and binding of MyoAAV 1A. Addition of *Erythrina cristagalli* lectin (ECL), which binds to terminal β-1,4 galactose on the cell surface, to NA-treated HEK293 cells significantly inhibited binding and transduction by both AAV9 and MyoAAV 1A, while it had no effect on AAV2 binding and transduction (Figures S6K and S6L). These results demonstrated that, similar to AAV9, MyoAAV 1A transduction and binding to cells is enhanced by removal of sialic acid and exposure of β-1,4 galactose on the cell surface.

We next evaluated the dependency of MyoAAV 1A transduction on the previously identified AAV receptor (AAVR), a rapidly endocytosed plasma membrane protein required for effective transduction of most known AAV serotypes except AAV4 and AAVrh32.33 (Dudek et al., 2018; Pillay et al., 2016). We transduced HEK293FT AAVR knockout (KO) and the parental HEK293FT WT cells with AAV4-, AAV2-, AAV9-, or MyoAAV 1A-CMV-Nluc and found that, similar to AAV2 and AAV9, MyoAAV 1A transduction requires AAVR expression (Figure S6M).

Finally, to investigate if integrin heterodimers and AAVR play redundant roles in MyoAAV 1A transduction, we overexpressed α8β1, αVβ1, αVβ3, αVβ6, or αVβ8 in the HEK293FT AAVR KO cells in the presence or absence of AAVR overexpression and then transduced the cells with MyoAAV 1A-CMV-Nluc. Our results demonstrated that, while overexpression of integrin heterodimers increased MyoAAV 1A transduction efficiency in AAVR KO cells compared to mock transfected controls, integrin overexpression was not sufficient to rescue transduction to levels observed in AAVR KO cells overexpressing AAVR or in WT HEK293FT cells (Figure S6N). These data suggest that integrin heterodimers and AAVR play distinct roles in and are likely utilized at different stages of MyoAAV 1A transduction.

Further rounds of *in vivo* evolution using DELIVER generates second-generation RGD-containing muscle-tropic variants in mice

Given the importance of interaction of the RGD motif with integrin heterodimers for transduction of myotubes by MyoAAV 1A, we hypothesized that modifying amino acids adjacent to this motif could generate even more potent muscle-tropic capsid variants by improving this interaction. Based on a predicted structure for the MyoAAV 1A hypervariable region VIII surface loop, we identified amino acids in positions 586, 587, and 588 upstream and positions 592, 593, 594, and 595 downstream of the RGD motif as likely to be located in the surface loop of MyoAAV 1A (Figure 5A). We then generated a diverse library of capsids, each with the RGD motif fixed at positions 589, 590, and 591 and varying amino acids in the above-mentioned flanking positions (Figure 5B).

With the aim of identifying potent second-generation muscle-tropic variants, we performed two rounds of *in vivo* selection with our RGD-fixed virus library using DELIVER in C57BL/6J and mdx mice. We injected the second-round library at two different

(C) Different tissues of 8-week-old C57BL/6J mice systemically injected with 2E+11 vg (~8E+12 vg/kg) of MyoAAV 1A-CMV-EGFP (left) or MyoAAV 2A-CMV-EGFP (right) illuminated by blue light.

(D) Whole-mount fluorescent images of gastrocnemius, triceps, tibialis anterior, and quadriceps of 8-week-old C57BL/6J mice systemically injected with 2E+11 vg of AAV9-, MyoAAV 1A-, or MyoAAV 2A-CMV-EGFP.

(E) Quantification of fold difference in EGFP mRNA expression in various tissues of 8-week-old C57BL/6J mice systemically injected with 2E+11 vg of MyoAAV 1A- or MyoAAV 2A-CMV-EGFP compared to mice injected with the same dose of AAV9-CMV-EGFP. Dashed red line indicates relative expression from AAV9-CMV-EGFP. Data are presented as mean ± SD (n = 11 for MyoAAV 1A and MyoAAV 2A, n = 8 for AAV9). p value calculated compared to the AAV9 group. *p < 0.05, **p < 0.01 (one-way ANOVA with Dunnett's MCT).

(F) Quantification of vector genome per diploid genome in various tissues of 8-week-old C57BL/6J mice injected with 2E+11 vg of AAV9-, MyoAAV 1A-, or MyoAAV 2A-CMV-EGFP. Data are presented as mean ± SD (n = 11 for MyoAAV 1A and MyoAAV 2A, n = 8 for AAV9). p value calculated between MyoAAV 2A and AAV9 groups; *p < 0.05, **p < 0.01 (Student's t test).

(G) Quantification of *in vitro* transduction in human primary myotubes transduced with AAV9-, MyoAAV 1A-, or MyoAAV 2A-CK8-Nluc. Data are presented as mean ± SD (n = 5). *p < 0.01 (one-way ANOVA with Tukey-Kramer MCT).

(H) *In vitro* transduction efficiency in human primary myotubes treated with different concentrations of GLPG-0187 integrin αV antagonists and transduced with AAV9- or MyoAAV 2A-CK8-Nluc. Data are presented as mean ± SD (n = 5). p value calculated compared to the 0 nM small molecule condition in each group. *p < 0.05, **p < 0.01 (one-way ANOVA with Dunnett's MCT).

(I and J) *In vitro* transduction efficiency in human primary myotubes transduced with MyoAAV 2A-CK8-Nluc (I) or AAV9-CK8-Nluc (J) incubated with different concentrations of αVβ1, αVβ3, αVβ6, αVβ8, or MBP recombinant proteins. Data are presented as mean ± SD (n = 5). **p < 0.01, ***p < 0.001 (one-way ANOVA with Dunnett's MCT with the 0 nM recombinant protein condition in each group as the control).

(K) *In vitro* transduction efficiency in human primary myotubes treated with different concentrations of anti-αVb6 antibody (left) or 10 ng/ul isotype control antibody (right) and transduced with AAV9- or first or second-generation RGD-containing capsid variants encoding for Nluc under the control of CK8 promoter. Data are presented as mean ± SD (n = 5). p value for the anti-αVb6 antibody data calculated between the first-generation and second-generation groups. *p < 0.05, **p < 0.01 (two-way ANOVA with Sidak's MCT). p value for the isotype control data calculated between the isotype control and 10 ng/ul anti-αVb6 antibody condition for each group; **p < 0.01 (Student's t test).

(L) Whole-body *in vivo* bioluminescence images of 8-week-old BALB/cJ mice systemically injected with 2E+11 vg (~8E+12 vg/kg) of AAVrh74-, AAV9-, or MyoAAV 2A-CMV-Fluc, taken over 21 days. Color scale: 6E+6 - 1E+9.

(M) Quantification of total luminescence from hindlimbs of animals injected with AAVrh74-, AAV9-, or MyoAAV 2A-CMV-Fluc, assessed over 21 days. p value calculated between AAVrh74, AAV9, and MyoAAV 2A groups by two-way ANOVA with Tukey-Kramer MCT; **p < 0.01 for both MyoAAV 2A versus AAVrh74 and MyoAAV 2A versus AAV9. Difference between AAVrh74 and AAV9 groups is not statistically significant at any of the time points.

doses (1E+12 vg and 1E+11 vg per mouse) to identify variants that effectively transduce muscle tissue both at high and low dose (Figure 5B). Among our top hits from these selections, glycine and alanine were enriched at position 588, and glutamine was enriched at position 592. A variant containing the GPGRGDQTTL sequence emerged as the most highly selected muscle-tropic capsid at both the 1E+12 and 1E+11 dose from the second round of selection (Figure 5B; Table S5). We named this second-generation variant MyoAAV 2A and used it for further characterization.

We investigated transduction efficiency of MyoAAV 2A in different mouse tissues after systemic delivery of a low dose of the virus. We injected C57BL/6J mice with 2E+11 vg (~8E+12 vg/kg) of AAV9-, MyoAAV 1A-, or MyoAAV 2A-CMV-EGFP and analyzed transgene expression and vector genome biodistribution in various tissues. Whole-tissue fluorescent imaging demonstrated that systemic gene delivery by MyoAAV 2A results in higher levels of transgene expression compared to MyoAAV 1A or AAV9 across different skeletal muscles (Figures 5C and 5D). Quantification of EGFP mRNA revealed that MyoAAV 2A transduces mouse skeletal muscles 10–80 times more efficiently and transduces the heart 17 times more efficiently than AAV9. Furthermore, transgene mRNA expression was 2.5 times lower in the liver of MyoAAV 2A-injected animals compared to AAV9-injected mice (Figure 5E). Similarly, vector genome biodistribution analysis showed that MyoAAV 2A-injected mice had significantly higher vg/dg in skeletal muscle and heart and significantly lower vg/dg in the liver compared to AAV9-injected animals (Figure 5F).

We next analyzed the efficiency and integrin dependency of MyoAAV 2A for transducing human primary myotubes. Remarkably, MyoAAV 2A transduced human primary myotubes 128 times more efficiently compared to AAV9 and 4.1 times higher than MyoAAV 1A (Figure 5G). Increasing concentrations of pan-αV integrin antagonist GLPG-0187 resulted in a dose-dependent decrease in the transduction efficiency of MyoAAV 2A (Figure 5H), confirming that MyoAAV 2A infectivity remains dependent on αV-containing integrin heterodimers expressed on target cells.

To evaluate the binding affinity of MyoAAV 2A for different individual αV integrin heterodimers, we pre-incubated MyoAAV 2A or AAV9 with αVβ1, αVβ3, αVβ6, αVβ8 recombinant proteins, or MBP as a control, before transducing human primary myotubes. Interestingly, and in contrast to results obtained in these same assays with MyoAAV 1A (Figure 4E), all four αV-containing integrin heterodimers tested inhibited transduction of human myotubes by MyoAAV 2A in a dose-dependent manner (Figure 5I), while there was no dose-dependent effect on AAV9 transduction (Figure 5J). This result suggests that amino acid substitutions included in MyoAAV 2A enable higher affinity binding to a broader class of αV integrin heterodimers when compared to MyoAAV 1A, which depends mainly on αVβ6.

We further examined the dependency of the top first-generation and second-generation capsid variants that we evolved using DELIVER in mice on αVβ6 heterodimer. We pre-incubated human primary myotubes with anti-αVβ6 antibody before transducing the cells with the top first-generation (MyoAAV 1A, MyoAAV 1B, MyoAAV 1C, MyoAAV 1E, MyoAAV 1F, see Figure 1F) and second-generation (MyoAAV 2A, MyoAAV 2B, MyoAAV 2C, MyoAAV 2D, MyoAAV 2E, MyoAAV 2F, see Figure 5B) mouse variants. While antibody binding inhibited transduction of human myotubes to some degree by all of these variants, the first-generation capsids were significantly more dependent on αVβ6 for myotube transduction (Figure 5K).

MyoAAV 2A shows great therapeutic potential after injection of a low dose of virus

In order to assess the potential future therapeutic relevance of MyoAAV 2A in comparison with capsids currently in clinical testing for human neuromuscular disease, we compared the transduction efficiency of MyoAAV 2A to both AAV9 and AAVrh74, which are being investigated in ongoing clinical trials for DMD (clinicaltrials.gov identifiers: NCT03362502, NCT03368742, and NCT03769116). Systemic administration of a function-complementing dystrophin mini-gene (termed micro-dystrophin), expressed from the muscle-specific MHCK7 promoter and delivered using the AAVrh74 vector, showed promising results in a recently reported clinical trial involving four DMD patients. In this trial, administering a high viral dose of 2E+14 vg/kg resulted in transgene expression in muscle and functional improvement in disease phenotype (Mendell et al., 2020).

We compared MyoAAV 2A-mediated gene delivery to that of both AAVrh74 and AAV9 vectors and further investigated performance in a DBA/2J-mdx mouse model of DMD. In a longitudinal *in vivo* imaging experiment, we injected adult BABL/cJ mice with a low dose (2E+11 vg, representing ~8E+12 vg/kg) of AAVrh74, AAV9, or MyoAAV 2A encoding the CMV-Fluc reporter gene. MyoAAV 2A-injected mice demonstrated dramatically higher bioluminescence signal in the limbs and throughout the body as compared to mice receiving AAVrh74 or AAV9 (Figures 5L and 5M). We also tested systemic delivery of MyoAAV 2A or AAV9 carrying a microdystrophin transgene (CK8-microdystrophin-FLAG) into the DBA/2J-mdx mouse model of DMD using an equivalent, low dose (2E+13 vg/kg) of each AAV.

MyoAAV 2A-injected animals demonstrated greater and more widespread expression of microdystrophin, localized at the sarcolemma, in multiple muscle groups as compared to AAV9-injected animals (Figure 6A). Western blot confirmed higher levels of microdystrophin protein in muscles of mice injected with MyoAAV 2A compared to AAV9 injected animals (Figure 6B). Quantitative RT-PCR indicated 7.6–15 times higher levels of microdystrophin mRNA in skeletal muscles of mice injected with MyoAAV 2A-CK8-microdystrophin-FLAG as compared to AAV9-CK8-microdystrophin-FLAG (Figure 6C).

Lastly, we assessed the abundance of vector genomes and muscle function in the MyoAAV 2A-injected mice as compared to AAV9-injected animals. MyoAAV 2A delivered 12–46 times higher numbers of vg/dg in skeletal muscles of DBA/2J-mdx mice and 2.5 times lower vg/dg in the liver, as compared to AAV9 (Figure 6D). Strikingly, while AAV9-injected animals had more than 40 times higher numbers of vg/dg in their liver compared to their muscles, the MyoAAV 2A-injected mice had similar levels in their liver and muscles. Quantification of muscle-specific force and percent force drop after eccentric damage demonstrated that TA muscles of MyoAAV 2A-injected DBA/2J-

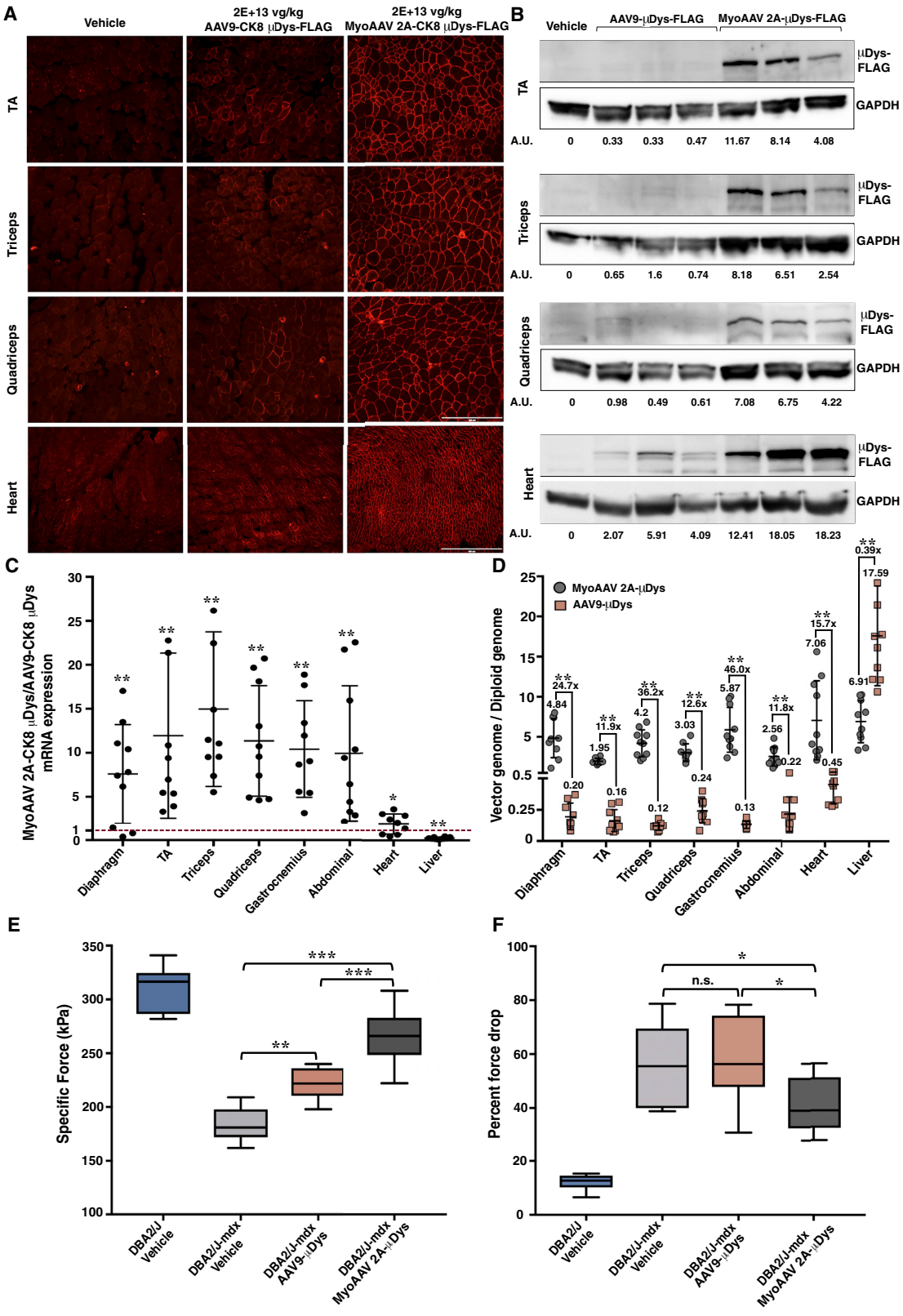

(legend on next page)

mdx mice recovered significantly greater specific force and were more protected from damage compared to muscles from mice receiving equal doses of AAV9 and to vehicle-injected animals (Figures 6E and 6F).

In vivo directed evolution identifies MyoAAV class of capsid variants as the top hits in cynomolgus macaques

Having demonstrated DELIVER's power to discover a class of muscle-tropic AAV variants with tissue-selective patterns of *in vivo* transduction and remarkably high potency in mice, we sought to determine whether this platform might prove equally effective for discovering potent muscle-directed capsid variants when applied directly in NHPs. We performed *in vivo* directed evolution of AAV9 using DELIVER in cynomolgus macaques. Two rounds of *in vivo* selections starting from a random 7-mer peptide insertion at the 588 site identified six variants containing the RGD motif as the top hits (Figure 7A; Table S6). These results provide evidence for high muscle tropism of the MyoAAV class of capsids in primates after systemic administration. To select for a further evolved MyoAAV class of variants that would enable potent muscle transduction across species, we also performed a round of *in vivo* selection in NHPs using the top 120,000 variants identified from the first round of our RGD-fixed selection in mice (Figure 7B; Table S7). Interestingly, the top hits from the RGD-fixed selection in macaques contained different amino acids surrounding the RGD motif compared to the top hits identified from the RGD-fixed selection in mice (Figures 5B and 7B; Tables S5 and S7).

We next benchmarked the transduction efficiency in both mice and NHPs of the 11 most highly muscle-tropic variants that we identified in NHPs (MyoAAV 3A-F and MyoAAV 4A-E, see Figures 7A and 7B) and 4 muscle-tropic variants identified in mice that transduced human primary myotubes with particularly high efficiency (MyoAAV 1C, MyoAAV 1E, MyoAAV 2A, and MyoAAV 2E, see Figures 5B and 7C) against AAVrh74 and AAV9. We generated rAAVs using each of these 15 capsid variants, as well as AAVrh74 and AAV9, to encode for the human Frataxin (h*FXN*) transgene under control of the constitutive CBh promoter. Recombinant AAVs produced with each of these capsids contained a unique set of barcodes at the 3′ untranslated region (3′ UTR) of the transgene (Figure 7D). We prepared a pool of rAAVs containing equal titer of each of the 17 viruses and administered this pool systemically to both cynomolgus macaques and mice. Quantification of transgene mRNA expression in NHP tissues identified MyoAAV 4A, MyoAAV 4E, MyoAAV 3A, and MyoAAV 4C as the most potent variants in transducing skeletal muscles in macaques, as compared to AAVrh74 and AAV9 (Figures 7D, 7E, and S7B). These four variants also transduced multiple skeletal muscles with significantly higher efficiency and were de-targeted from the liver compared to AAVrh74 and AAV9 in mice (Figures 7E and S7A).

Having identified the top four capsids, we evaluated their production yield. We produced rAAVs with MyoAAV 3A, 4A, 4C and 4E, as well as AAVrh74 and AAV9 using six different transgenes. Among the capsids we tested, AAV9 yielded the highest titers in HEK293 producer cells, and all of the MyoAAV variants produced similar or higher titers of virus compared to AAVrh74 (Figure 7F).

We next assessed these top four capsid variants' transduction dependency on and affinity for αV-containing integrin heterodimers, as well as their dependence on AAVR for transduction. Increasing concentrations of GLPG-0187 resulted in a dose-dependent decrease in transduction of human primary myotubes for all 4 variants (Figure 7G). Pre-incubation of the capsid variants with recombinant αVβ1, αVβ3, αVβ6, αVβ8, or MBP demonstrated that all four variants exhibit the highest affinity for αVβ6, followed by αVβ8 and αVβ3 (Figures 7H and 7I). Consistent with these results, treating human primary myotubes with increasing concentrations of the αVβ6 antibody resulted in a dose-dependent decrease in transduction by all four variants (Figure 7J). All four variants were also dependent on AAVR for transduction (Figure 7K).

Lastly, given the high dependency and affinity of the MyoAAV class of capsid variants for αVβ6, we analyzed expression in mouse, NHPs, and human muscles of integrin β6, which only exists on the cell surface as part of a heterodimer with integrin αV (Hynes, 2002). Immunofluorescence analysis demonstrated expression of integrin β6 in the muscles of all three species (Figure S7C).

DISCUSSION

In this study, we report a comprehensive strategy for engineering and selecting effective AAV capsid variants for potent gene delivery into any tissue and/or cell type of interest. DELIVER combines three critical features required for a stringent and widely applicable AAV capsid engineering strategy: (1) DELIVER enables selection of capsid variants that not only physically bind

Figure 6. Systemic injection of MyoAAV 2A-CK8-microdystrophin at the low dose of 2E+13 vg/kg results in widespread microdystrophin expression and effective restoration of muscle function in adult DBA/2J-mdx mice

(A) Representative immunofluorescence images for microdystrophin-FLAG (red) in muscles of 8-week-old DBA/2J-mdx mice injected with 2E+13 vg/kg AAV9- or MyoAAV 2A-CK8-microdystrophin. Scale bar: 400 μm.

(B) Western blots detecting microdystrophin-FLAG and GAPDH in muscles of 8-week-old DBA/2J-mdx mice injected with 2E+13 vg/kg AAV9- or MyoAAV 2A-CK8-microdystrophin, with relative signal intensity determined by densitometry at the bottom. A.U.: arbitrary unit, normalized to GAPDH.

(C) Quantification of fold difference in microdystrophin mRNA expression in various muscles and liver of 8-week-old DBA/2J-mdx mice systemically injected with 2E+13 vg/kg of MyoAAV 2A-CK8-microdystrophin compared to mice injected with the same dose of AAV9-CK8-microdystrophin. Dashed red line indicates relative expression from AAV9-CK8-microdystrophin. Data are presented as mean ± SD (n = 9–10); *p < 0.05, **p < 0.01 (Student's t test).

(D) Quantification of vector genome per diploid genome in various muscles and liver of DBA/2J-mdx mice injected with 2E+13 vg/kg of AAV9- or MyoAAV 2A-CK8-microdystrophin. Data are presented as mean ± SD (n = 9–10). **p < 0.01 (Student's t test).

(E and F) Muscle specific force (E) and decrease in isometric force after five eccentric contractions (F) for DBA/2J mice injected with vehicle (n = 10), and DBA/2J-mdx mice injected with vehicle (n = 10), 2E+13 vg/kg AAV9-CK8-microdystrophin (n = 10), or 2E+13 vg/kg MyoAAV 2A-CK8-microdystrophin (n = 10). *p < 0.05, **p < 0.01, ***p < 0.001 (one-way ANOVA with Tukey-Kramer MCT).

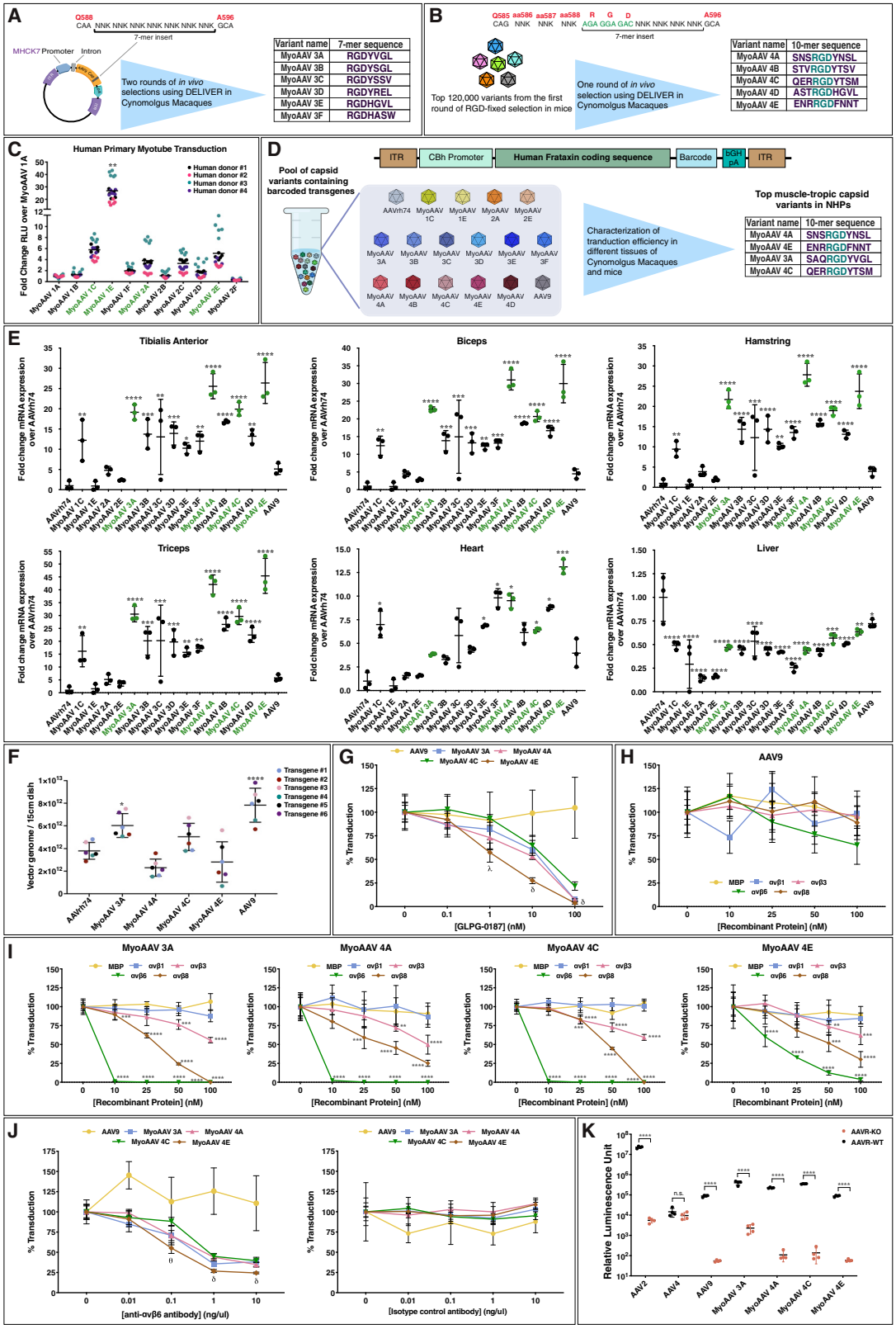

(legend on next page)

or enter the cells *in vivo*, but also functionally transduce the tissue and express their transgenes in specific cell types. (2) DELIVER can be applied in any mammalian species, *in vivo* or *in vitro*, enabling the identification of vector systems that can be translated directly from preclinical animal models to human applications. (3) DELIVER supports the screening of extremely diverse capsid libraries and is fully compatible with mechanism guided directed evolution approaches.

Ultimately, our interest in developing the DELIVER system was rooted in its potential benefits for advancing genomic medicine through the creation of more potent and selective viral vectors, and the muscle-directed AAV capsid variants identified in this study serve as an important proof-of-concept for this application. However, equally important to increasing muscle potency of the capsid was ensuring decreased transduction of the liver. The liver is a major site of transduction by naturally occurring AAV capsids and a target of toxicity associated with high-dose administration of AAV vectors in large animal models (Hinderer et al., 2018) and in human patients (Morales et al., 2020). In particular, two gene therapy trials (clinical trial identifiers NCT03368742 and NCT03199469) were put on clinical hold by the FDA due to severe adverse effects associated with liver toxicity. These recent setbacks in the clinical application of AAV-based gene therapy for genetic myopathies (Morales et al., 2020) highlight the exceptional challenges of delivery to the muscle and illustrate the clear need for potent-muscle directed AAV variants such as those described in this paper.

We applied DELIVER to develop engineered AAV capsids that, when administered systemically, transduce skeletal muscles throughout the body with greater efficiency and selectivity, and potentially a more favorable safety profile, than capsids currently used in clinical trials and preclinical discovery efforts. Through two rounds of stringent, transcript-based selection in C57BL/6J mice, we uncovered a class of RGD-containing capsid variants, including MyoAAV 1A, which exhibited more than 10 times greater efficiency for systemic muscle transduction compared to AAV9 in different mouse strains. Further evolution of MyoAAV 1A resulted in generation of improved muscle-tropic capsid variants in mice, including MyoAAV 2A. Independent application of DELIVER for *in vivo* directed evolution of muscle-tropic variants in NHPs identified the MyoAAV class of variants as the top hits, and additional evolution of RGD-containing variants in macaques resulted in identification of a few select highly muscle-tropic capsid variants that transduce both NHP and mouse muscles *in vivo* with extremely high efficiency. Furthermore, the muscle-directed capsid variants selected using DELIVER in mice and NHPs showed notably reduced targeting of the liver. These two attributes suggest that this class of AAV capsids could lower the dose of virus needed to achieve therapeutic levels of target cell transduction, lessening therapy-related risk for classical activation of complement by capsid/antibody complexes (Muhuri et al., 2021) and mitigating potentially detrimental consequences of transduction in liver cells. Consistent with this notion, we saw no evidence of liver toxicity or other adverse effects in any of the mice or NHP subjects receiving MyoAAV vectors in any of the studies reported here.

Application of DELIVER in both mice and NHPs identified numerous muscle-targeting capsid variants harboring a critical integrin-binding RGD motif as the first three amino acids of the inserted 7-mer peptide. The most enriched variants from our *in vivo* selections showed interaction with integrin heterodimers and could be blocked from target cell transduction by soluble integrin heterodimers, anti-integrin antibodies, and small molecule antagonists. This observed integrin dependency was conserved across mouse and human primary myotubes, suggesting a common mechanism of action for the MyoAAV class of capsids.

Figure 7. MyoAAV class of capsid variants evolved in NHPs transduce different muscles of cynomolgus macaques with high efficiency

(A and B) Schematic of virus library design and sequence of the top hits identified from NHP muscles after two rounds of *in vivo* selections in cynomolgus macaques starting from capsid variants containing a random 7-mer insert (A) or from one round of *in vivo* selection in cynomolgus macaques using the top 120,000 variants identified from the first round of RGD-fixed selection in mice (B).

(C) Comparison of *in vitro* transduction between the 11 muscle-tropic capsid variants selected in mice in human primary myotubes from four different donors. Data are presented as individual data points with mean; $^{**}p < 0.01$ (one-way ANOVA with Dunnett MCT with MyoAAV 1A as the control).

(D) Schematic of the barcoded human Frataxin transgene and the pool of capsid variants used for characterization of the top muscle-tropic variants in NHPs and mice.

(E) Fold change mRNA expression over AAVrh74 in different skeletal muscles, heart, and liver of three cynomolgus macaques 1 month after systemic administration of 3E+13 vg/kg of the pooled virus mix. mRNA expression quantified by deep sequencing of the barcodes associated with each capsid variant. Data are presented as mean ± SD (n = 3). $^{*}p < 0.05$, $^{**}p < 0.01$, $^{***}p < 0.001$, $^{****}p < 0.0001$ (one-way ANOVA with Dunnett's MCT with AAVrh74 as the control).

(F) Comparison of AAVrh74, MyoAAV 3A, MyoAAV 4A, MyoAAV 4C, and MyoAAV 4E, and AAV9 titers with six different transgenes. Data are presented as mean ± SD (n = 6). $^{*}p < 0.05$; $^{****}p < 0.0001$ (one-way ANOVA with Dunnett's MCT with AAVrh74 as the control).

(G) *In vitro* transduction efficiency in human primary myotubes treated with different concentrations of GLPG-0187 integrin αV antagonist and transduced with AAV9-, MyoAAV 3A-, MyoAAV 4A-, MyoAAV 4C-, or MyoAAV 4E-CK8-Nluc. Data are presented as mean ± SD (n = 5). p value calculated with a one-way ANOVA with Dunnett's MCT with the 0 nM condition for each group set as the control. δ: $p < 0.0001$ for MyoAAV 3A, MyoAAV 4A, MyoAAV 4C, and MyoAAV 4E; λ: $p < 0.0001$ for MyoAAV 4A and MyoAAV 4E.

(H and I) *In vitro* transduction efficiency in human primary myotubes transduced with AAV9-CK8-Nluc (H) or MyoAAV 3A-, MyoAAV 4A-, MyoAAV 4C-, or MyoAAV 4E-CK8-Nluc (I) incubated with different concentrations of αVβ1, αVβ3, αVβ6, αVβ8, or MBP recombinant proteins. Data are presented as mean ± SD (n = 5). $^{**}p < 0.01$, $^{***}p < 0.001$, $^{****}p < 0.0001$ (one-way ANOVA with Dunnett's MCT with the 0 nM recombinant protein condition in each group as the control).

(J) *In vitro* transduction efficiency in human primary myotubes treated with different concentrations of anti-αVβ6 antibody or mouse isotype control and transduced with AAV9-, MyoAAV 3A-, MyoAAV 4A-, MyoAAV 4C-, or MyoAAV 4E-CK8-Nluc. Data are presented as mean ± SD (n = 5). δ: $p < 0.0001$ for MyoAAV 3A, MyoAAV 4A, MyoAAV 4C, and MyoAAV 4E; θ: $p < 0.0001$ for MyoAAV 3A, MyoAAV 4A, and MyoAAV 4E (one-way ANOVA with Dunnett's MCT with the 0 nM condition for each group as the control).

(K) Comparison of *in vitro* transduction between HEK293FT and HEK293FT AAVR KO cells transduced with AAV2-, AAV4-, AAV9-, MyoAAV 3A-, MyoAAV 4A-, MyoAAV 4C-, or MyoAAV 4E-CMV-Nluc. Data are presented as mean ± SD (n = 4). $^{****}p < 0.0001$ (Student's t test on log transformed data).

See also Figure S7.

The required interaction of MyoAAV class of capsids with integrins appears to act in parallel with the previously identified AAV-binding protein AAVR, which was also necessary for target cell transduction by these variants. Among the RGD-binding integrin heterodimers, αVβ6 showed the highest affinity for MyoAAV binding and was specifically required on the surfaces of human muscle cells to enable their transduction by the top variants we identified. These observations are particularly interesting in light of prior studies of AAV2, which lacks the RGD motif but still utilizes integrin heterodimers, including α5β1 and αVβ5 as co-receptors for virus internalization, apparently via a related NGR motif (Asokan et al., 2006; Summerford et al., 1999).

Despite the highly effective and selective muscle transduction by the MyoAAV class of capsids in mice and NHPs, expression of RGD-binding integrin heterodimers is not specific to muscle tissue. Although more mechanistic studies are required to investigate the downstream signaling of integrin heterodimers after binding to MyoAAV, our working hypothesis to explain the muscle selectivity of these vectors despite the broader expression profile of integrin proteins is that expression of the integrin heterodimers on the cell surface is most likely required, but not sufficient, for potent functional transduction of cells and expression of the transgene. Since AAV transduction is a multi-step process (Figure S1A) and intracellular trafficking of the capsids and nuclear entry are also critical steps, downstream integrin signaling, which may differ in different cellular contexts, could be crucial for effective functional transduction by MyoAAV class of capsids. It is also possible that the muscle-tropism of MyoAAV reflects facilitation of transduction by other, potentially muscle-specific proteins that interact with integrin heterodimers.

While more work is needed to understand the molecular basis underlying the RGD-integrin heterodimer interaction for AAV-mediated gene delivery to muscle, its importance for our discovered class of muscle-directed vectors enabled us to further evolve these capsids by systematically varying the flanking residues around the essential RGD motif. This second evolution experiment identified additional variants capable of binding a broader subset of integrin heterodimers with even greater affinity than MyoAAV 1A. Our top second-generation variant in mice, MyoAAV 2A, showed dramatically increased potency for muscle transduction (up to 128 times that of AAV9) in both *in vivo* and *in vitro* assays while maintaining low liver transduction. Its success provides a framework for the iterative development of ultra-high potency vectors for other target tissues of interest.

With our goal of advancing genomic medicine, we tested MyoAAV 1A and MyoAAV 2A as delivery vectors for gene editing and gene therapy approaches that are currently under development and testing for human genetic myopathies. These studies employed well established mouse models of DMD and XLMTM, in which targeted DNA excision and transcript ''re-framing'' (Nelson et al., 2016; Tabebordbar et al., 2016), or genetic complementation with a full-length or miniaturized therapeutic transgene (Childers et al., 2014; Hakim et al., 2017), previously have shown functional benefit. In both models, we saw notable therapeutic effects, including rescue of expression of the disease-targeted proteins, significant increases in muscle strength and performance and, in the case of XLMTM, a striking rescue from disease-induced mortality that drastically extended the observed lifespan of MyoAAV 1A-treated animals beyond the average lifespan of untreated and AAV9-treated controls and with a similar survival trajectory to WT mice.

Our therapeutic results are all the more notable given that they were achieved after injecting 10–250 times lower doses of therapeutic vector than those used in previously published preclinical studies based on the same gene therapy approaches (Childers et al., 2014; Elverman et al., 2017; Hakim et al., 2017; Mack et al., 2017) or in currently ongoing human clinical trials (clinicaltrials.gov identifiers: NCT03362502, NCT03368742, NCT03769116, and NCT03199469). We anticipate that the lower dosage requirements for achieving therapeutic efficacy with these evolved AAV variants could have substantial benefits in clinical applications, including improved expression and safety profile and reduced manufacturing costs, although we note that vector doses used here for gene editing by CRISPR/Cas9 were higher than those needed for gene replacement, and may remain so given the requirement for co-delivery at appropriate ratios of the multiple components (AAV-SaCas9 + AAV-gRNAs) of this system.

Our results suggest direct applicability of the MyoAAV class of capsid variants across mice, NHPs, and human cells, as these variants showed broad activity for muscle transduction in multiple inbred mouse strains, including C57BL/6J, BALB/cJ, DBA/2J, mdx, and DBA/2J-mdx, as well as in cynomolgus macaques and cultures of human primary myoblasts obtained from multiple donors. Furthermore, the necessity of integrin heterodimers for MyoAAV class of capsids' infectivity in both mouse and human muscle cells strongly suggests a conserved mode of transduction in mouse and human muscle that could accelerate the timeline for developing and implementing new gene therapy approaches for a wide range of genetic myopathies.

While this paper was under peer review, Weinmann et al. (2020) reported identification of a muscle-tropic capsid variant containing an RGD motif in mice. Utilizing WT capsids, chimeric capsids, and modified capsids containing peptide insertions from previously published reports, they were able to identify this variant through testing transduction efficiency following systemic administration in mice of a panel of 183 total capsids. The two studies present important support for each other's findings, with work here going further in identifying a family of capsids containing the RGD motif starting from any potential amino acid sequence presented as a 7-mer peptide on the capsid surface, elucidating the dependency of transduction by RGD-containing variants on integrins, uncovering the significance of the RGD motif in this family of capsids and leveraging it to further evolve optimized capsid variants, documenting conserved, highly potent muscle-tropism in both mice and NHPs, and demonstrating therapeutic efficacy in multiple models of genetic myopathies after systemic administration of a low dose of rAAV generated using the identified muscle-tropic variants.

Our findings, applying *in vivo* directed evolution of capsids in both mice and NHPs, uncover critical capsid sequence features needed for potent muscle-directed gene delivery in different species. We found both the RGD motif itself and the sequence of amino acids immediately surrounding this motif play a crucial role in defining transduction efficiency and selectivity of capsids

in different species. In particular, while the most highly muscle-tropic variants we identified from our selections all contain the RGD motif, the amino acids around this motif differ for individual variants identified as the top hits in different species. For example, MyoAAV 2A is the top second-generation variant that we identified in mice and is highly potent in transducing mouse muscles; however, MyoAAV 2A does not transduce NHP muscles with high efficiency after systemic administration. In fact, all of the variants that we identified from our NHP selections outperformed the variants identified in mice when tested as rAAVs in NHPs for muscle transduction after systemic delivery. Fortunately, the top capsid variants from our NHP selections were highly potent in transducing mouse muscles as well, making them highly applicable for therapeutic development. These results highlight the importance of using *in vivo* directed evolution with diverse capsid libraries and a stringent selection strategy in order to evolve the most potent tissue-targeted capsid variants across species but also raise the important question of which variants will prove most potent for human application. While we anticipate that those selected in NHPs are very likely to perform well in humans, given the evolutionary relatedness of these species, it is possible that further optimization for human muscle transduction, perhaps using human muscle xenografts (Zhang et al., 2014), could further enhance the specificity and/or efficiency of this class of vectors for human applications.

In summary, we report here the evolution, engineering, and mechanistic characterization of a family of highly potent muscle-directed AAV capsid variants across species. We demonstrate these vectors' therapeutic efficacy, even at low dosage, in multiple mouse models of genetic muscle disease. These vectors have the potential to advance muscle-directed therapeutic gene delivery for a large number of musculoskeletal disorders. More broadly, the DELIVER system described here provides a highly adaptable platform for identifying precise AAV capsid variants for any tissue or cell type in the body that could greatly expand the clinical and experimental applications of this vector system across fields and disciplines. We anticipate that adoption of DELIVER to additional tissue and organ systems will have a far-reaching impact in accelerating the development and translation of gene therapy and other genomic medicine approaches for a variety of human diseases.

STAR★METHODS

Detailed methods are provided in the online version of this paper and include the following:

- KEY RESOURCES TABLE
- RESOURCE AVAILABILITY
  - Lead contact
  - Materials availability
  - Data and code availability
- EXPERIMENTAL MODEL AND SUBJECT DETAILS
  - Mice
  - Cynomolgus Macaques
  - Cell lines
  - Primary myoblasts and myotubes
- METHOD DETAILS
  - Constructs
  - First and second round capsid library generation
  - Recombinant AAV production
  - *In vivo* selection in mice and cynomolgus macaques
  - Next generation sequencing data analysis
  - Exon skipping, transgene expression, and vector genome quantification
  - Immunofluorescence
  - Western blot
  - *In vitro* AAV transduction and binding experiments
  - Small molecule and antibody inhibition experiments
  - Recombinant protein inhibition experiments
  - Lectin inhibition experiments
  - Flow cytometry
  - Mouse satellite cell isolation, culture, and differentiation
  - Alanine Aminotransferase (ALT) and Aspartate Aminotransferase (AST) assay
  - *In Vitro* Neutralizing Antibody Assay
  - Mouse activity measurement
  - Mouse muscle physiology analysis
  - Bioluminescence imaging
- QUANTIFICATION AND STATISTICAL ANALYSIS

SUPPLEMENTAL INFORMATION

Supplemental information can be found online at https://doi.org/10.1016/j.cell.2021.08.028.

ACKNOWLEDGMENTS

This work was made possible by a generous anonymous philanthropic gift to the P.C.S. lab at the Broad Institute of MIT and Harvard and a sponsored research agreement with Sarepta Therapeutics awarded to M.T. and P.C.S. It was additionally supported by grants from Howard Hughes Medical Institute to P.C.S., a Shark Tank award from the Chemical Biology and Therapeutic Sciences program at the Broad Institute and a career development award from the American Society of Gene & Cell Therapy to M.T., NIH (DP1 OD025432) and Glenn Foundation grants to A.J.W., and MDA602235 from the Muscular Dystrophy Association USA and generous support for therapy development from the Anderson Family Foundation to A.H.B. Mouse genotyping utilized the resources of the Boston Children's Hospital IDDRC Molecular Genetics Core Laboratory funded by NIH U54HD090255. The content is solely the responsibility of the authors and does not necessarily represent the official views of the American Society of Gene & Cell Therapy or other funding agencies. K.A. Lagerborg and A.S. were supported by the Herchel Smith graduate fellowship. We would like to thank Ben Deverman and Ken Chan for providing the Rep-AAP plasmid and for thoughtful discussions and technical assistance; the Harvard Department of Stem Cell and Regenerative Biology-Harvard Stem Cell Institute Flow Cytometry Core for technical assistance; Jan Carette for providing the HEK293FT AAVR KO cells and the HEK293FT WT control; and Aaron Lin, Steve Schaffner, Christopher Edwards, and Kian Sani for providing thoughtful feedback on the manuscript.

AUTHOR CONTRIBUTIONS

M.T. conceived the study, mentored graduate students and research associates involved in this project, and led the experimental design, technical, and logistical aspects of the study. M.T. wrote the paper with help from the co-authors. M.T., P.C.S., A.J.W, and A.H.B supervised the study. M.T., K.A. Lagerborg, E.M.K., A.S., L.T., S.T., J.J.W., K.A.M., A.K., E.C.T, B.M., B.L.P., K.A. Leacock, and N.H. performed experiments and data analysis.

S.Y. analyzed the next-generation sequencing data. All authors reviewed the manuscript.

DECLARATION OF INTERESTS

P.C.S. is a co-founder of, shareholder in, and advisor to Sherlock Biosciences, Inc, as well as a board member of and shareholder in Danaher Corporation. M.T. and P.C.S. are recipients of a sponsored research award from Sarepta Therapeutics. M.T. is a co-founder of, shareholder in, and advisor to Kate Therapeutics. A.H.B. has received sponsored research support from NIH, MDA (USA), AFM Telethon, Alexion Pharmaceuticals Inc., Audentes Therapeutics Inc., Dynacure SAS, and Pfizer Inc. He has consulted and received compensation or honoraria from Asklepios BioPharmaceutical Inc, Audentes Therapeutics, Biogen, F. Hoffman-La Roche AG, Kate Therapeutics, GLG Inc, and Guidepoint Global and holds equity in Ballard Biologics and Kate Therapeutics. A.J.W. is a consultant to Frequency Therapeutics, a recipient of a sponsored research award from Sarepta Therapeutics, and a co-founder of Elevian, a company that aims to develop medicines to restore regenerative capacity, and advises, receives sponsored research support, and holds private equity in the company. M.T., S.Y., and P.C.S. are inventors on patent applications filed by the Broad Institute related to this work.

Received: October 28, 2020
Revised: May 21, 2021
Accepted: August 20, 2021
Published: September 9, 2021

REFERENCES

Alexander, M.S., Casar, J.C., Motohashi, N., Vieira, N.M., Eisenberg, I., Marshall, J.L., Gasperini, M.J., Lek, A., Myers, J.A., Estrella, E.A., et al. (2014). MicroRNA-486-dependent modulation of DOCK3/PTEN/AKT signaling pathways improves muscular dystrophy-associated symptoms. J. Clin. Invest. *124*, 2651–2667. https://doi.org/10.1172/JCI73579.

Asokan, A., Hamra, J.B., Govindasamy, L., Agbandje-McKenna, M., and Samulski, R.J. (2006). Adeno-associated virus type 2 contains an integrin alpha5-beta1 binding domain essential for viral cell entry. J. Virol. *80*, 8961–8969. https://doi.org/10.1128/JVI.00843-06.

Bell, C.L., Vandenberghe, L.H., Bell, P., Limberis, M.P., Gao, G.P., Van Vliet, K., Agbandje-McKenna, M., and Wilson, J.M. (2011). The AAV9 receptor and its modification to improve in vivo lung gene transfer in mice. J. Clin. Invest. *121*, 2427–2435. https://doi.org/10.1172/JCI57367.

Bengtsson, N.E., Hall, J.K., Odom, G.L., Phelps, M.P., Andrus, C.R., Hawkins, R.D., Hauschka, S.D., Chamberlain, J.R., and Chamberlain, J.S. (2017). Muscle-specific CRISPR/Cas9 dystrophin gene editing ameliorates pathophysiology in a mouse model for Duchenne muscular dystrophy. Nat. Commun. *8*, 14454. https://doi.org/10.1038/ncomms14454.

Berry, G.E., and Asokan, A. (2016). Cellular transduction mechanisms of adeno-associated viral vectors. Curr. Opin. Virol. *21*, 54–60. https://doi.org/10.1016/j.coviro.2016.08.001.

Börner, K., Kienle, E., Huang, L.Y., Weinmann, J., Sacher, A., Bayer, P., Stüllein, C., Fakhiri, J., Zimmermann, L., Westhaus, A., et al. (2020). Pre-arrayed Pan-AAV Peptide Display Libraries for Rapid Single-Round Screening. Mol. Ther. *28*, 1016–1032. https://doi.org/10.1016/j.ymthe.2020.02.009.

Cerletti, M., Jurga, S., Witczak, C.A., Hirshman, M.F., Shadrach, J.L., Goodyear, L.J., and Wagers, A.J. (2008). Highly efficient, functional engraftment of skeletal muscle stem cells in dystrophic muscles. Cell *134*, 37–47. https://doi.org/10.1016/j.cell.2008.05.049.

Challis, R.C., Kumar, S.R., Chan, K.Y., Challis, C., Jang, M.J., Rajendran, P.S., Tompkins, J.D., Shivkumar, K., Deverman, B.E., and Gradinaru, V. (2018). Widespread and targeted gene expression by systemic AAV vectors: Production, purification, and administration. bioRxiv. https://doi.org/10.1101/246405.

Chan, S., Head, S.I., and Morley, J.W. (2007). Branched fibers in dystrophic mdx muscle are associated with a loss of force following lengthening contractions. Am. J. Physiol. Cell Physiol. *293*, C985–C992. https://doi.org/10.1152/ajpcell.00128.2007.

Childers, M.K., Joubert, R., Poulard, K., Moal, C., Grange, R.W., Doering, J.A., Lawlor, M.W., Rider, B.E., Jamet, T., Danièle, N., et al. (2014). Gene therapy prolongs survival and restores function in murine and canine models of myotubular myopathy. Sci. Transl. Med. *6*, 220ra10. https://doi.org/10.1126/scitranslmed.3007523.

Choudhury, S.R., Fitzpatrick, Z., Harris, A.F., Maitland, S.A., Ferreira, J.S., Zhang, Y., Ma, S., Sharma, R.B., Gray-Edwards, H.L., Johnson, J.A., et al. (2016). In Vivo Selection Yields AAV-B1 Capsid for Central Nervous System and Muscle Gene Therapy. Mol. Ther. *24*, 1247–1257. https://doi.org/10.1038/mt.2016.84.

Dalkara, D., Byrne, L.C., Klimczak, R.R., Visel, M., Yin, L., Merigan, W.H., Flannery, J.G., and Schaffer, D.V. (2013). In vivo-directed evolution of a new adeno-associated virus for therapeutic outer retinal gene delivery from the vitreous. Sci. Transl. Med. *5*, 189ra76. https://doi.org/10.1126/scitranslmed.3005708.

Deverman, B.E., Pravdo, P.L., Simpson, B.P., Kumar, S.R., Chan, K.Y., Banerjee, A., Wu, W.L., Yang, B., Huber, N., Pasca, S.P., and Gradinaru, V. (2016). Cre-dependent selection yields AAV variants for widespread gene transfer to the adult brain. Nat. Biotechnol. *34*, 204–209. https://doi.org/10.1038/nbt.3440.

DiMattia, M.A., Nam, H.J., Van Vliet, K., Mitchell, M., Bennett, A., Gurda, B.L., McKenna, R., Olson, N.H., Sinkovits, R.S., Potter, M., et al. (2012). Structural insight into the unique properties of adeno-associated virus serotype 9. J. Virol. *86*, 6947–6958. https://doi.org/10.1128/JVI.07232-11.

Ding, W., Zhang, L., Yan, Z., and Engelhardt, J.F. (2005). Intracellular trafficking of adeno-associated viral vectors. Gene Ther. *12*, 873–880. https://doi.org/10.1038/sj.gt.3302527.

Duan, D. (2018). Systemic AAV Micro-dystrophin Gene Therapy for Duchenne Muscular Dystrophy. Mol. Ther. *26*, 2337–2356. https://doi.org/10.1016/j.ymthe.2018.07.011.

Dudek, A.M., Pillay, S., Puschnik, A.S., Nagamine, C.M., Cheng, F., Qiu, J., Carette, J.E., and Vandenberghe, L.H. (2018). An Alternate Route for Adeno-associated Virus (AAV) Entry Independent of AAV Receptor. J. Virol. *92*. e02213-17. https://doi.org/10.1128/JVI.02213-17.

Elverman, M., Goddard, M.A., Mack, D., Snyder, J.M., Lawlor, M.W., Meng, H., Beggs, A.H., Buj-Bello, A., Poulard, K., Marsh, A.P., et al. (2017). Long-term effects of systemic gene therapy in a canine model of myotubular myopathy. Muscle Nerve *56*, 943–953. https://doi.org/10.1002/mus.25658.

Gao, G., Lu, Y., Calcedo, R., Grant, R.L., Bell, P., Wang, L., Figueredo, J., Lock, M., and Wilson, J.M. (2006). Biology of AAV serotype vectors in liver-directed gene transfer to nonhuman primates. Mol. Ther. *13*, 77–87. https://doi.org/10.1016/j.ymthe.2005.08.017.

Goldstein, J.M., Tabebordbar, M., Zhu, K., Wang, L.D., Messemer, K.A., Peacker, B., Ashrafi Kakhki, S., Gonzalez-Celeiro, M., Shwartz, Y., Cheng, J.K.W., et al. (2019). In Situ Modification of Tissue Stem and Progenitor Cell Genomes. Cell Rep. *27*, 1254–1264.e7. https://doi.org/10.1016/j.celrep.2019.03.105.

Hakim, C.H., Wasala, N.B., Pan, X., Kodippili, K., Yue, Y., Zhang, K., Yao, G., Haffner, B., Duan, S.X., Ramos, J., et al. (2017). A Five-Repeat Micro-Dystrophin Gene Ameliorated Dystrophic Phenotype in the Severe DBA/2J-mdx Model of Duchenne Muscular Dystrophy. Mol. Ther. Methods Clin. Dev. *6*, 216–230. https://doi.org/10.1016/j.omtm.2017.06.006.

Hinderer, C., Katz, N., Buza, E.L., Dyer, C., Goode, T., Bell, P., Richman, L.K., and Wilson, J.M. (2018). Severe Toxicity in Nonhuman Primates and Piglets Following High-Dose Intravenous Administration of an Adeno-Associated Virus Vector Expressing Human SMN. Hum. Gene Ther. *29*, 285–298. https://doi.org/10.1089/hum.2018.015.

Hordeaux, J., Wang, Q., Katz, N., Buza, E.L., Bell, P., and Wilson, J.M. (2018). The Neurotropic Properties of AAV-PHP.B Are Limited to C57BL/6J Mice. Mol. Ther. *26*, 664–668. https://doi.org/10.1016/j.ymthe.2018.01.018.

Hynes, R.O. (2002). Integrins: bidirectional, allosteric signaling machines. Cell *110*, 673–687. https://doi.org/10.1016/s0092-8674(02)00971-6.

Körbelin, J., Sieber, T., Michelfelder, S., Lunding, L., Spies, E., Hunger, A., Alawi, M., Rapti, K., Indenbirken, D., Müller, O.J., et al. (2016). Pulmonary Targeting of Adeno-associated Viral Vectors by Next-generation Sequencing-guided Screening of Random Capsid Displayed Peptide Libraries. Mol. Ther. *24*, 1050–1061. https://doi.org/10.1038/mt.2016.62.

Levitt, N., Briggs, D., Gil, A., and Proudfoot, N.J. (1989). Definition of an efficient synthetic poly(A) site. Genes Dev. *3*, 1019–1025. https://doi.org/10.1101/gad.3.7.1019.

Li, C., and Samulski, R.J. (2020). Engineering adeno-associated virus vectors for gene therapy. Nat. Rev. Genet. *21*, 255–272. https://doi.org/10.1038/s41576-019-0205-4.

Li, C., Wu, S., Albright, B., Hirsch, M., Li, W., Tseng, Y.S., Agbandje-McKenna, M., McPhee, S., Asokan, A., and Samulski, R.J. (2016). Development of Patient-specific AAV Vectors After Neutralizing Antibody Selection for Enhanced Muscle Gene Transfer. Mol. Ther. *24*, 53–65. https://doi.org/10.1038/mt.2015.134.

Mack, D.L., Poulard, K., Goddard, M.A., Latournerie, V., Snyder, J.M., Grange, R.W., Elverman, M.R., Denard, J., Veron, P., Buscara, L., et al. (2017). Systemic AAV8-Mediated Gene Therapy Drives Whole-Body Correction of Myotubular Myopathy in Dogs. Mol. Ther. *25*, 839–854. https://doi.org/10.1016/j.ymthe.2017.02.004.

Mendell, J.R., Sahenk, Z., Lehman, K., Nease, C., Lowes, L.P., Miller, N.F., Iammarino, M.A., Alfano, L.N., Nicholl, A., Al-Zaidy, S., et al. (2020). Assessment of Systemic Delivery of rAAVrh74.MHCK7.micro-dystrophin in Children With Duchenne Muscular Dystrophy: A Nonrandomized Controlled Trial. JAMA Neurol. *77*, 1122–1131. https://doi.org/10.1001/jamaneurol.2020.1484.

Michelfelder, S., Kohlschütter, J., Skorupa, A., Pfennings, S., Müller, O., Kleinschmidt, J.A., and Trepel, M. (2009). Successful expansion but not complete restriction of tropism of adeno-associated virus by in vivo biopanning of random virus display peptide libraries. PLoS ONE *4*, e5122. https://doi.org/10.1371/journal.pone.0005122.

Morales, L., Gambhir, Y., Bennett, J., and Stedman, H.H. (2020). Broader Implications of Progressive Liver Dysfunction and Lethal Sepsis in Two Boys following Systemic High-Dose AAV. Mol. Ther. *28*, 1753–1755. https://doi.org/10.1016/j.ymthe.2020.07.009.

Muhuri, M., Maeda, Y., Ma, H., Ram, S., Fitzgerald, K.A., Tai, P.W., and Gao, G. (2021). Overcoming innate immune barriers that impede AAV gene therapy vectors. J. Clin. Invest. *131*, 143780. https://doi.org/10.1172/JCI143780.

Murrey, D.A., Naughton, B.J., Duncan, F.J., Meadows, A.S., Ware, T.A., Campbell, K.J., Bremer, W.G., Walker, C.M., Goodchild, L., Bolon, B., et al. (2014). Feasibility and safety of systemic rAAV9-hNAGLU delivery for treating mucopolysaccharidosis IIIB: toxicology, biodistribution, and immunological assessments in primates. Hum. Gene Ther. Clin. Dev. *25*, 72–84. https://doi.org/10.1089/humc.2013.208.

Nelson, C.E., Hakim, C.H., Ousterout, D.G., Thakore, P.I., Moreb, E.A., Castellanos Rivera, R.M., Madhavan, S., Pan, X., Ran, F.A., Yan, W.X., et al. (2016). In vivo genome editing improves muscle function in a mouse model of Duchenne muscular dystrophy. Science *351*, 403–407. https://doi.org/10.1126/science.aad5143.

Nonnenmacher, M., Wang, W., Child, M.A., Ren, X.Q., Huang, C., Ren, A.Z., Tocci, J., Chen, Q., Bittner, K., Tyson, K., et al. (2020). Rapid evolution of blood-brain-barrier-penetrating AAV capsids by RNA-driven biopanning. Mol. Ther. Methods Clin. Dev. *20*, 366–378. https://doi.org/10.1016/j.omtm.2020.12.006.

Pierschbacher, M.D., and Ruoslahti, E. (1984). Cell attachment activity of fibronectin can be duplicated by small synthetic fragments of the molecule. Nature *309*, 30–33. https://doi.org/10.1038/309030a0.

Pillay, S., Meyer, N.L., Puschnik, A.S., Davulcu, O., Diep, J., Ishikawa, Y., Jae, L.T., Wosen, J.E., Nagamine, C.M., Chapman, M.S., and Carette, J.E. (2016). An essential receptor for adeno-associated virus infection. Nature *530*, 108–112. https://doi.org/10.1038/nature16465.

Pytela, R., Pierschbacher, M.D., and Ruoslahti, E. (1985). Identification and isolation of a 140 kd cell surface glycoprotein with properties expected of a fibronectin receptor. Cell *40*, 191–198. https://doi.org/10.1016/0092-8674(85)90322-8.

Ruoslahti, E. (1996). RGD and other recognition sequences for integrins. Annu. Rev. Cell Dev. Biol. *12*, 697–715. https://doi.org/10.1146/annurev.cellbio.12.1.697.

Salva, M.Z., Himeda, C.L., Tai, P.W., Nishiuchi, E., Gregorevic, P., Allen, J.M., Finn, E.E., Nguyen, Q.G., Blankinship, M.J., Meuse, L., et al. (2007). Design of tissue-specific regulatory cassettes for high-level rAAV-mediated expression in skeletal and cardiac muscle. Mol. Ther. *15*, 320–329. https://doi.org/10.1038/sj.mt.6300027.

Summerford, C., Bartlett, J.S., and Samulski, R.J. (1999). AlphaVbeta5 integrin: a co-receptor for adeno-associated virus type 2 infection. Nat. Med. *5*, 78–82. https://doi.org/10.1038/4768.

Tabebordbar, M., Zhu, K., Cheng, J.K.W., Chew, W.L., Widrick, J.J., Yan, W.X., Maesner, C., Wu, E.Y., Xiao, R., Ran, F.A., et al. (2016). In vivo gene editing in dystrophic mouse muscle and muscle stem cells. Science *351*, 407–411. https://doi.org/10.1126/science.aad5177.

Tse, L.V., Klinc, K.A., Madigan, V.J., Castellanos Rivera, R.M., Wells, L.F., Havlik, L.P., Smith, J.K., Agbandje-McKenna, M., and Asokan, A. (2017). Structure-guided evolution of antigenically distinct adeno-associated virus variants for immune evasion. Proc. Natl. Acad. Sci. USA *114*, E4812–E4821. https://doi.org/10.1073/pnas.1704766114.

Weinmann, J., Weis, S., Sippel, J., Tulalamba, W., Remes, A., El Andari, J., Herrmann, A.K., Pham, Q.H., Borowski, C., Hille, S., et al. (2020). Identification of a myotropic AAV by massively parallel in vivo evaluation of barcoded capsid variants. Nat. Commun. *11*, 5432. https://doi.org/10.1038/s41467-020-19230-w.

Yang, L., and Xiao, X. (2013). Creation of a cardiotropic adeno-associated virus: the story of viral directed evolution. Virol. J. *10*, 50. https://doi.org/10.1186/1743-422X-10-50.

Yang, L., Jiang, J., Drouin, L.M., Agbandje-McKenna, M., Chen, C., Qiao, C., Pu, D., Hu, X., Wang, D.Z., Li, J., and Xiao, X. (2009). A myocardium tropic adeno-associated virus (AAV) evolved by DNA shuffling and in vivo selection. Proc. Natl. Acad. Sci. USA *106*, 3946–3951. https://doi.org/10.1073/pnas.0813207106.

Zhang, Y., King, O.D., Rahimov, F., Jones, T.I., Ward, C.W., Kerr, J.P., Liu, N., Emerson, C.P., Jr., Kunkel, L.M., Partridge, T.A., and Wagner, K.R. (2014). Human skeletal muscle xenograft as a new preclinical model for muscle disorders. Hum. Mol. Genet. *23*, 3180–3188. https://doi.org/10.1093/hmg/ddu028.

Zincarelli, C., Soltys, S., Rengo, G., and Rabinowitz, J.E. (2008). Analysis of AAV serotypes 1-9 mediated gene expression and tropism in mice after systemic injection. Mol. Ther. *16*, 1073–1080. https://doi.org/10.1038/mt.2008.76.

STAR★METHODS

KEY RESOURCES TABLE

REAGENT or RESOURCE	SOURCE	IDENTIFIER
Antibodies		
Mouse anti-integrin alpha V antibody, PE conjugated	Biolegend	Cat #327910; RRID:AB_940564
Mouse anti-integrin alpha 5 antibody, PE conjugated	Biolegend	Cat #328010; RRID:AB_2280539
Mouse anti-integrin beta 1 antibody, APC conjugated	Biolegend	Cat #303008; RRID:AB_314323
Mouse anti-integrin beta 3 antibody, APC conjugated	Biolegend	Cat #336411; RRID:AB_10707694
Mouse anti-integrin beta 5 antibody, APC conjugated	Miltenyi	Cat #130-111-216; RRID:AB_2652485
Mouse anti-integrin beta 6 antibody, APC conjugated	Miltenyi	Cat #130-111-454; RRID:AB_2652496
Mouse anti-integrin beta 8 antibody, unconjugated	LSBio	Cat #LS-C70803-100; RRID:AB_1651323
Rabbit anti-FLAG antibody, unconjugated	Sigma	Cat #F7425; RRID:AB_439687
Rabbit anti-integrin beta 6 antibody, unconjugated	Abcam	Cat #ab187155; RRID:AB_2893159
Mouse anti-integrin alpha 8 antibody, unconjugated	Thermo Fisher	Cat #MA5-31449; RRID:AB_2787085
Rabbit anti-integrin alpha IIb antibody, unconjugated	Abcam	Cat #ab134131; RRID:AB_2732852
Goat anti-integrin beta 3 antibody, unconjugated	R&D systems	Cat #AF2266; RRID:AB_355209
Rabbit anti-integrin beta 8 antibody, unconjugated	Thermo Fisher	Cat #PA5-76390; RRID:AB_2720117
Mouse anti-eGFP antibody, unconjugated	Thermo Fisher	Cat #MA1-952; RRID:AB_889471
Goat anti-MTM1 antibody, unconjugated	Abnova	Cat #PAB6061; RRID:AB_1577478
Rabbit anti-dystrophin antibody, unconjugated	Abcam	Cat #ab15277; RRID:AB_301813
Mouse anti-GAPDH antibody, unconjugated	Santa Cruz	Cat #sc-32233; RRID:AB_627679
Mouse anti-alpha tubulin antibody, unconjugated	Abcam	Cat #ab7291; RRID:AB_2241126)
Mouse anti-Vinculin antibody, unconjugated	R&D systems	Cat #MAB6896; RRID:AB_10992930
Horse anti-mouse IgG, HRP conjugated	Cell Signaling	Cat #7076P2; RRID:AB_330924
Goat anti-rabbit IgG, HRP conjugated	Abcam	Cat #ab97051; RRID:AB_10679369
Donkey anti-goat IgG, HRP conjugated	Jackson Immunoresearch	Cat #705-035-147; RRID:AB_2313587
Mouse anti-integrin alpha V beta 6 antibody, unconjugated	Abcam	Cat #ab77906; RRID:AB_1603055
Mouse IgG2a isotype control	Biolegend	Cat #401508; RRID:AB_2893160
Goat anti-mouse IgG, PE conjugated	Invitrogen	Cat #12-4010-82; RRID:AB_11063706
Bacterial and Virus Strains		
Endura chemically competent cells	Lucigen	Cat #60240-2
Biological Samples		
Primary human skeletal muscle myoblasts	Lonza	Cat# CC-2580
Chemicals, Peptides, and Recombinant Proteins		
Horse Serum, New Zealand origin	Thermo Fisher	Cat #16050130
F10	Thermo Fisher	Cat #1155043
Glutamax	Thermo Fisher	Cat #35050061
Penicillin-Streptomycin	Thermo Fisher	Cat #15140122
hbFGF	Sigma	Cat #F0291-25 ug
Collagen	Thermo Fisher	Cat #A1048301
Laminin	Thermo Fisher	Cat #23017015
DMEM, high glucose, GlutaMAX™ Supplement, HEPES	Thermo Fisher	Cat #10564029
Fetal Bovine Serum, certified, One Shot™ format	Thermo Fisher	Cat #A3160402
PEI MAX	Polysciences	Cat #24765-1
TRIzol reagent	Thermo Fisher	Cat #15596026
Quickextract DNA extract solution	Lucigen	Cat #QE09050

(*Continued on next page*)

Continued

REAGENT or RESOURCE	SOURCE	IDENTIFIER
Hoechst 33342	Thermo Fisher	Cat #H3570
Vectashield antifade mounting medium without DAPI	Vector Laboratories	Cat #H-1400-10
Radioimmunoprecipitation assay (RIPA) buffer	Cell Signaling Technologies	Cat #9806S
Recombinant Human Integrin alpha V beta 1 Protein, CF	R&D systems	Cat #6579-AVB-050
Recombinant Human Integrin alpha V beta 3 Protein, CF	R&D systems	Cat #3050-AV-050
Recombinant Human Integrin alpha V beta 6 Protein, CF	R&D systems	Cat #3817-AV-050
Recombinant Human Integrin alpha V beta 8 Protein, CF	R&D systems	Cat #4135-AV-050
Maltose binding protein	Novus Biologicals	Cat #NBC1-18538
Critical Commercial Assays		
ALT Activity Assay	Sigma	Cat #MAK052
AST Activity Assay	Sigma	Cat #MAK055
Nano-Glo Luciferase Assay	Promega	Cat #N1120
SuperScript IV VILO Master Mix	Invitrogen	Cat #11754050
SuperScript IV reverse transcriptase	Invitrogen	Cat #18090050
Mouse GAPDH mRNA taqman assay	Integrated DNA technologies	Cat #Mm.PT.39a.1
Mouse beta actin mRNA taqman assay	Integrated DNA technologies	Cat #Mm.PT.39a.22214843.g
Deposited Data		
Next generation sequencing data	NCBI sequence read archive	bioproject ID PRJNA754792
Experimental Models: Cell Lines		
HEK293	ATCC	Cat #CRL-1573
Experimental Models: Organisms/Strains		
Mouse: C57BL/6J	Jackson Laboratories	Cat #000664
Mouse: C57BL/10ScSn-Dmdmdx/J	Jackson Laboratories	Cat #001801
Mouse: B6;129S6-Gt(ROSA)26Sortm9	Jackson Laboratories	Cat #007905
Mouse: BALB/cJ	Jackson Laboratories	Cat #000651
Mouse: DBA/2J	Jackson Laboratories	Cat #000671
Cynomolgus Macaque	Biomere Biomedical Research Models	N/A
Oligonucleotides		
Primers for cloning	See Table S1 for a list of cloning primers	N/A
Taqman assay primers and probes	See Table S2 for a list of primer and probe sequences	N/A
Recombinant DNA		
pAAV-Cre control plasmid	Cell Biolabs	Cat #AAV-401
Helper plasmid	Aldevron	Cat #pALDX-80
Software and Algorithms		
FlowJo v10.7.	FlowJo	https://www.flowjo.com/solutions/flowjo
Graphpad Prism v9	Graphpad Prism Inc	https://www.graphpad.com/scientific-software/prism/
Next generation sequencing analysis code	In house	https://doi.org/10.5281/zenodo.5210602

RESOURCE AVAILABILITY

Lead contact

Further information and requests for resources and reagents should be directed to and will be fulfilled by the lead contact, Mohammadsharif Tabebordbar (tabebord@fas.harvard.edu).

Materials availability

Reagents generated in this study will be made available on request, considering the terms of materials transfer agreement (MTA) for the modified reagents. We may require a completed MTA if there is potential for commercial application.

Data and code availability

- Next generation sequencing data have been deposited at NCBI Sequence Read Archive (SRA) with the bioproject ID PRJNA754792 and are publicly available as of the date of publication. Accession number is also listed in the key resources table.
- All original code has been deposited at Zenodo with the https://doi.org/10.5281/zenodo.5210602 DOI and is publicly available as of the date of publication. DOI is also listed in the key resources table.
- Any additional information required to reanalyze the data reported in this paper is available from the lead contact upon request.

EXPERIMENTAL MODEL AND SUBJECT DETAILS

Mice

All animal care and experimental procedures were in accordance with the Broad Institute Institutional Animal Care and Use Committee (IACUC), as well as, the Harvard University, Boston Children's hospital, and Biomere's IACUC. The following mice were purchased from the Jackson laboratories: mdx (JAX, #001801), C57BL/6J (JAX, #000664), DBA/2J (JAX, 000671), DBA/2J-mdx (JAX, 013141), and BALB/cJ mice (JAX, #000651). For the high dose systemic AAV-CMV-EGFP experiment, 8 weeks old male and female C57BL/6J, DBA/2J, and BALB/cJ mice were injected with AAV. For the low dose systemic AAV-CMV-EGFP experiment, 8 weeks old male C57BL/6J mice were used. For the intramuscular AAV-CMV-EGFP experiment, 8 weeks old male C57BL/6J mice were injected with vehicle (saline) or AAV. For the AAV-CRISPR experiments, 8 weeks old male mdx mice were used. For the *in vivo* imaging experiments, we injected 8 weeks old male BALB/cJ mice either with AAV or vehicle (saline). For the ALT and AST experiments, 8 weeks old male C57BL/6J mice were used. For the satellite cell transduction experiment, we injected 6 months old male mdx-Ai9 mice. For the AAV-MHCK7-h*MTM1* experiments, 4 weeks old male *Mtm1* KO mice were injected with AAV. For the AAV-CK8-microdystrophin experiments, we injected 8 weeks old male DBA/2J-mdx mice. For the pooled AAV-CBh-h*FXN* experiment, we injected 2 male and 3 female 8 weeks old C57BL/6J mice. Selection of the first-generation of MyoAAV variants in mice was performed in 2 male and 2 female 8 weeks old C57BL/6J mice in each of the two rounds of selection. Selection of the second-generation of MyoAAV variants in mice was performed in 2 male and 1 female 8 weeks old C57BL/6J and 2 male and 1 female 8 weeks old mdx mice. All the mouse injections were performed retro-orbitally

Cynomolgus Macaques

For the first round of selection of muscle-tropic variants in cynomolgus macaques (starting from a random 7-mer insert library), 1 male and 1 female 2 years old animals were injected with the capsid library. For the second round of selection in NHPs, 2 male and 1 female 2 years old cynomolgus macaques were injected with the capsid library. Selection of muscle-tropic variants in NHPs starting from the 120,000 RGD-fixed variants identified in mice, was performed in 2 female and 1 male 2 years old cynomolgus macaques and each animal was injected with the capsid library. For the pooled AAV-CBh-h*FXN* experiment, we injected 2 female and 1 male 2 years old cynomolgus macaques. The NHP injections were performed by intravenous infusion.

Cell lines

HEK293 was purchased from ATCC (ATCC, CRL-1573). HEK293FT, and HEK293FT AAVR KO cells were generous gift from Jan Carette.

Primary myoblasts and myotubes

Human and mouse primary myotubes were differentiated from human myoblasts and mouse satellite cells, respectively. Primary human skeletal muscle myoblasts were purchased from Lonza (Lonza, CC-2580). Primary mouse satellite cells were isolated from C57BL/6J mice as previously described (Cerletti et al., 2008).

METHOD DETAILS

Constructs

Plasmid used for generating AAV-CMV-EGFP was generated by cloning the Cytomegalovirus (CMV) promoter, EGFP coding sequencing, and the bovine growth hormone polyadenylation signal (bGH pA) into the pZac2.1 AAV plasmid backbone using Gibson assembly. The pZac2.1 construct was purchased from the University of Pennsylvania vector core. Constructs used for generating AAV-CMV-Nluc and AAV-CMV-Fluc were produced by replacing the EGFP coding sequence in the pZac2.1-CMV-EGFP-bGH pA with the Nluc and Fluc coding sequences, respectively. Plasmids used for generating the AAV-CMV-Cre and AAV-CRISPR viruses were described previously (Goldstein et al., 2019; Tabebordbar et al., 2016). The plasmid library recipient plasmid was generated by

cloning the CMV, MHCK7 (Salva et al., 2007), or CK8 (Bengtsson et al., 2017) promoters, splicing sequences of the AAV2 rep, AAV9 capsid coding sequence containing BsmBI restriction sites immediately after Q486 and Q588, and a SV40 polyadenylation signal, into an ITR-containing backbone using Gibson assembly. For generating constructs encoding for integrin proteins and AAVR, coding sequences of human integrin αV, α5, α8, αIIb, β1, β3, β5, β6, β8, and AAVR were amplified from human skeletal muscle cDNA using primers listed in table S1. The amplicons were inserted into a pUC57 backbone downstream of a human elongation factor 1 alpha (EF1α) promoter and upstream of the SV40 late polyadenylation signal sequence using Gibson assembly. Plasmid used for producing AAV-MHCK7-hMTM1 was generated by cloning the MHCK7 promoter, the chimeric intron from the pCI-neo mammalian expression vector (Promega, E184A), human MTM1 (hMTM1) coding sequence, and the bGH pA into the pZac2.1 AAV plasmid backbone using Gibson assembly. The pZac2.1-CK8-microdystrophin-FLAG was cloned by incorporating the CK8 promoter, coding sequence of a five repeat microdystrophin (Hakim et al., 2017), a FLAG tag, and a synthetic polyadenylation signal (Levitt et al., 1989) between the ITRs of the pZac2.1 backbone. The pZac2.1-CBh-h*FXN*-HA-bGH pA construct was cloned by incorporating the CBh promoter, human frataxin (h*FXN*) coding sequence, HA tag, and the bGH pA between the ITRs of the pZac2.1 backbone using gibson assembly. A pool of 50 unique 12-bp barcodes was inserted after the HA tag and the stop codon and before the bGH pA sequence in the pZac2.1-CBh-h*FXN*-HA-bGH pA plasmid used for generating recombinant AAV produced with each of the top MyoAAV variants for the pooled characterization experiment. Barcodes were randomly generated with a minimum Hamming edit distance of 4 between any two barcodes.

First and second round capsid library generation

For preparing capsid libraries for the first round of selection, we digested the AAV library recipient plasmid containing the CMV or MHCK7 promoter with BsmBI. We amplified a fragment encoding for the random 7-mer using the lib-F (5′-GCAACATGGCTGTC CAGGGAAGAAACTACATACCTG-3′) and NNK-R (5′-GTTTTGAACCCAGCCGGTCTGCGCCTGTGCMNNMNNMNNMNNMN NMNNMNNTTGGGCACTCTGGTGGTTTGTGGCC-3′) primers using the AAV9 capsid coding sequence as the template and incorporated this fragment into the digested library recipient plasmid using Gibson assembly. This library results in 32 possible DNA permutations and 20 amino acids encoded by each NNK codon resulting in a theoretical diversity of 327 (~34.36 billion) variants at the DNA level and 207 (~1.28 billion) variants at the amino acid level. However, diversity of the capsid library is dependent on the percentage of inserts that enable formation of capsid particles. We have been able to identify at least 5,000,000 unique capsid variants in our first-round virus libraries based on next generation sequencing analysis. For generating the second-round plasmid library, we used pools of oligonucleotides encoding for the variants selected in the first round, as well as the synonymous DNA codon replicates, synthesized by Agilent. The oligonucleotide library pools were used instead of the NNK-R primer to generate the amplicon for Gibson assembly into the digested library recipient plasmid. HEK293 cells were seeded in 15 cm dishes at a density of 2 x10^7 cells/dish 1 day before transfection. Each plate was transfected with 16 μg of the pALDX-80 helper plasmid (Aldevron), 8 μg of the Rep-AAP plasmid (a generous gift from Ben Deverman (Deverman et al., 2016), 8 μg pUC19 and 10 ng of the plasmid library using PEI MAX (Polysciences, 24765-1). Capsid library was harvested from cells and media, and purified by ultracentrifuge using a iodixanol gradient as previously described (Challis et al., 2018).

Recombinant AAV production

HEK293 cells were plated in 15 cm dishes at a density of 2 x10^7 cells/dish. The next day, each plate was transfected with 16 μg of the pALDX-80 helper plasmid (Aldevron), 8 μg of the Rep/Cap plasmid, and 8 μg of the ITR-containing plasmid using PEI MAX (Polysciences, 24765-1). Recombinant virus was harvested from the cells and media, and purified by ultracentrifuge using a iodixanol gradient as previously described (Challis et al., 2018). AAV titers were quantified by taqman-based qPCR. Primer and probe sequences for qPCR are listed in table S2.

In vivo selection in mice and cynomolgus macaques

For selection of the first-generation of MyoAAV variants in mice, we injected each mouse with 1E+12 vg of the capsid library. In the first round of selection for the second-generation MyoAAV variants, each mouse was injected with 1E+12 vg of the capsid library. In the second round of selection for identifying the second-generation MyoAAV variants in mice, one group of mice were injected with 1E+12 vg of the capsid library per mouse and another group with 1E+11 vg of the capsid library per mouse. For the first round of selection of muscle-tropic variants in cynomolgus macaques (starting from a random 7-mer insert library), animals were injected with 1E+13 vg/kg of the capsid library. For the second round of selection in NHPs, animals were injected with 3E+13 vg/kg of the capsid library. For selection of muscle-tropic variants in NHPs starting from the 120,000 RGD-fixed variants identified in mice, each animal was injected with 3E+13 vg/kg of the capsid library. Three weeks after injection, animals were perfused with saline and tibialis anterior, quadriceps, gastrocnemius, triceps, abdominal, pectoralis major, hamstring, biceps, and diaphragm, and heart muscles were harvested for analysis. Total RNA was extracted from all mouse tissues using TRIzol reagent (Thermo Fisher, 15596026) and DNA was extracted using the quickextract DNA extract solution (Lucigen, QE09050). mRNA was enriched from the total RNA samples using oligo dT beads (NEB, S1419S). Enriched mRNA was then treated with Turbo DNase (Thermo Fisher, AM2239) and cDNA synthesis was performed using SuperScript IV reverse transcriptase (Thermo Fisher, 18090050) and a capsid-specific primer (5′-GAAAGTTGCCGTCCGTGTGAGG-3′). Capsid variants DNA and expressed mRNA were amplified from the DNA and cDNA samples, respectively, with primers binding to upstream (5′-ACAAGTGGCCACAAACCACCA-3′) and

downstream (5′-GGTTTTGAACCCAGCCGGTC-3′) of the 7-mer insert using the Q5 High Fidelity 2x master mix. Amplicons containing the Illumina adapters and unique indices (NEB E7600S) were quantified using qubit, pooled at equimolar ratio, and sequenced on a Nextseq. For the pooled rAAV characterization experiment, rAAVs composed of each of the top 15 capsid variants, as well as AAVrh74 and AAV9 were produced individually using the barcoded pZac2.1-CBh-h*FXN*-HA-bGH pA plasmids. Plasmids used for producing the rAAV for each of the capsid variants contained a set of unique barcodes that was used to quantify transgene expression after transduction by that capsid variant. An equal amount of the rAAVs containing each of the 15 top capsid variants, as well as AAVrh74 and AAV9 were mixed with each other to prepare the virus mix injected to the animals. 2 female and 1 male 2 years old cynomolgus macaques, as well as 2 male and 3 female 8 weeks old C57BL/6J mice were injected with 3E+13 vg/kg of the pooled virus mix (1.76E+12 vg/kg for each capsid variant). Tissues were harvested from the animals 4 weeks after AAV administration. RNA extraction, mRNA enrichment, and Turbo DNase treatment was performed as described above. cDNA synthesis was performed using SuperScript IV reverse transcriptase (Thermo Fisher, 18090050) and a bGH pA-specific primer (5′- TTCACTGCATTCTA GTTGTGGTTTG-3′). Barcoded hFXN transcripts were amplified from cDNA samples with primers binding to upstream (5′-CCATAC GATGTTCCAGATTACGC-3′) and downstream (5′-CAATGTATCTTATCATGTCTGCTCGA-3′) of the barcodes using the Q5 High Fidelity 2x master mix. Amplicons containing the Illumina adapters and unique indices (NEB, E7600S) were quantified using qubit, pooled at equimolar ratio, and sequenced on a Nextseq.

Next generation sequencing data analysis

Illumina sequencing reads were demultiplexed using bcl2fastq2-v2.17.1. The resulting FASTQ sequences were filtered to keep only those which were directly matched to corresponding construct sequences surrounding the variable region, from which the 21 bp variant sequence was extracted. For paired end sequencing runs, the variant was further filtered to keep only variants that were consistent in both the forward and reverse reads. Variants were counted for each sample and normalized by the sequencing depth as reads per million (RPM). Additional normalization was also performed as necessary by dividing the RPM of variants by the RPM of the same variant in the matched virus library sample. To simplify further analysis, sample variants with fewer than 10 reads were discarded for future analysis. Variants were ranked using the RPM ratio of sample RPM divided by the virus library RPM, and the highest scoring variants were identified to be used in a second round of selection. For each selected amino acid variant, a variant encoding for the same amino acids with a synonymous DNA codon was included in the design of the second-round library as a control. For variants with synonymous variants already observed in the sequenced samples, the highest scoring synonymous variant was included in the second-round design. For variants with no synonymous version among the sequenced samples, a synonymous variant was computationally generated by randomizing each possible codon of the original amino acid sequence to a different codon if possible, thus maximally scrambling the original DNA sequence. Additionally, we designed 5% of the oligos to be random variants containing a stop codon to control for cross-packaging during the virus library production. Sequencing data from the second-round selection using designed variants was processed and counted as above, with the additional restriction that variants not matching the oligo design pool were filtered out. To analyze the data from the h*FXN* pooled virus experiment, sequencing reads were matched to the backbone template to identify the counts of all barcodes in the library pool. For each variant, the top 10 strongest and 5 weakest barcodes, as determined by overall rpm ratio compared to the virus library across the entire sequencing run, were excluded as outliers from downstream analysis, leaving 35 midrange barcodes to determine the average level of transgene expression for each specific capsid variant.

Exon skipping, transgene expression, and vector genome quantification

For the AAV-CRISPR, AAV-CMV-EGFP, AAV-MHCK7-h*MTM1* and AAV-CK8-microdystrophin-FLAG experiments, RNA was extracted from tissue samples using TRIzol (Thermo Fisher, 15596026). For samples from the AAV-CRISPR and microdystrophin experiments, extracted RNA was treated with Turbo DNase (Thermo Fisher, AM2239), and cDNA was made using the SuperScript IV VILO Master Mix (Thermo Fisher, 11754050). A taqman assay against exon 4-5 junction was used for quantification of total *Dmd* transcripts, and another assay against exon 22-24 junction was used for quantification of exon23-deleted transcripts (Table S2). For each of the exon 4-5 and exon 22-24 amplicons, a standard curve was generated by amplifying a gblock containing the taqman assay target sequences in each run. Total amount of *Dmd* transcripts and exon 23-deleted transcripts were quantified based on the standard curves. SaCas9 and gRNA expression in these tissue samples were quantified using taqman assays listed in table S2. Mouse GAPDH mRNA was used as the housekeeping control for quantification of SaCas9 and gRNA expression. For samples from the AAV-CMV-EGFP, AAV-MHCK7-h*MTM1* experiments, extracted RNA was treated with Turbo DNase (Thermo Fisher, AM2239), and cDNA was generated using SuperScript IV reverse transcriptase (Thermo Fisher, 18090050) with an oligo dT primer. Taqman assay used for quantifying EGFP in these samples are listed in table S2. Microdystrophin mRNA was quantified using the taqman assay listed in table S2 and mouse beta actin mRNA was used as the housekeeping control for quantification of microdystrophin expression. hMTM1 mRNA was quantified using the taqman assay listed in table S2 and mouse GAPDH mRNA was used as the housekeeping control for quantification of hMTM1 expression. Mouse GAPDH and beta actin mRNA (housekeeping controls) were quantified using predesigned taqman assays Mm.PT.39a.1 and Mm.PT.39a.22214843.g from IDT, respectively. For the vector genome quantification experiments, total DNA was extracted from tissue samples using the quickextract DNA extract solution (Lucigen, QE09050). Number of vector genomes per diploid genome was quantified based on qPCR using taqman assays designed to amplify the transgene (EGFP, microdystrophin, or hMTM1) or mouse GAPDH DNA (table S2). Absolute number of transgene and GAPDH molecules in

each sample was quantified using standard curves generated by amplifying different amounts of the taqman assay target sequences in each run.

Immunofluorescence

For tissues harvested from C67BL/6J mice injected with AAV-CMV-EGFP, samples were fixed with 4% paraformaldehyde (PFA) for 1 h at room temperature (RT) and washed 3 times with DPBS. Fixed tissues were immersed in 30% sucrose at 4°C until submersion, embedded in O.C.T compound (Tissue-Tek, 25608-930), and frozen in liquid nitrogen-cold isopentane. Muscles harvested from mdx mice injected with AAV-CRISPR were frozen in liquid nitrogen-cold isopentane immediately after dissection. Tissues were sectioned using CM1860 cryostat (Leica Biosciences) at the thickness of 12 μm. Laminin and DYSTROPHIN immunostaining of tissue sections was performed as previously described (Tabebordbar et al., 2016). For the microdystrophin-FLAG immunostaining, tissue sections were stained with a rabbit anti-FLAG antibody (Sigma, F7425) using the same protocol as Dystrophin immunostaining. For the Lectin staining of the liver samples, tissue sections were washed 3 × 5 min with PBST (PBS + 0.1% Tween-20), incubated with Lycopersicon Esculentum (Tomato) Lectin labeled with Dylight 594 (Vector laboratories, DL-1177-1) at 10 μg/mL for 10 min at RT, washed 3 × 5 min with PBST, stained with Hoechst 33342 (Thermo Fisher, H3570) at 10 μg/mL for 5 min, washed 2 × 5 min with PBST and mounted with Vectashield antifade mounting medium without DAPI (Vector Laboratories, H-1400-10). *In vitro* differentiated myotubes were immunostained for Myosin Heavy Chain (MHC) as previously described (Tabebordbar et al., 2016). For the integrin β6 (ITGB6) immunostaining, mouse, cynomolgus macaque, or human muscle tissue samples were stained with a rabbit monoclonal antibody to ITGB6 (abcam, ab187155) using the same protocol as Dystrophin staining.

Western blot

Protein lysates from tissue samples were prepared in radioimmunoprecipitation assay (RIPA) buffer (Cell Signaling Technologies, 9806S). Protein lysates from HEK293 cells overexpressing pUC19 or α8, αIIb, β3, or β8 integrin single chains were prepared by lysis in NP-40 lysis buffer (150 mM NaCl, 50 mM Tris-HCl pH7.5, 1% NP-40). All protein lysates were centrifuged to remove debris. Total protein concentrations were determined using the Pierce 660 protein assay reagent (Thermo Fisher, 22660) and measured on the Cytation 5 plate reader (BioTek). Equal amounts of total protein from each sample were loaded for all western blots.

For the dystrophin western blots, proteins were fractionated by SDS-PAGE on 3%–8% Tris-Acetate precast polyacrylamide gels (Bio-Rad, 3450129). For all western blots, proteins were fractionated on 4%–20% Mini-PROTEAN TGX precast polyacrylamide gels (Bio-Rad, 4561096). For the dystrophin blots, the first three lanes on each gel contain different percentages of wild-type muscle proteins diluted with mdx proteins from the same muscle type so that the total protein amount for all the lanes are the same. Tris-glycine SDS running buffer (25 mM Tris, 192 mM glycine, 0.1% SDS, pH 8.3) was used for electrophoresis except for in the dystrophin experiment, where XT Tricine buffer (Bio-Rad, 1610790) was used. All gels were transferred to PVDF membranes in Towbin transfer buffer (25 mM Tris, 192 mM glycine, 10% v/v methanol, pH 8.3), except for in the dystrophin experiment, where CAPS transfer buffer was used (10 mM CAPS, 10% v/v methanol, pH 11).

Membranes were blocked for 1 h in blocking buffer consisting of 5% w/v nonfat dry milk (Fisher Scientific, NC9959266) in TBST (TBS + 0.1% Tween-20). All membranes were then incubated for 16 h at 4þC in primary antibody diluted in blocking buffer. Primary antibodies used were against integrins α8 (Thermo Fisher MA5-31449, 1:1000), αIIb (Abcam ab134131, 1:5000), β3 (R&D Systems AF2266, 1 μg/mL), and β8 (Thermo Fisher PA5-76390, 1:500), eGFP (Thermo Fisher MA1-952, 1:2000), MTM1 (Abnova PAB6061, 1:1000), FLAG tag (Sigma F7425, 1:400), dystrophin (Abcam ab15277, 1:100), GAPDH (Santa Cruz sc-32233, 1:25,000), alpha tubulin (Abcam ab7291, 1:5000), and vinculin (R&D Systems MAB6896, 2 μg/mL). Blots were washed three times for 10 min each with TBST and then incubated with a secondary antibody diluted in blocking buffer for 2 h at room temperature. Secondary antibodies used were horse anti-mouse HRP (Cell Signaling Technologies 7076P2, 1:5000, for the mouse primary antibodies), goat anti-rabbit HRP (Abcam ab97051, 1:5000, for the rabbit primary antibodies), and donkey anti-goat HRP (Jackson Immunoresearch 705-035-147, 1:5000, for the goat anti-MTM1 primary antibody). Blots were washed three times with TBST and developed with SuperSignal West Dura substrate (Thermo Fisher, 34075, for dystrophin blots) or SuperSignal West Pico PLUS substrate (Thermo Fisher, 34580, all other blots). Blots were imaged on the FluorChem E CCD imager (Protein Simple), except for the integrin αIIb blot, which was imaged on X-ray film.

In vitro AAV transduction and binding experiments

HEK293, HEK293FT, and HEK293FT AAVR KO were maintained in DMEM (Thermo Fisher, 10564029) containing 5% fetal bovine serum (Thermo Fisher, A3160402). For the integrin overexpression experiments, HEK293 cells were transfected in 96 well plates (Thermo Fisher, 161093) with different pairs of integrin constructs at a total of 100 ng plasmid/well using PEI MAX (Polysciences, 24765-1) the next day. For transduction assays, 72 h after transfection, cells were transduced with 1E+4 vg/cell of AAV9- or MyoAAV 1A-CMV-Nluc and luminescence was measured with the Nano-Glo Luciferase Assay Reagent (Promega, N1120) on the SpectraMax L microplate reader (Molecular Devices) 24 h post transduction. For binding assays, cells were chilled on ice to inhibit endocytosis and AAV9-, or MyoAAV 1A-CMV-Nluc were added to the cells at 1E+4 vg/cell 72 h after transfection. Cells were kept on ice for 30 min and they were washed 3 times with PBS before they were lysed in quickextract DNA Extract solution (Lucigen, QE09050). Vector genomes and diploid genomes were quantified by taqman qPCR using assays targeting the Nluc coding sequence and human GAPDH genomic locus listed in table S2.

For the AAVR dependency experiments, HEK293FT AAVR KO and HEK293FT AAVR WT cells were transduced with AAV2-, AAV4-, AAV9-, MyoAAV 1A, MyoAAV 3A, MyoAAV 4A, MyoAAV 4C, or MyoAAV 4E-CMV-NLuc at 1E+3 vg/cell 24 h after being seeded into 96-well plates. For the AAVR rescue experiment, HEK293FT AAVR KO and HEK293FT WT cells were transfected with 33.3ng of each integrin construct or pUC19 and 33.3 ng of AAVR construct or pUC19, such that a total of 100 ng plasmid DNA was used per transfection. 48 after transfection, cells were transduced with MyoAAV 1A-CMV-Nluc at 1E+3 vg/cell and luminescence was measured with the Nano-Glo Luciferase Assay Reagent (Promega, N1120) on the SpectraMax L microplate (Molecular Devices) reader 24 h after transduction.

Small molecule and antibody inhibition experiments

Human primary myoblasts were maintained in SkGM-2 media (Lonza, CC-3245) at 37þC with 5% CO2. Mouse satellite cells were expanded in the mouse muscle stem cell growth media (20% horse serum (Thermo Fisher, 16050130) in F10 (Thermo Fisher, 1155043) containing 1% Glutamax (Thermo Fisher, 35050061), 1% penicillin-Streptomycin (Thermo Fisher, 15140122), and 5 ng/mL bFGF (Sigma, F0291-25 ug)) for 6 days. Human and mouse myoblasts were seeded into 96-well plates (Thermo Fisher, 161093) coated with collagen (Thermo Fisher, A1048301) and laminin (Thermo Fisher, 23017015) at a density of 15,000 cells/well. 24 h following plating, media was changed to DMEM (Thermo Fisher, 10564029) containing 2% horse serum (Thermo Fisher, 16050130) and myoblasts were allowed to differentiate into myotubes for 4-6 days.

Pan-alpha V integrin antagonists CWHM-12 (MedChem Express, HY-18644) and GLPG0187 (MedChem Express, HY-100506), anti-aVb6 antibody (Abcam, ab77906), and mouse IgG2a isotype control (BioLegend, 401508) were diluted in DMEM containing 2% horse serum at the specified concentrations. Media was removed from differentiated human skeletal muscle myotubes and replaced with the diluted inhibitors, after which the myotubes were incubated on ice for 30 min to inhibit endocytosis. Following this incubation, AAV9-, MyoAAV 1A-, MyoAAV 2A, MyoAAV 3A-, MyoAAV 4A-, MyoAAV 4C-, or MyoAAV 4E-CK8-Nluc were added to the cells at 1E+4 vg/cell and the plates were transferred back to the tissue culture incubators. 24 h after transduction, luciferase intensity was measured with the Nano-Glo Luciferase Assay (Promega, N1120).

Recombinant protein inhibition experiments

AAV9-, MyoAAV 1A-, MyoAAV 2A-, MyoAAV 3A-, MyoAAV 4A-, MyoAAV 4C-, or MyoAAV 4E-CK8-Nluc were pre-incubated with recombinant soluble human integrin heterodimers αVβ1 (R&D Systems, 6579-AVB-050), αVβ3 (R&D Systems, 3050-AV-050), αVβ6 (R&D Systems, 3817-AV-050), αVβ8 (R&D Systems, 4135-AV-050), or maltose-binding protein (Novus Biologicals, NBC1-18538) at 37þC for 30 min. Virus and protein were then added to human primary skeletal muscle myotubes in 96-well plates at 1E+4 vg/cell. Cells were returned to 37þC for 24 h before luciferase intensity was measured with the Nano-Glo Luciferase Assay (Promega, N1120).

Lectin inhibition experiments

24 h after being seeded into poly-D-lysine coated 96-well plates (Corning, 356690) that were additionally coated with 0.1% gelatin (Sigma, ES-006-B), HEK293 cells were treated with 50 mU/mL Neuraminidase (NA) type III from *Vibrio cholerae* (Sigma, N7885-1UN) in 100 μL serum-free DMEM for 2 h at 37þC. Cells were then washed three times with cold DMEM before being treated with 50 μg/mL *Erythrina cristagalli* lectin (ECL, Vector Laboratories, L-1140-10) in 100 μL serum-free DMEM for 15 min at 4þC. The lectin solution was then removed, and the cells were treated with a mixture of 1E+4 vg/cell of AAV2-, AAV9-, or MyoAAV 1A-CMV-Nluc and 50 μg/mL ECL, or vector alone for control cells, for 1 h at 4þC. Cells were washed three times with cold DMEM. For the transduction experiments, warm complete medium was added to the cells, which were incubated for 24 h before luciferase intensity was measured with the Nano-Glo Luciferase Assay (Promega, N1120). For binding experiments, cells were lysed in quickextract DNA extract solution (Lucigen, QE09050) and vector genomes and diploid genomes were quantified by taqman qPCR as described above.

Flow cytometry

HEK293 cells overexpressing pUC19 or integrin single chains were harvested in PBS containing 5 mM EDTA and washed 3 times with staining buffer (2% FBS in PBS). The cells were then stained for 1 h at 4þC in primary antibody (listed in table S3) diluted in staining buffer. Cells were washed 3 times with staining buffer. For samples stained with the integrin β8 antibody, cells were incubated for 30 min at 4þC with a PE-conjugated goat anti-mouse IgG secondary antibody (Invitrogen, 12-4010-82, 1:80) diluted in staining buffer. Cells were washed 3 times, resuspended in staining buffer, and analyzed using a CytoFLEX S flow cytometer (Beckman). The flow cytometry data was analyzed with Flow Jo v10.7.

Mouse satellite cell isolation, culture, and differentiation

Satellite cell isolation from mdx-Ai9 mice injected with AAV-CMV-Cre was performed as previously described (Goldstein et al., 2019). Satellite cells isolated from the injected animals were seeded on collagen/laminin-coated plates in satellite cell growth media (20% horse serum (Thermo Fisher, 16050130) in F10 (Thermo Fisher, 1155043) containing 1% Glutamax (Thermo Fisher, 35050061), 1% penicillin-Streptomycin (Thermo Fisher, 15140122), and 5 ng/mL bFGF (Sigma, F0291-25 ug)). Growth media was changed every other day. After 6 days, satellite cells were harvested, cell numbers were counted and cells were re-plated in multiple wells of a 96 well plate at a density of 10,000 cells/well for differentiation. The next day, growth media was changed to differentiation media

(DMEM (Thermo Fisher, 10564029)) containing 2% donor horse serum (Thermo Fisher, 16050130)). Myotubes were fixed with 4% PFA 60 h after start of the differentiation.

Alanine Aminotransferase (ALT) and Aspartate Aminotransferase (AST) assay

8 weeks old male C57BL6/J mice were injected retro-orbitally with either saline, or 1E+12 vg (~4E+13 vg/kg) AAV9-, or MyoAAV 1A-CMV-EGFP (n = 5 per group). Prior to injection, a pre-bleed sample was collected. Blood was collected using a submandibular bleed and spun down in a serum separator tube (BD). Serum samples were collected again at 14 days and 28 days post injection. ALT activity was measured using an ALT Activity Assay from Sigma (Catalog #:MAK052) based on manufacturer's instructions for fluorometric detection using a 1:25 serum dilution. AST activity was measured with an AST Activity Assay from Sigma (Catalog #:MAK055). AST activity was also measured in duplicates according to the manufacturer's instructions for colorimetric detection using a 1:5 serum dilution.

In Vitro Neutralizing Antibody Assay

Titers of AAV neutralizing antibodies (NAbs) were determined via an *in vitro* neutralizing antibody assay. For the cross-reactivity experiment, serum from 8 weeks old C57BL/6J mice was collected 1 week after injection with either 1E+12 vg AAV9- or MyoAAV 1A-CMV-EGFP (n = 5 mouse serum samples per group, n = 3 technical replicates for each assay condition). Cells were seeded in 96-well poly-D-lysine coated plates (Corning, 356690) at a density of 35,000 cells/well. Twenty-four h later, serum from the mice was serially diluted and then incubated with 2.5E+3 vg/cell AAV9- or MyoAAV 1A-CMV-Nluc for 1 h at 37þC. The neutralized sample was then added in triplicate to the cells and returned to 37þC for 24 h. Luminescence was then measured with the Nano-Glo Luciferase Assay Reagent (Promega, N1120) on the SpectraMax L microplate reader (Molecular Devices). Serum samples from NHPs were analyzed for the presence of the anti-AAV9 (for the *in vivo* the selection experiments), or anti-AAV9 and anti-AAVrh74 (for the pooled hFXN experiments) using the protocol mentioned above and AAV9- or AAVrh74-CMV-Nluc virus with 1:1, 1:3, 1:5, 1:8, 1:10, and 1:31.6 dilutions of the serum. Animals with less than 50% inhibition at the 1:3 dilution were selected for the experiments.

Mouse activity measurement

The compact infrared actimeter (Harvard Apparatus, item numbers 76-0128, 76-0132, 76-0134, 76-0130, 76-0406, 76-0608, 76-0003) was used to measure the number of rearing events for each mouse every two weeks. Each animal was placed in the actimeter cage for 5 min and the number of rearing events were quantified for that period of time using the ACTITRACK V2.7 software. For measuring the spontaneous running wheel rotation, mice were housed individually at 5 weeks of age and throughout their lives in cages equipped with low-profile wireless running wheels (Med Associates, ENV-047). Animals had free access to their running wheels and could voluntarily run on them. The rotation of each wheel was continuously recorded, and the data was downloaded once a week when the running wheels were cleaned and inspected for proper operation. To normalize the data, the total activity of each week was expressed as the mean of total wheel rotations per h.

Mouse muscle physiology analysis

Mice were prepared for *in situ* evaluation of the tibialis anterior (TA) as previously described (Tabebordbar et al., 2016). The distal tendon of the TA was attached to a muscle lever system (Aurora Scientific, 305C) and adjusted to its optimal length for tetanic tension. Force was recorded over a range of stimulation frequencies. Sub-maximal forces were expressed relative to the muscles peak force. The resulting relative force data were fit by a sigmoidal curve of the form $p = P_{min} + ((P_{max} - P_{min}) / (1 + (K/f)H))$, where P is force at stimulation frequency f, P_{min} is the minimum force, P_{max} is the maximum force, K is the stimulation frequency at the inflection point of the curve, and H is the slope (Chan et al., 2007). The TA was then subjected to a series of 5 isometric-eccentric contractions to assess its susceptibility to injury. These contractions consisted of a 100 ms fixed-end contraction followed immediately by active lengthening at 4 fiber lengths/s to a final length of 1.2 fiber length, assuming a fiber length to muscle length ratio of 0.60. The series was bracketed by a pre- and a post-trial isometric contraction that were used to evaluate the change in isometric force. TA physiological cross-sectional area was calculated as previously described (Tabebordbar et al., 2016). Extensor digitorum longus (EDL) muscles were dissected from anesthetized mice and prepared for *in vitro* analysis as previously described (Alexander et al., 2014). Muscles were attached to a muscle lever system (Aurora Scientific, 300B-LR) and studied in a mammalian bicarbonate buffer maintained at 35°C and continually equilibrated with 95% O_2, 5% CO_2. Optimal length and the force-frequency relationship were determined in a manner similar to that used for the *in situ* TA. Muscle physiological cross-sectional area was calculated as previously described (Alexander et al., 2014).

Bioluminescence imaging

Mice were injected with 150 mg/kg of D-luciferin (Goldbio, LUCK-500) and anesthetized with isoflurane before imaging. The bioluminescence images were acquired 5 min after D-luciferin injection with a rate of one image per 2 min for 25 minutes using the IVIS spectrum CT *in vivo* imaging system (PerkinElmer, 128201). Total and average radiance was measured from the same size of the region of interest (ROI) using Living Image 4.7.3 software (PerkinElmer). The highest captured radiance over imaging time was determined as the peak of the kinetic curve and picked for analysis. To measure the radiance from the dissected muscles,

the mice were euthanized 12 min after D-luciferin injection. The dissected muscles were placed in a Petri dish followed by bioluminescence imaging using the IVIS spectrum CT *in vivo* imaging system.

QUANTIFICATION AND STATISTICAL ANALYSIS

All statistical analysis was performed with Graphpad Prism v9 (GraphPad Software, Inc., La Jolla, CA, USA). All data are presented as mean ± SD (standard deviation). Datasets with an unequal variance between groups were log transformed prior to statistical analysis and this information has been noted in the figure legends. Assumptions of equal variance and normality were assumed for all other datasets. Comparisons between three or more groups were analyzed with a one-way or two-way ANOVA. Two-way ANOVA was used for datasets with two groups with multiple comparisons (in Figures 5K and S3K, L). For Figures 3G, I and S4G, the difference between the AAV9- and MyoAAV 1A-MHCK7-h*MTM1* groups were analyzed with multiple t tests with the Holm-Sidak multiple comparison test (MCT), since the number of animals in the AAV9 groups changed over time, as they reached the humane endpoint for euthanized, and two-way ANOVA could not be performed on these datasets. Post hoc tests for the ANOVA were performed using either the Dunnett multiple comparison test (MCT) when there was a control mean (as defined in the figure legend), the Tukey-Kramer MCT, or the Sidak's MCT (for comparison between two datasets with multiple comparisons in Figures 5K and S3K, L). For datasets with only two groups without multiple comparisons, a unpaired two-tailed Student's t test was performed. The post hoc test employed for datasets using multiple t tests was the Holm-Sidak MCT with $\alpha = 0.05$. The Kaplan-Meier plot in Figure 3J was analyzed using the Mantel-Cox test for AAV9 and MyoAAV 1A groups. A significance cutoff of $\alpha = 0.05$ was used for all datasets except Figures 4A, 4B, 7G-J which had a significance cutoff of $\alpha = 0.01$. The n for each dataset is defined in the figure legends.

CellPress
OPEN ACCESS

Supplemental figures

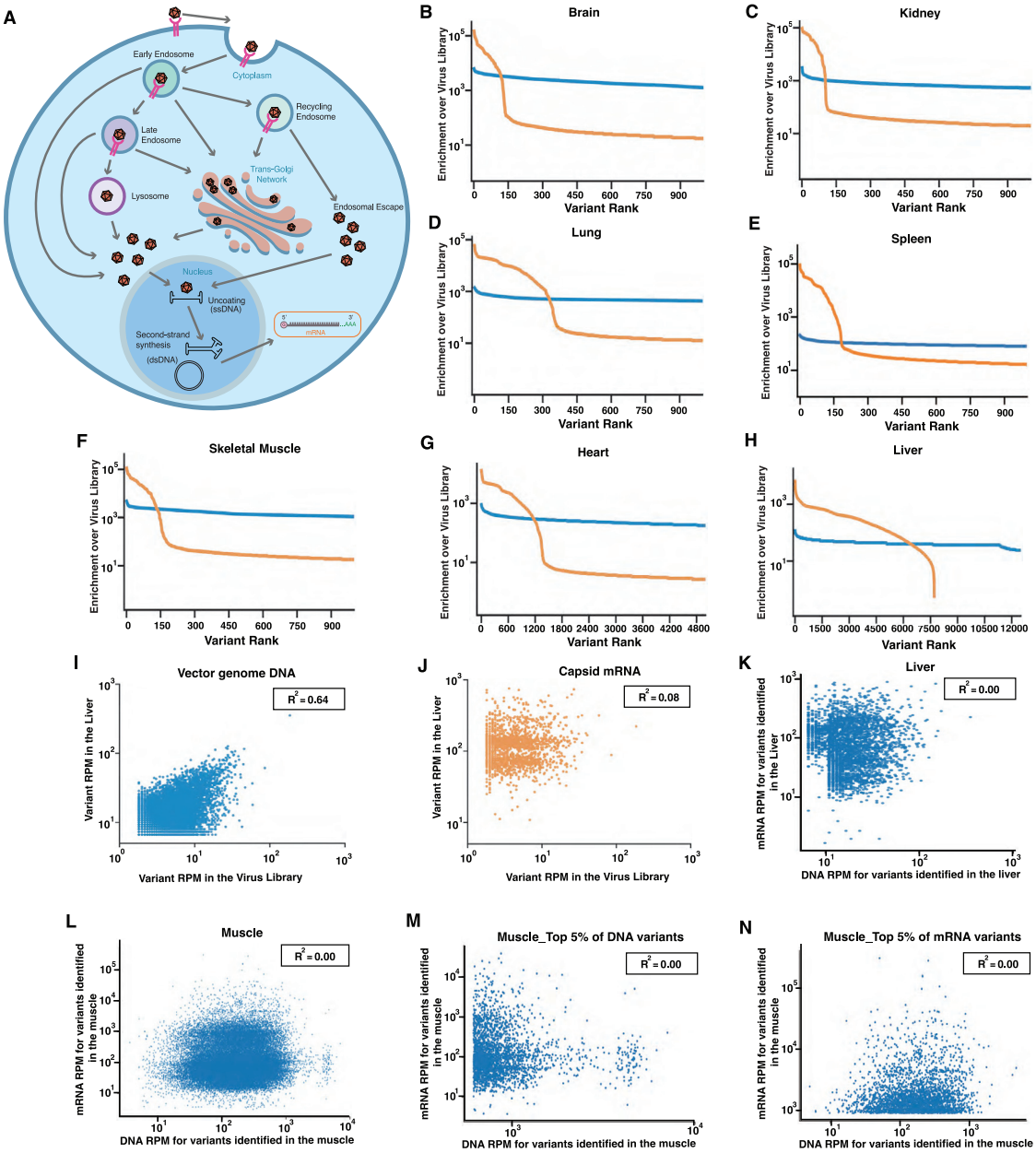

Figure S1. DELIVER allows selection of capsid variants capable of functional transduction in various tissues

(A) Schematic representation of different steps in AAV transduction.

(B–H) Graphs showing enrichment of capsid variants expressed under the ubiquitous CMV promoter over virus library at the DNA and mRNA level in Brain (B), Kidney (C), Lung (D), Spleen (E), Skeletal Muscle (F), Heart (G), and Liver (H) of 8 weeks old C57BL/6J mice injected with 1E+12 vg of the AAV capsid library. Transcript-based selection as used in DELIVER enables more stringent identification of functional capsid variants compared to DNA-based selections. Enrichment over the virus library is calculated by dividing reads per million (RPM) for each variant identified in the tissue by RPM of the same variant in the virus library.

(I and J) Correlation between abundance of each capsid variant in the virus library with abundance of vector genome DNA (I) or expressed mRNA (under the control of CMV promoter, J) from that variant identified in the liver of mice injected with the virus library. While the relative amount of the vector genome DNA from

(legend continued on next page)

each variant is correlated with the abundance of that variant in the virus library, there is almost no correlation between the levels of capsid mRNA expression from each variant and quantity of that variant in the virus library based on the linear regression between the two sample types.
(K and L) Correlation between abundance of each capsid variant identified in the liver (K), or muscle (L), at the vector genome DNA and transgene mRNA levels.
(M and N) Correlation between abundance of the top 5% DNA (M) or top 5% mRNA (N) variants identified in muscle, at the vector genome DNA and transgene mRNA levels. RPM: Reads Per Million.
Related to Figure 1.

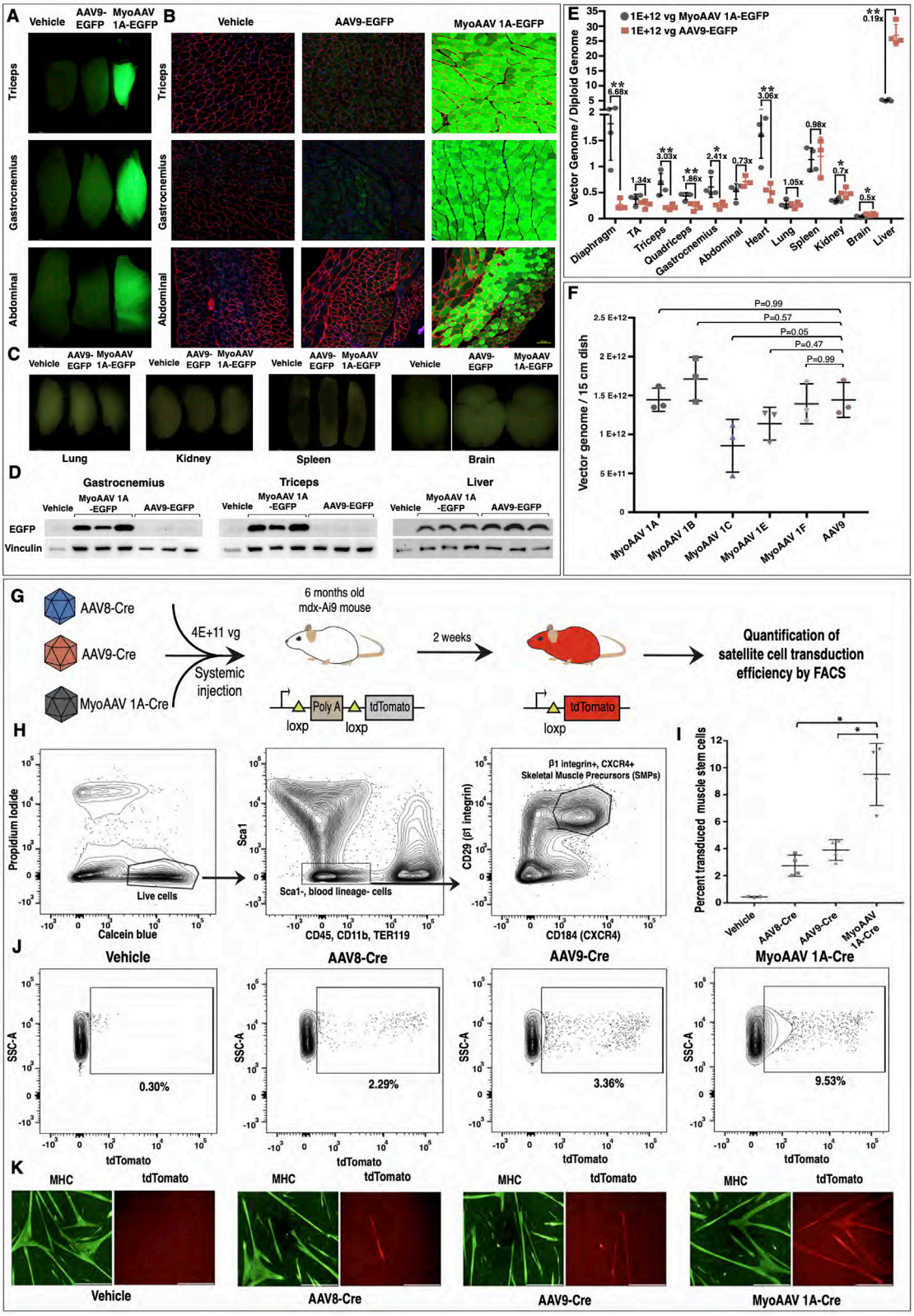

(legend on next page)

Figure S2. MyoAAV 1A produces recombinant AAV with similar titers compared to AAV9 and transduces muscle stem cells more effectively than AAV8 and AAV9 after systemic delivery to adult mdx-Ai9 mice

(A and B) Whole mount fluorescent (A) and cross section (B) images of Triceps, Gastrocnemius, and Abdominal muscles from 8 weeks old C57BL/6J mice systemically injected with 1E+12 vg of AAV9- or MyoAAV 1A-CMV-EGFP. Tissues were harvested 2 weeks after injection. Green: EGFP, Red: laminin, Blue: Hoechst. Scale bar in cross sections: 100 μm.

(C) Whole mount fluorescent images of Lung, Kidney, Spleen, and Brain from 8 weeks old C57BL/6J mice systemically injected with 1E+12 vg of AAV9- or MyoAAV 1A-CMV-EGFP.

(D) western blots detecting EGFP and Vinculin in muscles of 8 weeks old C57BL/6J mice injected with vehicle, or 1E+12 vg of AAV9- or MyoAAV 1A-CMV-EGFP.

(E) Quantification of vector genome per diploid genome in various tissues of 8 weeks old C57BL/6J mice injected with 1E+12 vg of AAV9 or MyoAAV 1A-CMV-EGFP. Data are presented as mean ± SD (n = 4); *: $p < 0.05$, **: $p < 0.01$ (Student t test).

(F) Comparison of recombinant AAV titers produced by the top RGD-containing capsid variants with wild type AAV9. Data are presented as mean ± SD (n = 3). P value calculated by one-way ANOVA with Dunnett's MCT with AAV9 as the control.

(G) Schematic of the satellite cell transduction analysis experiment. Delivery of Cre recombinase to cells containing the Ai9 locus results in removal of the STOP cassette from the genome and expression of tdTomato.

(H) Gating strategy for isolating skeletal muscle precursors from the mononuclear cells in the muscle.

(I) Percent tdTomato+ transduced muscle stem cells isolated from 6 months old mdx-Ai9 mice, 2 weeks after systemic injection with 4E+11 vg of AAV8-, AAV9-, or MyoAAV 1A-CMV-Cre. Data are presented as mean ± SD (n = 4); **: $p < 0.01$ (one-way ANOVA with Tukey-Kramer MCT).

(J) Representative FACS plots from muscle stem cells isolated from the injected mdx-Ai9 mice.

(K) Representative immunofluorescence images of myotubes differentiated from FACS sorted muscle stem cells isolated from 6 months old mdx-Ai9 mice injected systemically with 4E+11 vg of AAV8-, AAV9-, or MyoAAV 1A-CMV-Cre. Green, myosin heavy chain (MHC); red, tdTomato; blue, Hoechst. Scale bar: 400 μm.

Related to Figure 2.

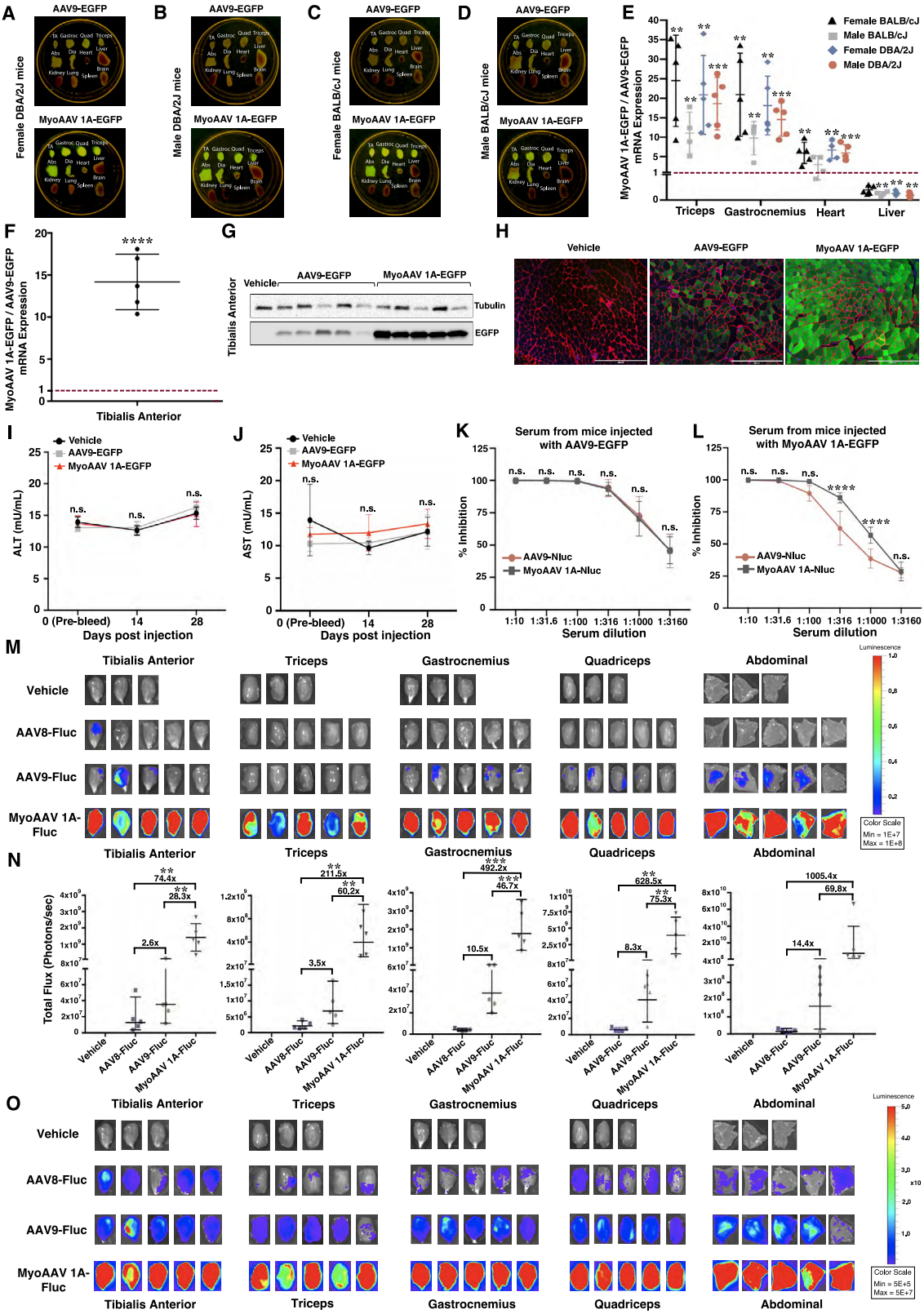

(legend on next page)

Figure S3. MyoAAV 1A effectively transduces different skeletal muscles after systemic administration in mice from DBA/2J and BALB/cJ backgrounds and is highly potent in muscle transduction after intramuscular delivery

(A–D) Different tissues of 8 weeks old female DBA/2J (A), male DBA/2J (B), female BALB/cJ (C), and male BALB/cJ (D) mice systemically injected with 1E+12 vg of AAV9-CMV-EGFP (top) or MyoAAV 1A-CMV-EGFP (bottom) illuminated by blue light. Tissues were harvested 2 weeks after AAV administration.

(E) Quantification of fold difference in EGFP mRNA expression in triceps, gastrocnemius, heart, and liver of 8 weeks old male and female DBA/2J and BALB/cJ mice systemically injected with 1E+12 vg of AAV9- or MyoAAV 1A-CMV-EGFP. Dashed red line indicates relative expression from AAV9-CMV-EGFP. Data are presented as mean ± SD (n = 4-5); **: $p < 0.01$, ***: $p < 0.001$ (Student t test between AAV9 and MyoAAV 1A injected mice for each group).

(F) Quantification of fold difference in EGFP mRNA expression in TA of 8 weeks old C57BL/6J mice intramuscularly injected with 2E+10 vg of AAV9- or MyoAAV 1A-CMV-EGFP. Dashed red line indicates relative expression from AAV9-CMV-EGFP. Data are presented as mean ± SD (n = 5); ****: $p < 0.0001$ (Student t test).

(G) western blots detecting EGFP and Tubulin in TA muscles of 8 weeks old C57BL/6J mice injected intramuscularly with vehicle, or 2E+10 vg of AAV9- or MyoAAV 1A-CMV-EGFP.

(H) Immunofluorescence images of the TA from 8 weeks old C57BL/6J mice intramuscularly injected with vehicle, or 2E+10 vg of AAV9- or MyoAAV 1A-CMV-EGFP. Green: EGFP, Red: laminin, Blue: Hoechst. Scale bar in cross sections: 400 μm.

(I and J) Quantification of ALT (I) and AST (J) enzyme levels in serums of 8 weeks old C57BL/6J mice before injection, as well as 14 and 28 days after systemic injection of vehicle, or 1E+12 vg AAV9- or MyoAAV 1A-CMV-EGFP. Data are presented as mean ± SD (n = 5). P value calculated by two-way ANOVA with Tukey-Kramer MCT. Significance threshold: $p < 0.05$. Difference between any two groups at each time point is not significant.

(K and L) Inhibition of AAV9- or MyoAAV 1A-CMV-Nluc transduction in HEK293 cells by serum isolated from 8 weeks old C57BL/6J mice injected with 1E+12 vg of AAV9-CMV-EGFP (K) or MyoAAV 1A-CMV EGFP (L); Data are presented as mean ± SD (n = 5); ****: $p < 0.0001$ (two-way ANOVA with Sidak's MCT).

(M) Whole organ luminescence images of TA, Triceps, Gastrocnemius, Quadriceps, and Abdominal muscles from BALB/cJ mice injected with 4E+11 vg of AAV8-, AAV9-, or MyoAAV 1A-CMV-Fluc harvested 4 months after injection. Color scale: 1E+7 – 1E+8.

(N) Quantification of total luminescence from different muscles of animals injected with 4E+11 vg of AAV8-, AAV9-, or MyoAAV 1A-CMV-Fluc harvested 120 days after injection. Data are presented as mean ± SD (n = 5); **: $p < 0.01$, ***: $p < 0.001$ (one-way ANOVA with Tukey-Kramer MCT).

(O) Whole organ luminescence images of TA, Triceps, Gastrocnemius, Quadriceps, and Abdominal muscles from BALB/cJ mice injected with 4E+11 vg of AAV8-, AAV9-, or MyoAAV 1A-CMV-Fluc harvested 4 months after injection. This image shows the luminescence signal from the same mice shown in Figure 3C with a different color scale (5E+5 – 5E+7) to enable detection of the signal in muscles of mice injected with AAV8- and AAV9-CMV-Fluc.

Related to Figure 2.

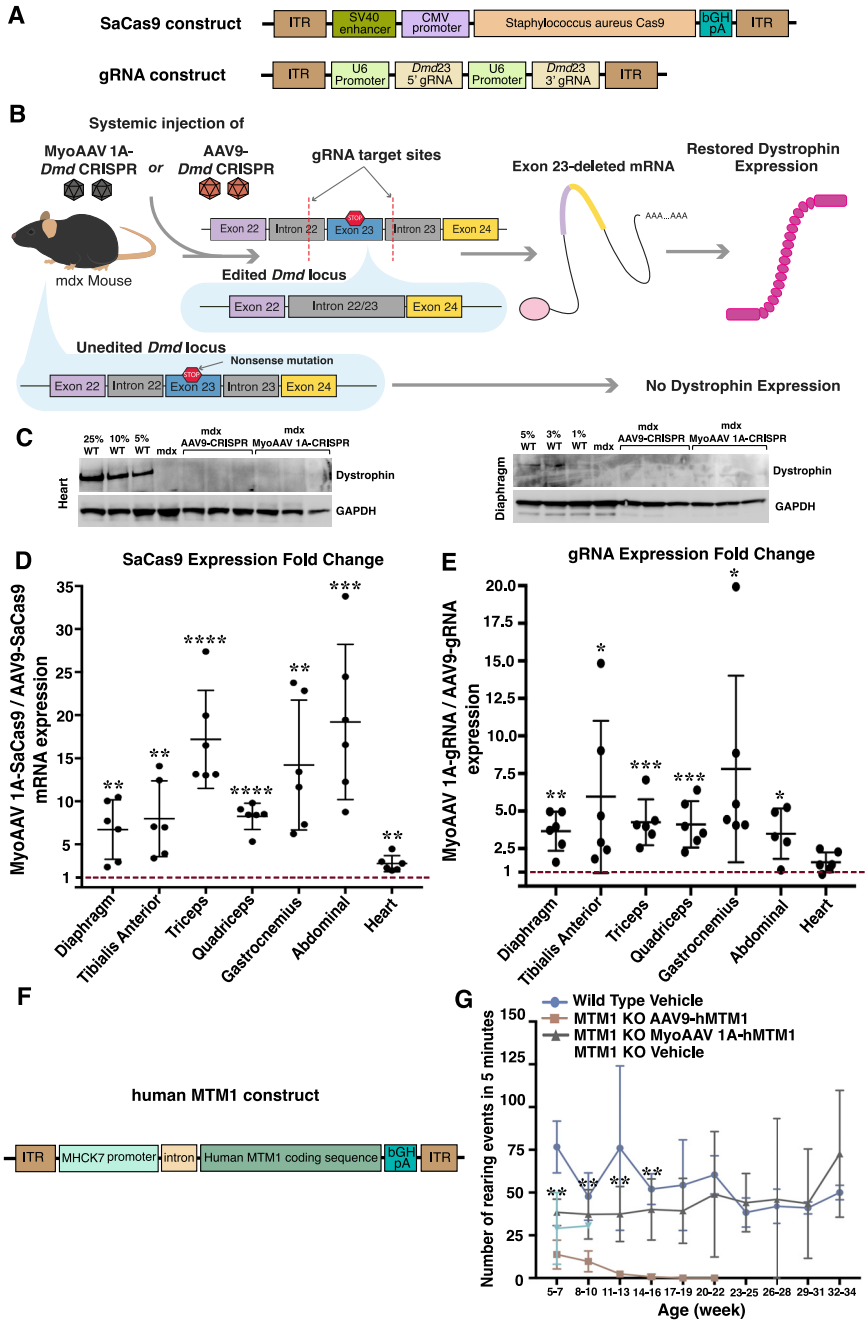

Figure S4. MyoAAV 1A-*Dmd* CRISPR systemic administration results in higher levels of SaCas9 and gRNA expression compared to AAV9-*Dmd* CRISPR in multiple muscles throughout the body

(A) Schematic of the AAV constructs used to generate the AAV9- and MyoAAV 1A-*Dmd* CRISPR viruses.

(B) Schematic of dystrophin restoration after AAV-*Dmd* CRISPR administration to 8 weeks old mdx mice. Mice were injected with 4.5E+12 vg of SaCas9 and 9E+12 vg of gRNA AAV. Tissues were harvested 1 month after injection.

(C) western blots detecting dystrophin and GAPDH in the heart (left) and diaphragm (right) from 8 weeks old mdx mice injected with AAV9- or MyoAAV 1A-*Dmd* CRISPR.

(D and E) Quantification of fold difference in SaCas9 mRNA (D) or gRNA (E) expression in different muscles of 8 weeks old mdx mice systemically injected with 4.5E+12 vg of AAV9- or MyoAAV 1A-CMV-SaCas9 and 9E+12 vg of AAV9- or MyoAAV 1A-gRNA. Dashed red line indicates relative expression from AAV9-CMV-SaCas9 (C) and AAV9-gRNA (D). Data are presented as mean ± SD (n = 5-6); *: $p < 0.05$, **: $p < 0.01$, ***: $p < 0.001$, ****: $p < 0.0001$ (Student t test).

(F) Schematic of the AAV construct used to generate the AAV9- and MyoAAV 1A-MHCK7-h*MTM1* viruses.

(legend continued on next page)

(G) Number of rearing events in 5 min by wild type mice, or *Mtm1* KO mice injected with vehicle, AAV9-h*MTM1*, or MyoAAV 1A-h*MTM1*, both at 2E+12 vg/kg. Data are presented as mean ± SD (n = 6 for KO AAV9, n = 6 for KO MyoAAV 1A, n = 3 for wild type vehicle, n = 4 for KO vehicle) for weekly measurements averaged across three-week time periods. Data points for the *Mtm1* KO mice injected with vehicle are from a previous experiment. P value calculated between MyoAAV 1A and AAV9 groups; **: $p < 0.01$ (Multiple t tests with Holm-Sidak MCT).
Related to Figure 3.

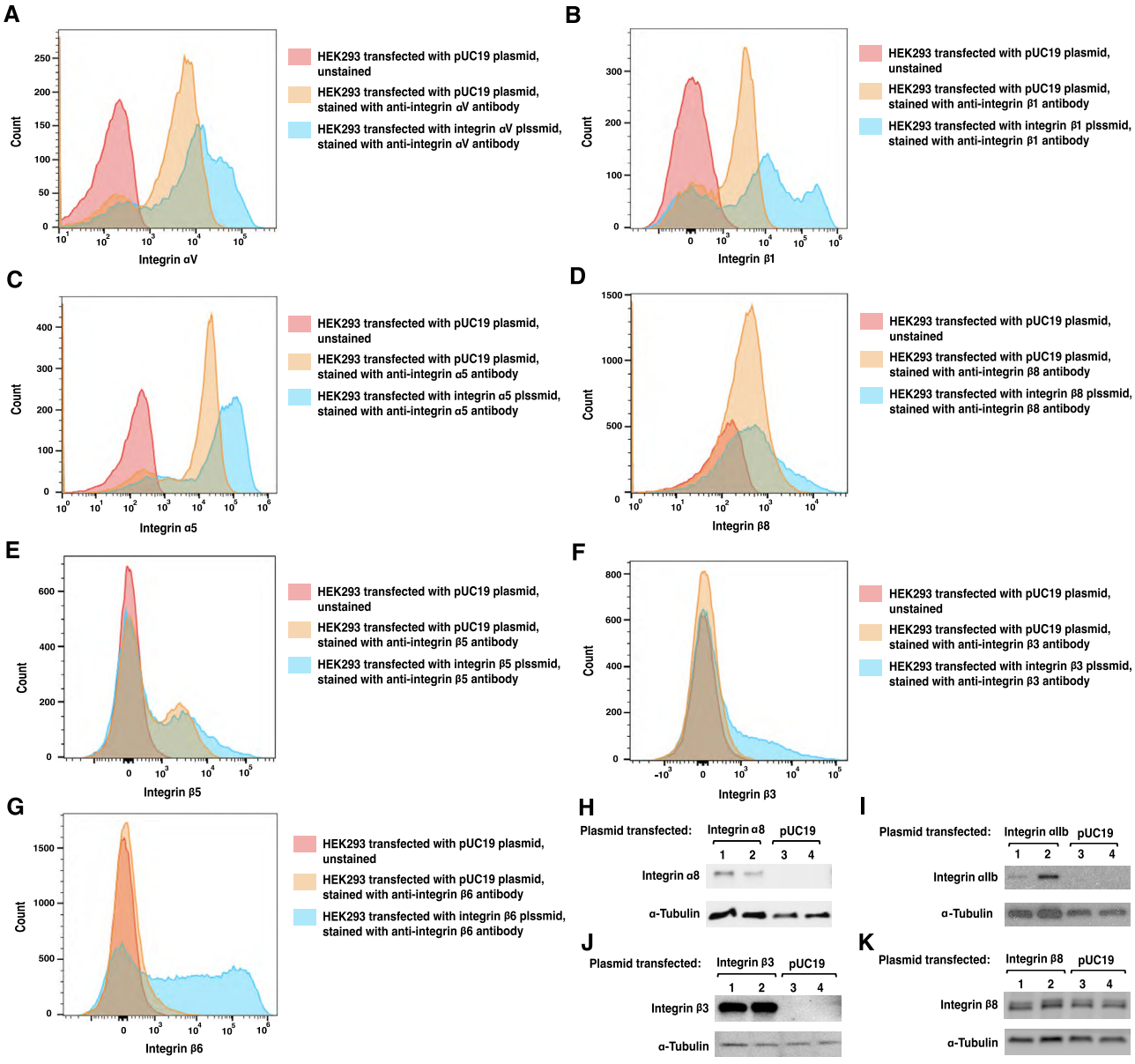

Figure S5. Flow cytometry and western blot confirms overexpression of integrin alpha and beta proteins after plasmid transfection in HEK293 cells

(A–G) Representative histograms from flow cytometry analysis of HEK293 cells transfected with pUC19 or plasmids expressing integrin αV (A), β1 (B), α5 (C), β8 (D), β5 (E), β3 (F), or β6 (G) under the control of EF1α promoter and stained with antibodies against the overexpressed protein.

(H and I) western blots showing overexpression of integrin α8 (H), αIIb (I), β3 (J), and β8 (K) in HEK293 cells transfected with the corresponding integrin plasmid (lanes 1 and 2) compared to the cells transfected with pUC19 (lanes 3 and 4).

Related to Figure 4.

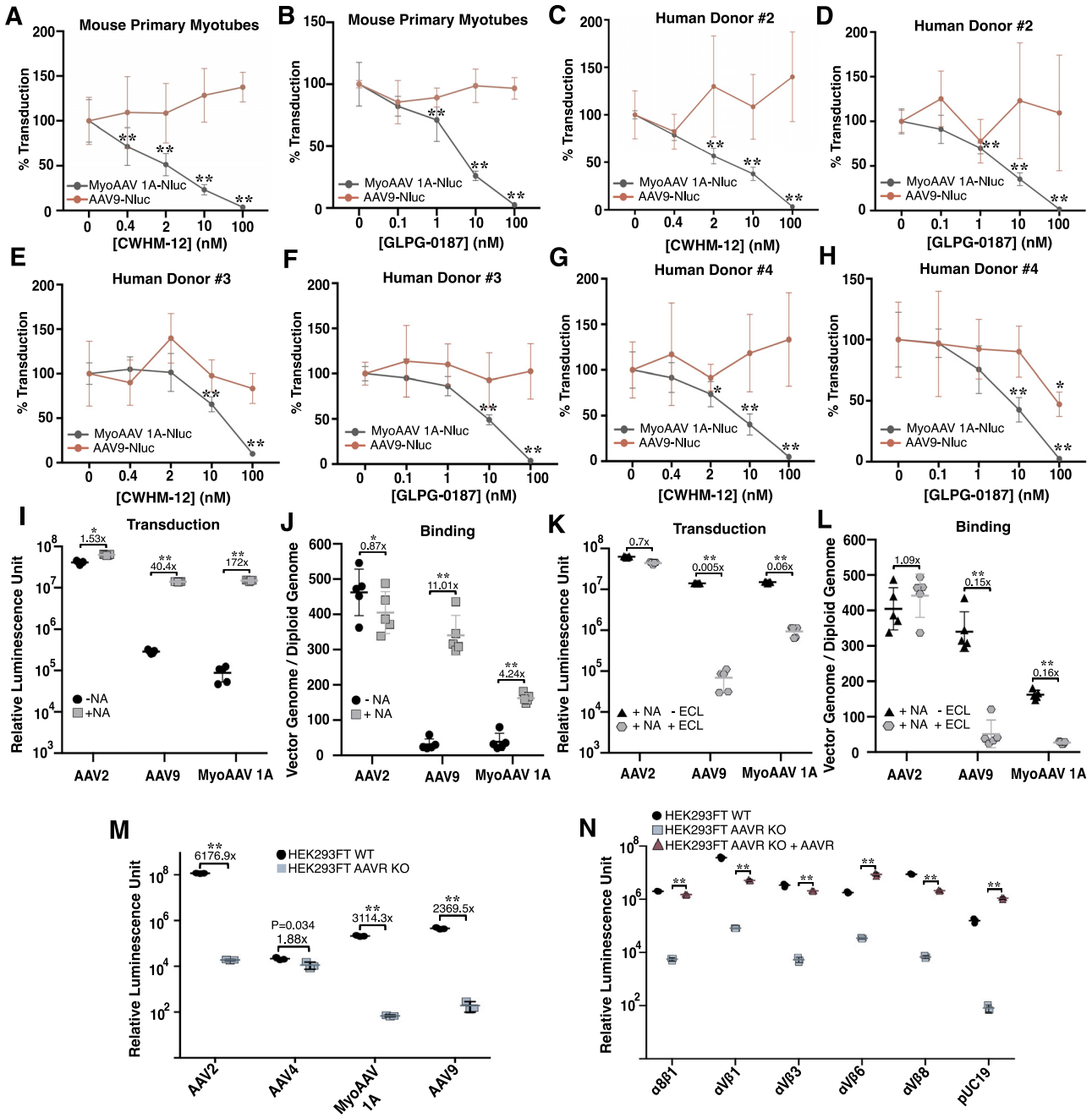

Figure S6. CWHM-12 and GLPG-1087 integrin αV antagonists suppress MyoAAV 1A but not AAV9 transduction in primary mouse myotubes, as well as primary human myotubes from different donors.

(A and B) *In vitro* transduction efficiency in mouse primary myotubes treated with different concentrations of CWHM-12 (A) or GLPG-0187 (B) integrin αV antagonists and transduced with AAV9- or MyoAAV 1A-CK8-Nluc. Data are presented as mean ± SD (n = 5). *: $p < 0.05$, **: $p < 0.01$ (one-way ANOVA with Dunnett's MCT with the 0 nM condition for each group as the control).

(C–H) *In vitro* transduction efficiency in human primary myotubes from three different donors treated with different concentrations of CWHM-12 (C, E, G) or GLPG-0187 (D, F, H) integrin αV antagonists and transduced with AAV9- or MyoAAV 1A-CK8-Nluc. Data are presented as mean ± SD (n = 5). *: $p < 0.05$, **: $p < 0.01$ (one-way ANOVA with Dunnett's MCT with the 0 nM condition for each group as the control). I, J) Quantification of *in vitro* transduction (I) and binding (J) of untreated HEK293 cells or cells pre-treated with NA and transduced with AAV2-, AAV9-, or MyoAAV 1A-CMV-Nluc. Data are presented as mean ± SD (n = 5); *: $p < 0.01$, **: $p < 0.0001$ (Student t test using log transformed data).

(K and L) Quantification of *in vitro* transduction (K) and binding (L) of HEK293 cells pre-treated with NA and ECL or NA alone with AAV2-, AAV9-, or MyoAAV 1A-CMV-Nluc. Data are presented as mean ± SD (n = 5); *: $p < 0.01$, **: $p < 0.0001$ (Student t test using log transformed data).

(legend continued on next page)

(M) Comparison of *in vitro* transduction between HEK293FT and HEK293FT AAVR KO cells transduced with AAV2-, AAV4-, AAV9-, or MyoAAV 1A-CMV-Nluc. Data are presented as mean ± SD (n = 3). **: $p < 0.0001$ (Student t test using the log transformed data).
(N) Quantification of *in vitro* transduction in HEK293FT cells, HEK293FT AAVR KO cells, and HEK293FT AAVR KO cells overexpressing AAVR, transfected with plasmids encoding for RGD-binding integrin heterodimers or with pUC19, and transduced with MyoAAV 1A-CMV-Nluc. Data are presented as mean ± SD (n = 3). **: $p < 0.0001$ (Student t test using the log transformed data).
Related to Figure 4.

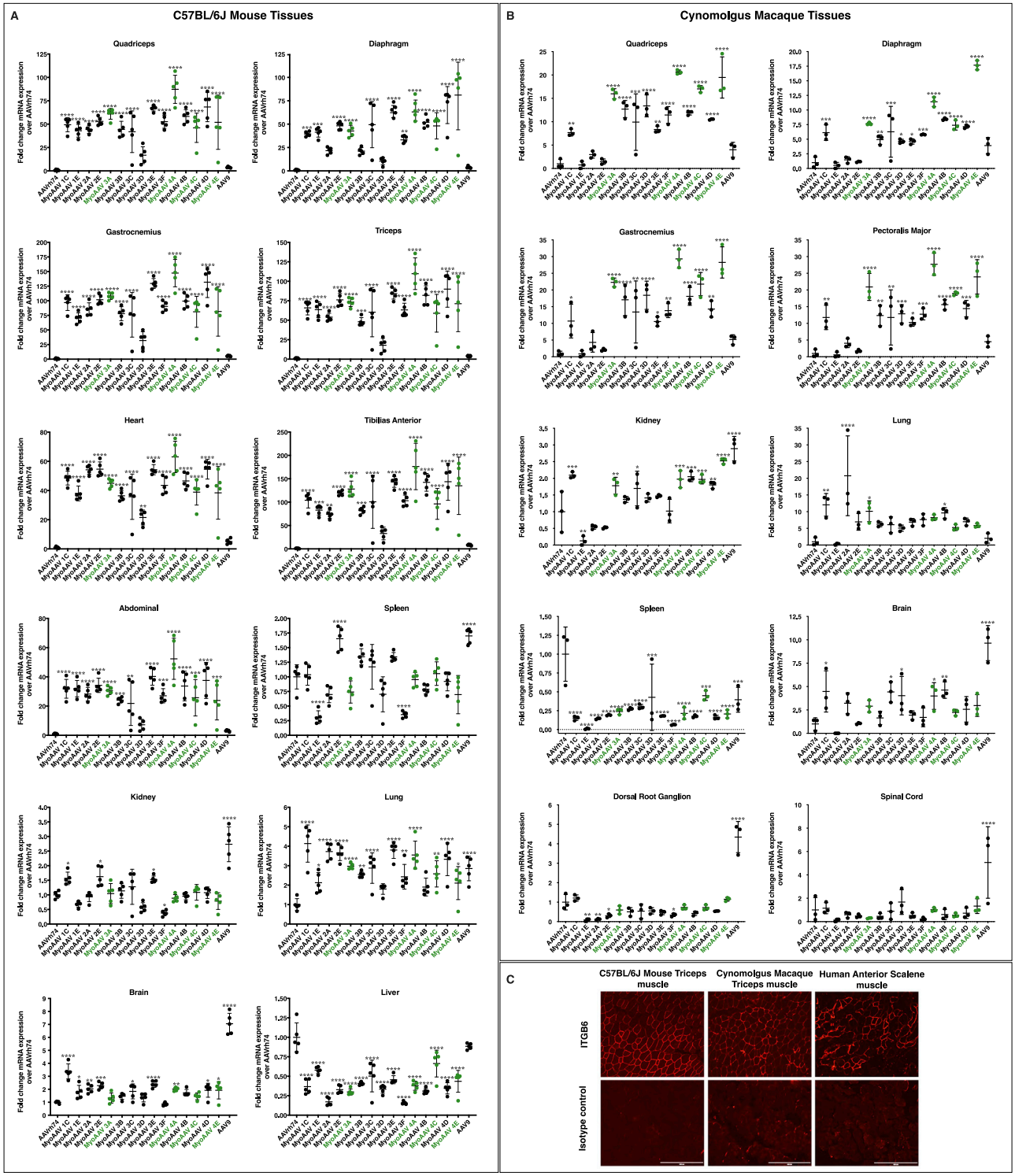

Figure S7. Characterization of muscle-tropic capsid variants evolved in cynomolgus macaque

(A and B) Fold change mRNA expression over AAVrh74 in different tissues of 8 weeks old C57BL/6J mice (A) or 2- 3 years old cynomolgus macaques (B) 1 month after injection of 3E+13 vg/kg of the pooled virus mix. mRNA expression was quantified by deep sequencing of the barcodes associated with each capsid variant.

(legend continued on next page)

Data are presented as mean ± SD (n = 5 for mice and n = 3 for macaques). *: $p < 0.05$, **: $p < 0.01$, ***: $p < 0.001$, ****: $p < 0.0001$ (one-way ANOVA with Dunnett's MCT with AAVrh74 as the control).

(C) Representative immunofluorescence images for integrin β6 (ITGB6, red) and an isotype control (red) in C57BL/6J Mouse Triceps muscle, cynomolgus macaque Triceps muscle, and Human Anterior Scalene muscle. Scale bar: 400 μm.

Related to Figure 7.